HHS Public Access

Author manuscript

Nat Cardiovasc Res. Author manuscript; available in PMC 2024 July 31.

Published in final edited form as:

Nat Cardiovasc Res. 2024 May ; 3(5): 567–593. doi:10.1038/s44161-024-00471-7.

Primitive macrophages induce sarcomeric maturation and functional enhancement of developing human cardiac microtissues via efferocytic pathways

Homaira Hamidzada[1,2,3], **Simon Pascual-Gil**[1,2], **Qinghua Wu**[4], **Gregory M. Kent**[5,6], **Stéphane Massé**[7], **Crystal Kantores**[1,2], **Uros Kuzmanov**[8], **M. Juliana Gomez-Garcia**[4,5], **Naimeh Rafatian**[4], **Renée A. Gorman**[9], **Marianne Wauchop**[9], **Wenliang Chen**[10], **Shira Landau**[4], **Tasnia Subha**[7], **Michael H. Atkins**[5,6], **Yimu Zhao**[1,4], **Erika Beroncal**[11], **Ian Fernandes**[5,6], **Jared Nanthakumar**[1,2], **Shabana Vohra**[1,2], **Erika Y. Wang**[12], **Tamilla Valdman Sadikov**[5], **Babak Razani**[13,14], **Tracy L. McGaha**[3,15], **Ana C. Andreazza**[16,17], **Anthony Gramolini**[1,2,8], **Peter H. Backx**[1,8,9], **Kumaraswamy Nanthakumar**[7], **Michael A. Laflamme**[5,18,19,#], **Gordon Keller**[5,6,15,#], **Milica Radisic**[1,4,20,21,#], **Slava Epelman**[1,2,3,18,19,#]

[1.]Toronto General Hospital Research Institute, University Health Network, Toronto, ON

[2.]Ted Rogers Centre for Heart Research, Translational Biology and Engineering Program, Toronto, ON

[3.]Department of Immunology, University of Toronto, Toronto, ON

[4.]Institute of Biomedical Engineering, University of Toronto, Toronto, ON

[5.]McEwen Stem Cell Institute, University Health Network, Toronto, ON

[6.]Department of Medical Biophysics, University of Toronto, Toronto, ON

[7.]The Hull Family Cardiac Fibrillation Management Laboratory, Toronto General Hospital, Toronto, ON

[8.]Department of Physiology, University of Toronto, Toronto, ON

[9.]Department of Biology, York University, Toronto, ON

Corresponding Author: Slava Epelman, MD, PhD, Toronto Medical Discovery Tower, MaRS Building, 101 College St, 3rd Floor, Room TMDT 3-903, Toronto, ON. Canada. M5G 1L7, slava.epelman@uhn.ca.

[#]These authors jointly supervised this work.

Author contributions

H.H. designed and performed experiments with the help of S.P-G., Q.W., S.M., C.K., U.K., N.R., R.A.G., M.W., W.C., S.L., T.S., Y.Z., E.B., J.N., and S.V. H.H. performed the bioinformatics analyses. Q.W., G.M.K., M.H.A., M.J.G-G., E.Y.W., I.F., and T.V.S. generated bioengineering platforms and produced and differentiated cells. B.R., T.M., A.C.A., A.G., P.B., K.N., M.A.L., G.K., and M.R. contributed to data interpretation and provided expertise. S.E. and M.R. conceived the study and obtained funding. H.H. and S.E. wrote the manuscript. All authors reviewed and approved the manuscript.

Code availability

This manuscript does not report original code. Scripts for the analysis of bulk RNA sequencing and single-cell RNA sequencing data are available at https://github.com/HomairaH/EpelmanLab_Human-cardiac-microtissues.

Competing interests

M. R. and Y.Z. are inventors on patents for cardiac tissue cultivation that are licensed to Valo Health. They receive licensing royalty from this invention. Q.W., M.R., and Y.Z. have a filed patent application on thermoplastic polymer composition for micro 3D printing and uses thereof. All other authors declare no competing interests.

[10]Scientific Research Center, the Second Affiliated Hospital of Guangdong Medical University, Guangdong Medical University, Zhanjiang, 524023, China

[11]Department of Pharmacology and Toxicology, University of Toronto, Toronto, ON

[12]David H. Koch Institute for Integrative Cancer Research at MIT, Cambridge, Massachusetts, United States

[13]Vascular Medicine Institute, Department of Medicine, University of Pittsburgh School of Medicine and UPMC, Pittsburgh, PA, United States

[14]Department of Cardiology, Pittsburgh VA Medical Center, Pittsburgh, PA, United States

[15]Princess Margaret Cancer Centre, University Health Network, Toronto, ON

[16]Department of Psychiatry, University of Toronto, Toronto, ON

[17]Mitochondrial Innovation Initiative, Toronto, ON

[18]Peter Munk Cardiac Centre, University Health Network, Toronto, ON

[19]Department of Laboratory Medicine and Pathobiology, University of Toronto, Toronto, ON

[20]Department of Chemical Engineering and Applied Chemistry, University of Toronto, Toronto, ON

[21]Terrence Donnelly Centre for Cellular & Biomolecular Research, University of Toronto, ON

Abstract

Yolk sac macrophages are the first to seed the developing heart, however we have no understanding of their roles in human heart development and function due to a lack of accessible tissue. Here, we bridge this gap by differentiating human embryonic stem cells (hESCs) into primitive LYVE1^{+} macrophages (hESC-macrophages) that stably engraft within contractile cardiac microtissues composed of hESC-cardiomyocytes and fibroblasts. Engraftment induces a human fetal cardiac macrophage gene program enriched in efferocytic pathways. Functionally, hESC-macrophages trigger cardiomyocyte sarcomeric protein maturation, enhance contractile force and improve relaxation kinetics. Mechanistically, hESC-macrophages engage in phosphatidylserine dependent ingestion of apoptotic cardiomyocyte cargo, which reduces microtissue stress, leading hESC-cardiomyocytes to more closely resemble early human fetal ventricular cardiomyocytes, both transcriptionally and metabolically. Inhibiting hESC-macrophage efferocytosis impairs sarcomeric protein maturation and reduces cardiac microtissue function. Taken together, macrophage-engineered human cardiac microtissues represent a considerably improved model for human heart development, and reveal a major beneficial role for human primitive macrophages in enhancing early cardiac tissue function.

Introduction

Resident cardiac macrophages arise from yolk sac and fetal monocyte precursors that seed the heart during early embryonic development[1–4]. These embryonically derived primitive macrophages persist into adulthood where they are primarily maintained through self-renewal[1–9]. Functionally, murine studies show that macrophages directly interact with cardiomyocytes, can facilitate electrical conduction[10], trigger cardiomyocyte proliferation

after injury leading to regeneration (in neonatal animals)[11,12] and promote cardiac tissue repair (in adult animals)[1,3,4,11,13–19]. Macrophages also possess key efferocytic functions, where they can ingest apoptotic cells during cardiac stress or ischemic injury[20,21], and help shape matrix formation and degradation[22–24], which together reveal broad cardioprotective functions attributed to resident macrophages.

In contrast to our expanding knowledge of cardiac macrophages in adulthood, the role of macrophages during cardiac development is poorly understood. Developing organs undergo major macro-environmental changes due to rapid cellular proliferation, migration and death. In the developing murine heart, embryonic macrophages modulate aspects of coronary development[25] and lymphatic growth[26], however beyond these roles very little is known. Importantly, all of these studies were performed in murine models, and the role of macrophages within human cardiac tissue or during human cardiac development is entirely unknown. One of the obvious barriers is the lack of access to developing human cardiac tissue and cells. To overcome these challenges, *in vitro* organoid or engineered tissue models of the human heart using human pluripotent stem cells (hPSCs) have been developed. The versatile use of beating engineered tissues has led to significant progress in (1) modeling human heart development and disease[27–31]; (2) modeling patient-specific genetic disease[32–34] and (3) studying cardiomyocyte maturation[35–37]. To model the *in vivo* environment more accurately, studies have begun to include some key non-myocyte cell populations (fibroblasts, endothelial cells)[31,38–40]. Macrophages are present from the earliest stages of human cardiac development before the presence of a fully formed heart (as early as 5 post-conception weeks)[2,41]. Importantly, macrophages may possess key functions that could support developing cardiomyocytes[3,4,10,42]. Primitive hematopoietic progenitors generated from hPSCs will differentiate to give rise to macrophages under appropriate culture conditions, mimicking human yolk sac hematopoiesis[43,44]. However, primitive hPSC-derived macrophages have not been included in cardiac bioengineering or organoid approaches, representing a critical gap in the field.

In this study, we developed immuno-engineered human cardiac microtissues using human embryonic stem cell (hESC)-derived primitive macrophages to define the critical reciprocal interactions between developing cardiac microtissues and macrophages, and importantly, whether those interactions lead to improved microtissue function. We used the Biowire system, a human heart-on-a-chip platform[45–47] which forms a 3D contractile microtissue composed of hESC- or iPSC-derived cardiomyocytes and fibroblasts suspended in a hydrogel matrix. The tissue is cylindrically shaped and grows in suspension attached at the ends by two parallel, flexible wires. hESC-macrophages engrafted cardiac microtissues, which instructed the development of a tissue resident yolk sac program in hESC-macrophages akin to human fetal development. Using a combination of functional assessments, proteomics and transcriptomics, we show that hESC-macrophages markedly improved contractile force, relaxation properties and electrical stability, and enhanced maturation of cardiomyocyte contractile machinery. The primary role of hESC-macrophages was during early tissue remodeling and formation where they were critical for the reduction of cytotoxicity, cardiomyocyte stress and apoptosis. hESC-macrophage efferocytosis of cardiomyocyte cargo via recognition of phosphatidylserine led to developmentally-staged cardiomyocyte maturation and enhanced cardiac microtissue function. We report major

improvements in modelling human cardiac tissue formation, maturation and function, highlighting novel, previously unappreciated roles of human primitive macrophages in cardiac development, which has major implications, from *in vitro* studies using engineered cardiac tissues to *in vivo* cell-based therapies for regeneration.

Results

Human ESC-derived macrophages resemble macrophages in human fetal development

We do not understand the reciprocal interactions between early human fetal macrophages and developing cardiac tissue the obvious lack of samples and inability to model this developmental stage. To better understand these events, we examined macrophage transcriptional signatures in early human development *in vivo*, and subsequently, whether we can educate hESC-derived macrophages to a similar fate *in vitro*. We aimed to emulate primitive macrophages from *in vivo* human embryonic development, previously shown to be regenerative in neonates and broadly cardioprotective in adult mice[1,3,11,13,17,19]. We analyzed publicly available single-cell RNA sequencing (scRNA-seq) data of the human yolk sac at 4 weeks post-conception (PCW)[9]. We found that all macrophages (*C1QC*$^{+}$ *CD64*$^{+}$ *CD68*$^{+}$ *CD14*$^{+}$) expressed high levels of *TIMD4*, *LYVE1* and *FOLR2*, and other genes comprising the previously defined "TLF" macrophage signature (*MRC1, CD163, F13A1*)[2] and lacked expression of the monocyte and monocyte-derived macrophage marker *CCR2* (Fig. 1A, Supplementary Table 1). Human fetal cardiac macrophages *in vivo* (19–22 post-conception weeks)[48] expressed a similar yolk sac macrophage signature, including *LYVE1*, *CD163*, and *MRC1*, and lacked *CCR2,* which was found primarily on monocytes and dendritic cells (Fig. 1B, Supplementary Table 1). Next, we focused on lineage-specified macrophage production from pluripotent stem cells. hESC-macrophages were specified from a primitive yolk sac hematopoietic program as shown recently[43] (Fig. 1C). Flow cytometric analyses showed that the day 15 populations uniformly expressed canonical macrophage lineage markers including CD14, CD64, CD68 and CD163 (Fig. 1D), embryonic-derived marker LYVE1, and lacked CCR2 (Fig. 1E, gating strategy Supplementary Fig. S1A), suggesting hESC-macrophages were specified to a program resembling macrophages present during early development in the yolk sac and fetal heart.

Engrafted hESC-macrophages acquire a fetal cardiac macrophage program

To study hESC-macrophage education, we generated immuno-engineered human cardiac microtissues using hESC-derived cardiomyocytes[49,50] (Extended Data Fig. 1A, gating strategy Supplementary Fig. S1B, high expression and purity of cardiac troponin T [98%]), human primary cardiac fibroblasts (Extended Data Fig. 1B, expressing *GATA4* and *WT1*), and hESC-macrophages. We utilized a high throughput plate-based Biowire platform[47] (termed HT-Biowires) wherein 3D printed nanocomposite microwires are fabricated over multi-well plates. Cardiac microtissues began to beat at ~day 3–4 post seeding. After 14 days, CD68^{+} macrophages were found throughout the microtissues, wrapped between adjacent cardiomyocytes and fibroblasts (Extended Data Fig. 1C-D), indicating hESC-macrophages stably integrated. Long-term survival of hESC-macrophages without exogenous growth factors (M-CSF) required the presence of fibroblasts or fibroblast-conditioned media (Extended Data Fig. 1E-F), indicating that cell circuits were formed.

To dissect whether hESC-cardiomyocytes and fibroblasts transcriptionally program hESC-macrophages when they engraft, we created microtissues in a combinatorial fashion to recapitulate the following: (1) Cardiac environment: hESC-macrophages, hESC-cardiomyocytes and fibroblasts; (2) General tissue environment: hESC-macrophages and fibroblasts; and (3) hESC-macrophages alone (Fig. 1F-G), all within a hydrogel matrix. We then performed two sets of bulk RNA-seq experiments to specifically dissect hESC-macrophage education within cardiac microtissues.

First, we defined “contaminating RNA signatures” associated with dissociation and ambient RNA contamination. To delineate *de novo* transcription from contaminating transcripts, we profiled hESC-macrophages in the presence of a transcription inhibitor, which we confirmed prevented LPS-induced transcription (Extended Data Fig. 2A). To define an “ambient RNA signature”, hESC-macrophages were incubated alone, with fibroblasts, or with fibroblasts and cardiomyocytes, in the presence of a transcription inhibitor. hESC-macrophages from each group were sorted for bulk RNA-seq (Extended Data Fig. 2B-D). Upon addition of fibroblasts, 291 differentially expressed genes (DEGs) were found in hESC-macrophages, which were comprised largely of fibroblast-specific or collagen genes (*POSTN, COL1A1, COL5A1*; Extended Data Fig. 2E, Supplementary Table 2). Addition of both hESC-cardiomyocytes and fibroblasts resulted in 451 DEGs, comprised of contractile machinery components unique to cardiomyocytes (*MYH6, MYL4, MYH7*; Supplementary Table 2). The transcription inhibitor was included in all subsequent RNA-seq experiments and these “contaminating genes” were excluded from macrophage analyses.

Next, we performed bulk RNA-seq on sorted live hESC-macrophages ($DAPI^{-}$ $CD45^{+}CD14^{+}RFP^{+}$; Extended Data Fig. 2F-G) from microtissues (HT-Biowires) from each of the 3 groups (day 14) to define how fibroblasts and the combination of fibroblasts and hESC-cardiomyocytes instruct hESC-macrophages. Contaminating transcripts identified by the control experiment were removed (Supplementary Table 3, Extended Data Fig. 2H). We found that fibroblasts and hESC-cardiomyocytes induced distinct and overlapping genes and pathways in hESC-macrophages. For example, hESC-macrophages isolated from microtissues composed of fibroblasts + hESC-macrophages had 566 upregulated DEGs, while hESC-macrophages isolated from hESC-cardiomyocytes + fibroblasts + hESC-macrophages had 1790 upregulated DEGs, of which 373 were overlapping (Fig. 1H, Supplementary Table 3). To assess transcriptional similarity to *in vivo* human embryonic macrophages, we benchmarked hESC-macrophages against a gene signature generated from human yolk sac macrophages (4 PCW)[9] and human fetal cardiac macrophages (19–22 PCW)[48] relative to monocytes. hESC-macrophages exhibited a stepwise upregulation of both the human yolk sac macrophage program and fetal cardiac macrophage program (Fig. 1I, Supplementary Table 1), indicating *in vitro* education within microtissues. General core macrophage functions such as endocytosis, phagocytosis and antigen presentation were more enhanced when hESC-macrophages were instructed by both cardiomyocytes and fibroblasts, while fibroblasts uniquely programmed hESC-macrophages to be enriched in genes regulating lipid transport and storage (Fig. 1J, Supplementary Table 3). Lastly, a tissue environment containing both fibroblasts and cardiomyocytes induced the largest upregulation of core macrophage genes required for lineage, survival and identity (*CSF1R, MAFB, MAF, CD14*) (Fig. 1K) and the embryonically derived TLF^{+} macrophage core

signature (Fig. 1L; *LYVE1, FOLR2, STAB1, MRC1, F13A1*, etc.)[2]. Upregulation of these genes occurred in a stepwise fashion by fibroblasts, with further induction upon cardiomyocyte addition (Fig. 1K-L). For example, *LYVE1* was upregulated ~10 fold by fibroblasts, and ~400 fold by the combination of hESC-cardiomyocytes and fibroblasts (P_{adj}<0.05). These data indicate a microenvironment generated by cardiomyocytes and fibroblasts was required to more fully program hESC-macrophages and induce an *in vivo* yolk sac derived tissue resident macrophage program seen in humans during early development.

hESC-macrophages broadly enhance cardiac microtissue functions

Next, we defined whether hESC-macrophages improved electromechanical properties of developing human cardiac microtissues. We varied both the cardiomyocyte source and bioengineering platform used to ensure reproducibility and compared the Biowire II platform[46] seeded with commercial iPSC-derived cardiomyocytes (iCells) to the HT-Biowire platform (Fig. 1)[47] seeded with hESC-cardiomyocytes[50]. Biowires in both groups were seeded with or without hESC-macrophages and a variety of electromechanical properties were assessed (Fig. 2A). We observed that hESC-macrophages reduced tissue width (increased compaction) relative to controls, which is a process of tissue formation driven by fibroblast ECM synthesis and remodeling, using iCells in the Biowire II platform (Fig. 2B, day 2–7). Moreover, passive tension was also increased, which is generally attributed to fibroblast functions, ECM deposition and myofilaments (Fig. 2C).

To investigate contractile force generated in cardiac microtissues we measured the elastic anchor wire displacement with each beat during pacing (1 Hz)[45]. hESC-macrophages increased the active force generated upon contraction relative to control microtissues without hESC-macrophages (Fig. 2D). hESC-macrophage-containing microtissues also had reduced excitation threshold voltage, increased maximum capture rate, and substantially increased contraction and relaxation slopes (Fig. 2G-H), which was reproducible across multiple batches (Extended Data Fig. 3A). Qualitatively, we observed greater variation in the force of successive paced contractions, as well as intermittent conduction abnormalities, which led to a more chaotic appearance in force tracking of developing microtissues that lacked hESC-macrophages (Extended Data Fig. 3B). To assess the degree of this electrical instability in microtissues, we paced microtissues at increasing frequencies (0 to 4 Hz) and quantified the presence of reduced force as a measurement of instability (Extended Data Fig. 3B-C, zoomed tracing of reduced force). Microtissues without hESC-macrophages exhibited asynchronous contractions during spontaneous beating, while during pacing (1–4 Hz), they exhibited a contractile pattern that oscillated in strength, likely due to the immature nature of the microtissues (Extended Data Fig. 3B). In contrast, microtissues with hESC-macrophages had an increased pacing threshold below which tissues were electrically and mechanically stable, as well as a lower fraction of beats exhibiting reduced amplitudes or conduction blocks (Extended Data Fig. 3D-E). Aspects of this variation are seen in humans with severe cardiac dysfunction (termed mechanical alternans)[51,52]. Together, these data indicate that electromechanical properties of cardiomyocyte function, including systolic and diastolic function, and electrical stability, are improved by hESC-macrophage incorporation in cardiac microtissues.

We next used HT-Biowires seeded with hESC-cardiomyocytes to assess whether the benefit of hESC-macrophages occurs with a different cardiomyocyte source and platform. As before, hESC-macrophages triggered greater compaction and passive tension (Fig. 2I-J). Importantly, active force generated by microtissues with hESC-macrophages was increased compared to control microtissues (Fig. 2K, Extended Data Fig. 4A). A low macrophage input (5%) did not impact contractile force generation, with peak force generated in tissues with 20% hESC-macrophages (Fig. 2L), while a high content of hESC-macrophages (30%) led to significant reduction in active force, indicating the cellular composition is critical for optimal function. As observed in our earlier experiments, microtissues that contained hESC-macrophages reproducibly exhibited increased contraction slopes and increased relaxation slopes (Fig. 2M-N), indicating faster contraction and relaxation.

Collectively, we utilized numerous cardiomyocyte batches and different stem cell sources, and observed a broad range of baseline spontaneous resting heart rates in control cardiac microtissues without macrophages (between 20–130 BPM), reflecting a combination of cardiomyocyte immaturity and purity. On average, when the baseline heart rate was low (~20–40 BPM), addition of hESC-macrophages increased the heart rate, whereas when the baseline was high (>60 BPM), hESC-macrophages reduced the heart rate (Extended Data Fig. 4B). Irrespective of their effect on heart rate, in all cases, hESC-macrophages resulted in an increased active force (Extended Data Fig. 4C). These data suggested that hESC-macrophages modulate (or fine tune) the heart rate in a context dependent fashion, while improved cardiac microtissue function was independent of heart rate. Since the combination of hESC-cardiomyocytes with hESC-macrophages is a step closer towards a common stem cell source for tissue engineering and *in vivo* delivery approaches, we used hESC-cardiomyocytes in HT-Biowires for the remainder of our study.

Unbiased proteomics reveal hESC-macrophages drive sarcomeric maturation

To dissect how hESC-macrophages improved cardiomyocyte function, we performed unbiased proteomics analyses using liquid chromatography mass spectrometry (LC-MS) on individual cardiac microtissues with and without hESC-macrophages during early microtissue formation (day 3) and during functional evaluation (day 14). We identified ~3500 proteins per sample (Extended Data Fig. 5A-B), with principal component analysis highlighting the greatest differences were driven by the presence of hESC-macrophages followed by the timepoint (Fig. 3A; Supplementary Table 4). We focused our analyses on proteins only expressed by cardiomyocytes, in particular, those that change as cardiomyocytes mature. We found that a broad range of sarcomeric (contractile machinery) proteins were significantly upregulated in microtissues with hESC-macrophages, including proteins of the troponin-tropomyosin complex (day 14: TNNT2, TNNI1, TPM1, TPM2, TPM3, TPM4), myosin heavy chain proteins (MYH7), and myosin light chain proteins (MYL6, MYL4, MLY3; Fig. 3B). hESC-macrophage driven upregulation of sarcomeric proteins was also observed at day 3 (timepoint where microtissues begin to beat), indicating cardiomyocyte maturation began in the earliest stages of microtissue development (Extended Data Fig. 5C). We found an increase in the ratio of adult to fetal isoforms of myosin heavy chains (MYH7 to MYH6) and adult to fetal isoforms of myosin regulatory light chains (MYL2 to MYL7), indicating improved cardiomyocyte maturation (Fig. 3C). Moreover,

cardiac desmosomal proteins, which provide strength and structural integrity, were increased by hESC-macrophages (DSC2, DSG2 and DSP [Fig. 3D]), suggesting improved mechanical transduction. Juntophillin-2 (JPH2), a key junction protein involved in excitation-contraction coupling[53], was also upregulated with hESC-macrophages (Extended Data Fig. 5D). These protein level changes correlated with increased cardiomyocyte size without an obvious change in cardiomyocyte cell numbers (Fig. 3E-F, gating strategy Supplementary Fig. S2A). hESC-macrophages induced increased elongation of sarcomeres (quantified by eccentricity; Fig. 3G), without an obvious change in myofibril alignment (Extended Data Fig. 5E). These data are consistent with pathway enrichment analyses, where hESC-macrophages led to upregulation of muscle contraction, fiber organization, structural constituent of muscle, and proteoglycan binding pathways (Fig. 3H, Supplementary Table 4). Elongation of sarcomeres, increased cardiomyocyte size and higher production of sarcomeric proteins that drive contractility revealed widespread cardiomyocyte structural changes occur when macrophages are integrated into cardiac microtissues, which leads to improved cardiac performance.

ECM composition is also critical to cardiomyocyte function, in particular fibrillar collagens which govern structural integrity and force transmission[54,55]. We observed that fibrillar collagens COL1A2 and COL3A1 were upregulated in microtissues with hESC-macrophages as early as day 3 (Extended Data Fig. 5F), however, the majority of changes were observed at day 14, including upregulation of fibrillar (COL1A1, COL1A2, COL3A1) and non-fibrillar (COL8A1) collagens, and downregulation of fibrillar COL5A1 and COL5A2 (Fig. 3I), without a change in total fibroblast numbers (Fig. 3J, gating strategy Supplementary Fig. S2B, day 3). We also observed complex reorganization of proteoglycans primarily at day 14, including downregulation of VCAN, DCN, and FN1, and upregulation of LUM (Fig. 3K), which also possess non-structural functions[54]. Fewer differences were found on day 3 during microtissue development, including downregulation of FMOD, and upregulation of POSTN (Extended Data Fig. 5G).

hESC-macrophages increase Ca^{2+} amplitude without changes in kinetics

We detected only a handful of calcium handling proteins, of which we noted upregulation of the calcium binding protein HRC, which governs calcium uptake, storage and release, while the L-type calcium channel CACNA2D1 was downregulated (Extended Data Fig. 6A). Functionally, we observed increased calcium amplitude in microtissues with hESC-macrophages (Extended Data Fig. 6B). We did not observe differences in conduction velocity, calcium transient duration, or relaxation time and time to peak of the calcium transient (Extended Data Fig. 6C-G). To assess whether single cardiomyocytes were altered, we dissociated microtissues with and without hESC-macrophages and performed whole-clamp voltage-clamp recordings of single hESC-cardiomyocytes (Extended Data Fig. 6H). We observed no significant differences in either amplitudes or activation properties (i.e. Boltzmann fits to conductance) of voltage-gates Na^+ channels or Ca^{2+} channels (Extended Data Fig. 6I-K), and no differences in whole-cell current-clamp recordings (action potential parameters; Extended Data Fig. 6L). Therefore, the primary electrophysiological effect on hESC-cardiomyocytes was likely attributed to increased systolic calcium release, resulting

in improved contractile force, without major alterations in ion channel functions within individual cardiomyocytes.

hESC-macrophages reduce mitochondrial protein containing debris

Cardiac function is highly energy dependent, therefore we wondered whether addition of hESC-macrophages alters metabolic pathways within cardiomyocytes. Given our proteomics data was performed in bulk tissue, we performed single cell protein phenotyping by developing a multi-dimensional cytometry by time-of-flight (CyTOF) workflow using 36 markers (cell death, cell identity, and metabolic pathways). We focused on the early phase of microtissue formation (day 3), included multiple replicates (n=6 per group) and analyzed 580,776 cells (live and dead) (Fig. 4A, Extended Data Fig. 7A). We could clearly differentiate $cTnT^+$ hESC-cardiomyocytes from $CD14^+CD45^+$ hESC-macrophages and $CD36^+$ ($CD14^-CD45^-$) fibroblasts (Fig. 4B). Strikingly, we found that the major difference in abundance was that control microtissues without hESC-macrophages accumulated a sizable population (~43% of all events) of dead cells/material expressing high levels of ATP5A and citrate synthase (CS), both mitochondrial localized proteins, DNA, and glucose-6-phosphate dehydrogenase (G6PD), but no additional lineage or metabolic markers (Fig. 4A-C, Extended Data Fig. 7B; named “dead $ATP5A^{hi}$”). In the presence of hESC-macrophages this population was markedly reduced by >95% (Fig. 4D), without differences in the number of live cardiomyocytes or fibroblasts (Extended Data Fig. 7C). Immunofluorescence confirmed accumulation of punctate $ATP5A^+$ material markedly reduced in microtissues with hESC-macrophages (Fig. 4E). We also observed a second population of dead cells/material expressing moderate levels of ATP5A, but not CS, with moderate levels of GLUT1, MCT1 and GAPDH, likely representing an earlier stage of death, where more proteins remained detectable. This population represented ~10% of all events in control microtissues, and was reduced by ~40% by hESC-macrophages (Extended Data Fig. 7B, 7D).

In line with these data (loss of mitochondrial protein debris), we found that hESC-macrophages also reduced the accumulation of a broad range of mitochondrial-localized proteins, including mitochondrial membrane, structural and ribosomal proteins on both day 3 and 14 using whole microtissue proteomics (LC-MS; Fig. 4F-G, Extended Data Fig. 7E, Supplementary Table 4). We examined proteins involved in the Krebs Cycle and found that cytosolic isoforms (MDH1, ACO1, IDH1) were upregulated in cardiac microtissues with hESC-macrophages, while all the remaining mitochondrial isoforms (MDH2, ACO2, IDH2, IDH3A, IDH3B, IDH3G) were reduced in abundance (Fig. 4G). Together, these data support a compartment-specific pattern where mitochondrial protein containing debris and therefore proteins localized to the mitochondria are reduced, likely representing the dead $ATP5A^{hi}$ subset accumulation detected by CyTOF. We reasoned this reduction was secondary to ingestion of cardiomyocyte-derived cargo potentially containing mitochondrial proteins. A similar pathway was described in murine studies, where macrophages ingested expelled mitochondria, improving cardiomyocyte mitochondrial quality control that results in optimal ATP generation[42]. Importantly, despite the above changes, we found that inclusion of hESC-macrophages led to higher ATP content in cardiac microtissues with hESC-macrophages relative to controls (Fig. 4H), indicative of a more energized state.

hESC-macrophages induce cardiomyocyte metabolic shifts akin to the fetal heart

We understand very little about human fetal cardiac development, including dynamic metabolic changes occurring during rapid organ growth and remodeling. To better understand these early stages, we analyzed publicly available scRNA-seq data of the developing human fetal heart and focused on ventricular cardiomyocytes (Supplementary Table 5)[41]. We observed (as did the authors), that human fetal cardiomyocytes downregulated pathways related to mitochondrial metabolism between 5- and 22-weeks post-conception (Fig. 4I). To understand whether metabolic pathways were altered in cardiac microtissues with hESC-macrophages, we subclustered live hESC-cardiomyocytes from our CyTOF data and observed four distinct clusters, two unique to each group (CM-1, CM-2) and two shared across groups (CM-3, CM-4; Fig. 4J-K). CM-1 and CM-2 appeared to be the most metabolically active, while CM-3 and CM-4 were relatively quiescent (Fig. 4L). CM-4 contained less DNA and slightly higher expression of the dead label suggesting cellular stress, and addition of hESC-macrophages reduced expression of this dead cell label (Extended Data Fig. 7F-G). To understand how hESC-cardiomyocytes differ across groups, we first focused on directly comparing the most metabolically active states. CM-2 was unique to cardiac microtissues with hESC-macrophages, and relative to CM-1 (unique to controls), CM-2 was more glycolytic (GLUT1, MCT1) and had increased expression of phosphorylated NRF2, which has detoxifying roles in the heart *in vivo*[56] (Fig. 4M). In contrast, CM-1 had higher expression of mitochondrial proteins ATP5A, CS, CPT1A (fatty acid oxidation) and the transcription factor NRF1 (drives cellular stress and mitochondrial biogenesis). These data suggest that hESC-macrophages reduced mitochondrial oxidative proteins in a subset of hESC-cardiomyocytes, potentially in favour of glycolytic pathways. In accordance, flow cytometric analyses demonstrated that hESC-macrophages reduced mitochondrial abundance within hESC-cardiomyocytes and fibroblasts (Extended Data Fig. 7H), suggesting reduced mitochondrial proteins detected by proteomics analyses (LC-MS) may reflect both reduced mitochondrial protein debris and a reduction of mitochondria within viable cells. Indeed, these changes existed in all subclusters, highlighting a common pattern induced by hESC-macrophages (Fig. 4N-O). Finally, cardiac troponin T protein expression was increased in CM-2 and CM-4 in microtissues with hESC-macrophages, supporting our LC-MS-based proteomics and indicating that the upregulation of contractile proteins is cell intrinsic, occurring at the single cell level (Extended Data Fig. 7I).

We also found four fibroblast subclusters, including two unique to each group and two shared (Extended Data Fig. 8A-B). FB-1 and FB-2 were the most metabolically active, while FB-3 and FB-4 were relatively quiescent (Extended Data Fig. 8C). We directly compared FB-1 (in control group) to FB-2 (in hESC-macrophage group) and found reduced abundance of metabolic proteins across both oxidative and glycolytic pathways driven by hESC-macrophages (Extended Data Fig. 8D). The only protein that was upregulated in microtissues with hESC-macrophages was phosphorylated NRF2. Similar patterns were observed in comparing groups within FB-3 and FB-4 (Extended Data Fig. 8E-F), highlighting that in general, addition of hESC-macrophages results in a more quiescent fibroblast state.

These complex data suggest that hESC-macrophages increase ATP stores in cardiac microtissues while simultaneously reducing the accumulation of mitochondrial protein containing debris and altering metabolic proteins in cardiomyocytes and fibroblasts. In this setting, hESC-cardiomyocytes become more similar to early human fetal ventricular cardiomyocytes (reduced mitochondrial pathways).

hESC-macrophages improve the cardiac microtissue environment

Given that macrophages cleared potentially toxic cellular debris (Fig. 4D) we wondered whether hESC-macrophages improved the early tissue microenvironment. We measured a variety of cytotoxicity markers and found that cardiac specific creatine kinase (CKMB), lactate dehydrogenase (LDH), adenylate kinase and G6PD release were significantly lower in microtissues with hESC-macrophages (Fig. 5A), which was reproducible across distinct stem cell sources of both primitive macrophages (H1 hESC-macrophages; Fig. 5B) and cardiomyocytes (hES2 hESC-cardiomyocytes; Fig. 5C). In addition, both cell-free double-stranded (ds)DNA and mitochondrial DNA were reduced by hESC-macrophages (Fig. 5D-E). Finally, microtissues with hESC-macrophages had decreased cellular oxidative stress due to reactive oxygen species (ROS; Fig. 5F), indicating that hESC-macrophages markedly reduce cell stress during tissue formation.

Next, we explored how hESC-cardiomyocytes behave in the altered environment induced by hESC-macrophages. We performed bulk RNA-seq of sorted live hESC-cardiomyocytes ($DAPI^{-}CD45^{-}CD14^{-}CD90^{-}RFP^{-}$) from microtissues with or without hESC-macrophages and found 998 upregulated DEGs and 787 downregulated DEGs (Extended Data Fig. 9A-D, 5G, Supplementary Table 6). We benchmarked hESC-cardiomyocytes isolated from microtissues to those present during early human fetal cardiac development using publicly available scRNA-seq data (as in Fig. 4)[41]. hESC-cardiomyocytes from microtissues with hESC-macrophages were transcriptionally more similar to *in vivo* human fetal ventricular cardiomyocytes (Fig. 5H). More specifically, hESC-cardiomyocytes educated by hESC-macrophages most closely resembled ventricular cardiomyocytes in early fetal development (5–9 PCW) rather than later development (17–24 PCW) (Fig. 5I). The major pathways that were enriched were cell cycle and proliferation processes, as well as pathways related to glycolysis and protein binding, while lipid metabolism was downregulated (Fig. 5J-K). We also found hESC-macrophages induced downregulation of *NPPA* and to a lesser extent, *NPPB* (Fig. 5L), indicative of maturation-like changes and/or reduced stress. Therefore, the early microenvironment is improved in the presence of hESC-macrophages, which triggers gene expression in hESC-cardiomyocytes that more closely resemble early human fetal heart development.

Efferocytosis of cardiomyocytes reprograms hESC-macrophages

Using Transwell co-cultures, we found that reduced cytotoxicity in the presence of hESC-macrophages was contact dependent (Fig. 6A) and hypothesized that efferocytosis of stressed hESC-cardiomyocytes (or their cargo) facilitates improved cardiac function. Efferocytic genes were induced by both fibroblasts and cardiomyocytes, but their combined effect resulted in the largest upregulation in hESC-macrophages during their tissue instruction (Fig. 6B; e.g. *MERTK, AXL, GAS6, FCGR3A*). To test this functionally, we

focused on phosphatidylserine, a cell membrane component that is exposed on the surface of stressed or apoptotic cells and is recognized by macrophages to trigger efferocytosis[57,58]. hESC-macrophages reduced apoptotic cardiomyocytes (Phosphatidylserine^{+} DAPI^{-}), with a smaller effect on fibroblasts (Fig. 6C). To assess whether hESC-macrophages sample cardiomyocytes or fibroblasts, we pre-labeled cardiomyocytes or fibroblasts with CFSE prior to seeding microtissues and found cardiomyocyte or fibroblast-derived material was detected within hESC-macrophages (Fig. 6D, gating strategy Supplementary Fig. S2), with a preferential uptake of cardiomyocytes. In accordance, hESC-macrophages also strongly upregulated key metabolism genes (*ABCA1*, *ABCG1*, *NR1H3* [LXR], *SLC2A1* [GLUT1], *ALOX12*) and proliferation genes (*MKI67, TOP2A*) in microtissues with cardiomyocytes, in line with reports highlighting activation of these pathways following efferocytosis[59] (Extended Data Fig. 10A, Supplementary Table 3).

hESC-macrophage efferocytosis reduces mitochondrial protein content

To determine whether hESC-macrophage efferocytosis was functionally relevant within tissues, we used Annexin V to block phosphatidylserine specifically on cardiomyocytes before seeding[60,61]. Microtissues with annexin-treated cardiomyocytes showed markedly reduced macrophage uptake of cardiomyocyte-derived material (Fig. 6E, gating strategy Supplementary Fig. S2), indicating a phosphatidylserine-specific uptake mechanism. Fibroblasts demonstrated some phosphatidylserine-specific sampling (~12% were sampling), however the majority of sampling was done by hESC-macrophages (~80%; Fig. 6E-F). Moreover, when ingestion occurred, macrophages contained greater (3-fold) cardiomyocyte cargo than did fibroblasts (Fig. 6G). Therefore, hESC-macrophages are the primary cell type undergoing efferocytosis of hESC-cardiomyocytes during early microtissue formation through recognition of phosphatidylserine.

Next, we explored the downstream consequences of disrupting macrophage-mediated efferocytosis of cardiomyocytes. We performed unbiased proteomics using LC-MS of total individual microtissues (day 14) with or without hESC-macrophages, with cardiomyocytes that were pre-treated with either Annexin V or PBS. In cardiac microtissues with hESC-macrophages, a total of 102 proteins were significantly upregulated in annexin-treated groups, and 92 proteins were significantly upregulated in PBS-treated groups (adjusted p-value<0.05, Fig. 6H, Supplementary Table 7). As we demonstrated earlier, mitochondrial proteins (membrane, ribosomal, Krebs cycle, ATP synthases, etc.) and mitochondrial containing debris were markedly reduced by hESC-macrophages within microtissues (Fig. 4). Here we show that this reduction was almost completely dependent on efferocytosis (Fig. 6I, Extended Data Fig. 10C, Supplementary Table 7). For example, the mitochondrial isoforms of Krebs cycle proteins were reduced by hESC-macrophages, however this reduction was inhibited with annexin (Fig. 6J). The cytosolic isoforms of the Krebs cycle (MDH1, ACO1, IDH1) were upregulated by hESC-macrophages, and annexin had no effect, indicating efferocytosis had a compartment specific effect, even within the same pathway.

Lastly, we examined macrophage-specific proteins (i.e. those detected only in microtissues with hESC-macrophages) to determine if inhibiting efferocytosis altered macrophage protein signatures. While blocking efferocytosis had no effect on canonical core macrophage

proteins (CD163, C1QB, C1QC) or changes in the number of hESC-macrophages or cardiomyocytes (Extended Data Fig. 10B), pathways related to lysosome and vesicle trafficking were downregulated in annexin-treated microtissues with hESC-macrophages, as well as other macrophage proteins (F13A1, NRP1, STAB1; Extended Data Fig. 10C, Supplementary Table 7) we had shown were induced in hESC-macrophages as they engrafted microtissues (Fig. 1). There was also an ~50% reduction of detected efferocytosis and lineage proteins (ITGAX, MARCO, STAB1, DOCK2; Fig. 6K). These data suggest hESC-macrophage differentiation/education is blunted when efferocytosis is inhibited.

hESC-macrophage efferocytosis upregulates cardiomyocyte contractile machinery

As observed earlier, hESC-macrophages markedly increased contractile proteins in cardiac microtissues, and this effect was blunted in annexin-treated microtissues with hESC-macrophages (Fig. 7A-B). Cardiomyocyte maturation, as measured by the ratio of adult to fetal isoforms MYH7:MYH6, was also reduced when efferocytosis was blocked (Fig. 7C), indicating that uptake of dying cardiomyocytes/cargo within the microtissue was important for maturation of contractile machinery. Furthermore, proteins comprising intercalated discs (e.g. CDH2, DSG2) were reduced in annexin-treated microtissues with hESC-macrophages (Fig. 7D), suggesting reduced structural integrity and/or mechanical transduction.

Not all upregulated sarcomeric proteins were inhibited by annexin treatment. For example, 7 out of 11 sarcomeric proteins induced by hESC-macrophages were inhibited by annexin, and the average inhibition was ~20%, suggesting either residual (non-phosphatidylserine mediated) efferocytosis or non-efferocytic pathways were present. Indeed, we found marked modulation of the secretome by hESC-macrophages, with an average of 22–31 cytokines at each timepoint differentially secreted (out of 85; Extended Data Fig. 10D, Supplementary Table 8). These included upregulation of the immunoregulatory, anti-apoptotic cytokine IL-10, and suppression of cytokines known to cause cardiomyocyte injury *in vivo* (IL-17A)[62–64]. We also observed blunted secretion of the damage associated molecular pattern IL-33, which is released from stressed cells, suggesting soluble factors may be involved (Extended Data Fig. 10E). Lastly, we assessed whether the ECM composition is altered when efferocytosis is blocked (Fig. 7E). hESC-macrophage inclusion resulted in increased non-fibrillar collagens (COL6A1, COL6A2, COL4A1, COL4A2), which were reduced in annexin-treated microtissues with hESC-macrophages (Fig. 7F). Furthermore, ECM glycoproteins LAMA4 and BGN, and proteoglycan PRELP were also reduced (Fig. 7F), indicating that in addition to the secretome, the ECM (and by extension fibroblast function), were altered by hESC-macrophage-mediated efferocytosis.

hESC-macrophage efferocytosis improves cardiac microtissue function

To determine whether macrophage efferocytosis was responsible for improved cardiac microtissue performance, we assessed microtissues both early (cytotoxicity) and late (cardiac function and cytotoxicity). Blocking efferocytosis led to increased cytotoxicity (day 3 & 14; Fig. 7G). The ability of hESC-macrophages to induce tissue compaction was not inhibited by blocking efferocytosis. In fact, compaction was further induced, suggesting altered fibroblast activation (Fig. 7H). Functionally, reduced efferocytosis by hESC-macrophages led to a substantial loss (~50%) of the beneficial effect of hESC-

macrophages in the microtissue, with reduced contractile force, reduced contraction slope (speed of contraction) and reduced relaxation slope (diastolic function; Fig. 7I-J, Extended Data Fig. 10F). Spearman's correlation analysis revealed that the top proteins associated with enhanced active force were a combination of contractile (e.g. MYL3, TNNT2, MYH7), ECM (e.g. LAMA4), and macrophage proteins (e.g. GPNMB [Supplementary Table 7]).

Taken together, these data show that efferocytosis of stressed or dying cardiomyocytes by hESC-macrophages via phosphatidylserine recognition results in reduced cardiomyocyte apoptosis, stress and cell death during early microtissue development. Ultimately, these processes lead to enhanced production and maturation of contractile machinery proteins and improved electromechanical function (Fig. 8 – schematic).

Discussion

In this study, we successfully integrated hESC-derived macrophages into human cardiac microtissues, focusing on two key goals. The first defines the beneficial role macrophages play in the earliest stages of heart maturation and function, while the second explores how the tissue triggers primitive macrophage specification, revealing complex reciprocal interactions that are nearly impossible to dissect *in vivo* in humans. Our study provides a critical advancement to understanding what aspects of cardiac tissue maturation are enhanced by human macrophages in a system that brings us closer to the cellular composition present during fetal development.

Murine fate mapping studies reveal the developing myocardium is first seeded by primitive (yolk sac-derived) macrophages as early as E10.5[3]. As time passes and macrophages proliferate in tissue, we see the environment instruct and maintain macrophage transcriptional identity, and when separated from their environment, macrophages lose these signatures[65–67]. hESC-macrophages we used can be considered general uneducated "*in vitro*" primitive macrophages, yet when they integrate within complex cardiac microtissues, they are rapidly instructed to more closely resemble both human yolk sac and fetal heart macrophages. In this way, we show specification towards both an "*in vivo*" and cardiac specific transcriptional identity. Signals that drive specification are numerous, involving general survival signals, such as those delivered through fibroblast derived MCSF[68], and more specific imprinting via processes[69]. It is important to appreciate that fibroblasts create a 3D ECM network in which the hESC-macrophages reside, which can trigger a variety of integrin mediated signals that differ from plastic or hydrogel alone[70,71]. Similarly, cardiomyocytes trigger rhythmical contraction that activate mechanosensor gated ion channels, inducing macrophage proliferation and cytokine secretion[17]. Intriguingly, fibroblasts and cardiomyocytes induced both unique and overlapping education patterns in hESC-macrophages, however both were required for optimal induction of key macrophage lineage genes (*LYVE1, FOLR2, CD163, CD14*), transcription factors driving fate (*SPI1, ZEB2, MAFB, MAF*)[65,72–76] and imprinting of key functions, such as efferocytosis. Our cardiac microtissue platform provides an ideal system to investigate combinatorial assessments of these and other cell types (i.e., endothelial cells, pericytes, monocyte-derived macrophages), as we reconstruct more complex tissues and better model maturation pathways.

Macrophages are professional efferocytic cells, and our data point to efferocytosis as a program both induced within tissue, but also required to improve systolic and diastolic function. Embryonic macrophages within the brain (microglia) govern neuronal patterning by regulating both survival of cortical neurons[77], as well as the developmental induction of cell death of neurons that is accompanied by ingestion of apoptotic cells, suggesting these functions may be conserved[78,79]. This also occurs following myocardial infarction where efferocytosis of apoptotic cardiomyocytes is required to prevent downstream arrythmias[80], or for proper calcium mobilization in adult mice[81]. Without macrophages ingesting cells in the earliest phases of cell death, those apoptotic cells die via necroptotic pathways, liberating toxic stimuli, increasing oxidative stress and potentially amplifying injury. In our studies, increased oxidative stress and cytotoxicity in the absence of macrophages was likely related to, at least in part, release of inflammatory molecules secondary to cell death within developing cardiac microtissues. This is expected as we try to recreate the earliest stage of development in an *in vitro* environment.

Cardiac microtissues or organoids are typically seeded with immature cardiomyocytes (iPSC- or hESC-derived), which resemble an early fetal rather than post-natal state[82–84]. Rather than focus on mature microtissues (i.e., paced for 6 weeks[46]), we focused on the first 2 weeks of tissue formation, a time where spontaneous contraction begins as the tissue is still organizing itself in the setting of cell stress. Addition of hESC-macrophages led to increased cardiomyocyte size, marked upregulation of numerous cardiomyocyte sarcomeric and desmosomal proteins, maturation of myosin isoforms, and greater elongation of cardiomyocytes, without a change in overall numbers and stoichiometry of hESC-cardiomyocytes and fibroblasts. We demonstrate here that whereas inclusion of hESC-macrophages stops short of inducing an advanced maturation phenotype that biophysical approaches can induce (e.g. electrical or mechanical stimulation)[46,85,86], an important developmental-stage specific impact on metabolism and contractile maturation is seen. In previous studies, chronic electrical stimulation was effective in maturing ion channel machinery and electrophysiological parameters in cardiac microtissues[46], opening the possibility for unified systems (electrical stimulation + hESC-macrophages).

Along those lines, we also observed changes in ECM composition, which is a factor that can mature cardiomyocytes. For example, cardiomyocytes contract against ECM components, which modulates sarcomere organization[87]. We observed hESC-macrophages rapidly reduced the width of cardiac microtissues (termed compaction), which is similar to the ability of iPSC-derived macrophages to reduce the size of brain organoids[88], suggesting macrophages may restrain excessive growth or expansion of developing tissues. Our work identified that a key role of hESC-macrophages is during the tissue formation phase, and it is plausible their role during early microtissue development subsequently results in a better functioning tissue at later times due to a better microenvironment. Selective macrophage deletion from mature microtissues would define how they contribute to later stages. These systems represent a complex environment generated with dissociated cells that are combined to form a tissue, which differs from an entirely homeostatic condition. Therefore, our findings are specific to how hESC-macrophages behave in the context of stressed cells integrating into a dynamic developmental formation process.

We observed that in the setting of increased ATP stores and improved microtissue function, hESC-macrophages also induced a marked, and efferocytosis dependent reduction of mitochondrial protein containing debris at the single cell level using CyTOF and at the total microtissue level using LC-MS. We also observed a reduction in mitochondrial proteins and mitochondria within individual cardiomyocytes, reminiscent of murine studies that demonstrated macrophages facilitate ongoing ejection of dysfunctional mitochondria and subsequently ingest them[42]. In the absence of macrophages, toxic mitochondrial constituents can accumulate extracellularly, reducing ATP production and cardiac function[42]. Similarly, murine macrophages cleared cardiomyocyte-derived mitochondria following ischemic injury, reducing cardiomyocyte death[80]. How hESC-macrophages drive metabolic changes within individual cells requires additional studies, however our CyTOF data point to reduced oxygen metabolism in these early stages, which in fact mirrors what is observed in very early human ventricular cardiomyocytes *in vivo*[41]and is consistent with the hypoxic environment of the developing embryo that triggers heart development[89]. Our data also suggest some glycolysis pathways may be increased (GLUT1, MCT1), but we suspect this is a very dynamic process that changes as very immature cardiomyocytes gradually mature over time, in particular, after birth. Of note, metabolism within 3D contractile microtissues is complex as the density of the tissue may drive a shift towards reduced reliance on oxidative phosphorylation due to reduced oxygen availability at the core.

In conclusion, we provide the first functional and mechanistic evidence that hESC-macrophages rapidly detoxify the developing cardiac microtissue microenvironment through efferocytotic uptake of toxic cargo, that leads to improved cardiomyocyte sarcomeric maturation and function, and reciprocal macrophage education. In the field of tissue engineering and cell therapy, organoids and transferred cells are not developing in a nurturing, hospitable and evolutionary optimized *in utero* environment. Rather, the earliest, and potentially most difficult steps of tissue assembly, cellular growth, organization and maturation are occurring either *ex vivo* or in a hostile *in vivo* environment following transplant (i.e., into a scar tissue). Addition of primitive hESC-macrophages provides an important opportunity towards developing multicellular organoids in a manner that more closely replicates the physiological and cellular properties of native human tissues, and for detailed mechanistic studies using human microtissues.

Methods

Cell lines

Human pluripotent stem cell derived macrophages—Differentiation of the td-RFP variant of HES-2 hESCs (ES Cell International; karyotype 46XX)[90,91], or H1 hESCs (WiCell Research Institute Inc.; karyotype 46XY)[92] to the primitive hematopoietic fate was performed as previously described[43]. On day 9 of differentiation, $CD43^+$ primitive hematopoietic progenitors were isolated by magnetic-activated cell sorting (MACS) and grown in suspension cultures in base media consisting of 25% v/v StemPro-34 (Gibco) in IMDM (Gibco) supplemented with M-CSF (30ng/mL, R&D), IL-3 (50ng/mL, R&D) and SCF (100ng/mL, R&D) for 3 days followed by M-CSF (30ng/mL) alone for another 12 days. Macrophage cultures were maintained in a normoxic incubator (5% CO_2, 20% O_2).

Human pluripotent stem cell derived cardiomyocytes

ESI-17 hESC-cardiomyocytes: We used a modified version of previously reported growth factor-based cardiac differentiation protocol[49,50]. Briefly, undifferentiated ESI-17 hESCs (BioTime) were dissociated using TrypLE (Gibco) and re-aggregated on an orbital shaker to form embryoid bodies (EBs) in StemPro-34 media (Gibco) supplemented with bone morphogenetic protein-4 (BMP4, 1 ng/mL, R&D), L-glutamine (2mM, Gibco), transferrin (150μg/mL, Roche), ascorbic acid (50μg/mL, Sigma), monothioglycerol (50μg/mL, Sigma), and ROCK inhibitor Y-27632 (10μM, StemCell Technologies) in a low oxygen environment (5% CO_2, 5% O_2, 90% N_2). After 20 hours, the EBs were transferred to mesoderm induction media consisting of base StemPro-34 media supplemented with BMP4 (10ng/mL, R&D), activin A (6ng/mL, R&D), and fibroblast growth factor (5ng/mL, R&D) in static condition. Two days later, the aggregates were washed with Iscove's Modified Dulbecco's medium (Gibco) and suspended in StemPro-34 media supplemented with Wnt inhibitor IWP2 (2μM, Tocris) and vascular endothelial growth factor (VEGF, 10ng/mL, R&D). Three days later, the EBs were dissociated into single cells using TrypLe and plated onto growth factor-reduced Matrigel (Corning) coated plates at a density of 120,000 cells per cm^2 in StemPro-34 with VEGF (5ng/mL) and Y-27632 (10μM). Media was changed the next day to remove Y-27632 and every other day thereafter. From days 12 to 20 of differentiation, the cultures were transferred to a normoxic incubator (5% CO_2, 20% O_2) and fed with RPMI 1640 medium with insulin-containing B27 supplement (Gibco). On day 20, cultures were dissociated to single cells using trypsin (0.125% solution, Corning), neutralized with defined trypsin inhibitor (Gibco), and cryopreserved at 10 million cells/mL in CryoStor (StemCell Technologies).

HES-2 GFP hESC-cardiomyocytes: For ventricular differentiation, we used a modified version of our embryoid body (EB)-based protocol[50,93,94]. hESC populations (HES-2 GFP; ES Cell International) were dissociated into single cells (TrypLE, ThermoFisher) and re-aggregated to form EBs in StemPro-34 media (ThermoFisher) containing penicillin/streptomycin (1%, ThermoFisher), L-glutamine (2mM, ThermoFisher), transferrin (150mg/mL, ROCHE), ascorbic acid (50 mg/mL, Sigma), and monothioglycerol (50mg/mL, Sigma), ROCK inhibitor Y-27632 (5μM, TOCRIS) and rhBMP4 (1ng/mL, R&D) for 16 h on an orbital shaker (70 rpm). On day 1, the EBs were transferred to mesoderm induction media consisting of StemPro-34 with the above supplements (-ROCK inhibitor Y-27632) and rhBMP4 (12ng/mL), rhActivinA (8ng/ml, R&D) and rhbFGF (5ng/mL, R&D). At day 3, the EBs were harvested, dissociated into two to three cell clusters (TrypLE), and re-aggregated in cardiac mesoderm specification media consisting of StemPro-34, the Wnt inhibitor IWP2 (2μM, TOCRIS) and rhVEGF (10ng/mL, R&D). At day 5, the EBs were transferred to StemPro-34 containing basal supplements [(L-glutamine (2mM, ThermoFisher), transferrin (150mg/mL, ROCHE), ascorbic acid (50mg/mL, Sigma), and monothioglycerol (50 mg/ml, Sigma)] and with rhVEGF (5ng/mL) for another 5 days. From days 10 to 16, EBs were cultured in StemPro-34 containing basal supplements [(L-glutamine (2mM, ThermoFisher), transferrin (150mg/mL, ROCHE), ascorbic acid (50mg/mL, Sigma), and monothioglycerol (50mg/ml, Sigma)]. Cultures were incubated in a low oxygen environment (5% CO_2, 5% O_2, 90% N_2).

Human primary cardiac fibroblasts: Human primary cardiac fibroblasts (PromoCell Cat# C-12375) were cultured according the manufacturer's protocols. Fibroblasts were thawed and cultured in 75cm^2 flasks with Fibroblast Growth Medium 3 (PromoCell) and detached for passaging using 0.04%/0.03% Trypsin-EDTA for 5 minutes at room temperature. Passages 3–5 were used in our studies.

Biowire II platform

The Biowire II device used in experiments presented in Fig. 2 were fabricated and designed as we previously published[46].

Fabrication of 96-well or 24-well plate-based high-throughput Biowire device

The high-throughout Biowires (HT-Biowires) were fabricated as we previously published[47]. A polystyrene base plate was fabricated by a hot-embossing machine (EVG 520) at a temperature of 180°C and a pressing force of 3000 N, using a flat polystyrene sheet (0.032 inches thick, Jerry's Artarama) to be placed on a polydimethylsiloxane (PDMS) mold. The PDMS mold was produced by mixing a curing agent and silicone elastomer base at a ratio of 1:5 using Sylgard 184 silicone elastomer kit (Dow Corning). The negative PDMS mold was made from a SU-8 photoresist master mold fabricated by soft-lithography using a photomask. Patterns designed with AutoCAD was used to produce the photomask, with repeated rectangular microwells (5×1 mm^2, L×W) and groves (78×0.2 mm^3, L×W). The distances of adjacent microwells in the patterns were adjusted to be compatible with the 96-well plate dimension. The PDMS mold was fixed to a silicon wafer (University Wafers) using a plasma generator (model BD-20A, Electro-Technic Products). A thermoplastic elastomer-based nanocomposite ink was prepared by mixing core-shell CdSe/ZnS quantum dots and poly(styrene) (ethylene/butylene)–(styrene) co-polymers. The ink was directly deposited onto the polystyrene plate through temperature-controlled 3D printing (RegenHU Ltd., Switzerland). The polystyrene plate base with printed microwires was assembled onto a bottomless 96-well plate (Greiner-BioOne) using polyurethane glue (GS Polymers).

Generation of bioengineered cardiac microtissues

A collagen-Matrigel hydrogel (500μL volume) was prepared using rat tail collagen I (to a final concentration of 3mg/mL; Corning), Matrigel (15% v/v, 75μL; Corning), 1X Medium 199 (50μL; Sigma), 2.2mg/mL $NaHCO_3$ (50μL), 1M NaOH (4μL), and deionized sterile H_2O to a final volume of 500μL. Biowire polystyrene strips (8 microwells per strip) were seeded within a 10cm tissue culture dish. Biowire strips or wells within 24-well or 96-well Biowire plates were soaked in either media (strips) or PBS (plates) overnight. On the day of seeding, strips or plates were coated with 5% (w/v) Pluronic acid (Sigma) for 5 minutes, and then aspirated and dried in the biosafety cabinet for 2 hours. Cardiomyocytes (iPSC-cardiomyocytes FUJIFLIM, or in-house produced hESC-derived cardiomyocytes) were thawed for direct seeding into the Biowires. Fibroblasts were dissociated from culture flasks and macrophages were collected from culture wells. Cells were mixed to attain 100,000 iPSC- or hESC-cardiomyocytes and 15,000 human primary cardiac fibroblasts per microtissue, with an additional 10% (Biowire II platform, Fig. 2) or 20% (plate-based HT-Biowires, Fig. 1–7) of hESC-macrophages. Cell mixtures were pelleted at

300g for 5 minutes at 22°C, followed by an additional 3 minutes, and resuspended in a volume of 2.5μL of hydrogel per microtissue. This results in 100,000 cardiomyocytes per microtissue, and a final cell concentration of 4.6×10^7 cells/mL (control), 5×10^7 cells/mL (10% macrophages) or 5.5×10^7 cells/mL (20% macrophages) in hydrogel. Following seeding, Biowires were baked at 37°C (5% CO_2) for 10 minutes, after which media was immediately added to the dish or to each well. Biowires were cultured in StemPro-34 SFM (1X) medium (ThermoFisher) containing 2-phospho-L-ascorbic acid (64mg/mL; Sigma), 2% v/v HEPES (1M; ThermoFisher), 1% v/v GlutaMax (100X; ThermoFisher), 1% v/v Penicillin-Streptomycin (10,000U/mL; ThermoFisher), Transferrin (30mg/mL; ROCHE). Media was sterile filtered. The pH of the culture media was ~7.4 upon incubation at 37°C (5% CO_2). Biowires were cultured at 37°C (5% CO_2) and imaged daily for the first seven days to assess tissue compaction and formation (Zeiss AxioObserver Widefield). Biowires formed 3D contractile tissues by day 7 of culture, and culture media was changed every week (strips) or every 3 days (plates). Videos focused on the fluorescent wire were acquired on day 11 or day 14 (Zeiss AxioObserver Widefield) to track wire movement during each contraction (10X objective, 100 frames/second, 10ms exposure time). 5X brightfield images of each tissue were also acquired. The width of each tissue as well as the length of the tissue attached to the wire were measured using ImageJ. Finally, functional measurements (passive force, active force, contraction and relaxation slopes, beating kinetics) were measured using a custom MATLAB code as previously described in detail[46].

Immunofluorescence and confocal microscopy

HT-Biowires (day 14 post-seeding) were fixed with 4% paraformaldehyde for 24 hours, then permeabilized and blocked using 0.1% Triton X-100 in 5% FBS in PBS for 2 hours at room temperature. Immunostaining was performed overnight at 4°C with the following primary antibodies: mouse anti-cardiac troponin T (Clone 13–11; ThermoFisher Cat#: MA5–12960; 1:100), rabbit anti-CD68 (ThermoFisher Cat#: PA5–109344; 1:50), rabbit anti-vimentin (abcam ab92547; 1:100). For alignment and eccentricity measurements, HT-Biowires were stained with mouse anti-α-actinin (abcam ab9465; 1:200) and rabbit-anti-MLC2v (abcam 79935; 1:200) primary antibodies. Microtissues were washed six times for 15 minutes each in PBS then stained for 2 hours at room temperature with secondary antibodies: goat anti-rabbit IgG secondary antibody Alexa Fluor™ Plus 647 (ThermoFisher A32733; 1:500) and goat anti-mouse IgG Alexa Fluor™ Plus 488 (ThermoFisher A32723; 1:500). Tissues were washed six times for 15 minutes each in PBS, then mounted using SlowFade™ Diamond Antifade Mountant with DAPI (ThermoFisher). Confocal microscopy was used to acquire images using the Nikon A1R confocal microscope with resonant scanner. For images in Extended Data Fig. 1, surface versus deep were defined based on the relative plane of visualization.

Myofibril alignment and eccentricity analysis

To quantify cardiac tissue development, we assessed cardiac tissue elongation using a custom-made MATLAB code (link to code available at: https://www.epelmanlab.com/resources). Eccentricity was employed as a metric to quantify the degree of ellipticity of cardiomyocytes, with perfectly circular cells assigned a score of 0. As cardiomyocytes became more elongated or compressed, their scores progressively approached 1. To achieve

this, we first converted the images into binary format and then employed the imageprops function to quantify eccentricity. For cell alignment, the angle of each element was measured using the imageprops function, after which the variance in orientation was calculated

Cell surface staining, intracellular staining and flow cytometry

To assess cell surface markers on hESC-macrophages over the course of differentiation, cells were stained for 20 minutes at 4°C with the following antibodies: mouse anti-human CD45 (clone 2D1; BioLegend Cat# 368503; 1:100), mouse anti-human CD14 (M5E2; BioLegend Cat# 301814; 1:100), mouse anti-human LYVE1 (clone FAB20892G; R&D Cat# 537028; 1:100), mouse anti-human CCR2 (clone K036C2; BioLegend Cat# 357207; 1:100). Cells were washed once in FACS buffer (2% heat-inactivated bovine serum in PBS containing 1mM EDTA) and spun down 300xg for 5 minutes at 4°C. Cells were resuspended FACS buffer, filtered through a 40um filter and acquired on the cytometer (BD LSRFortessa™). To perform intracellular staining of hESC-cardiomyocytes to validate purity, cells were fixed in 4% (w/v) paraformaldehyde for 10 minutes at 4°C. Fixed cells were washed twice in PBS with 5% fetal bovine serum for 5 minutes each. Cells were then permeabilized with methanol (90% v/v in PBS) for 20 minutes on ice, followed by staining with APC-conjugated anti-cardiac troponin T (clone REA400; Miltenyi Biotec; 1:100) and a PE-conjugated anti-MLC2v (clone REA401; Miltenyi Biotec; 1:100) antibodies in PBS with 5% fetal bovine serum for 1 hour at 4°C. Stained cells were washed twice, resuspended in FACS buffer and filtered through a 40um filter prior to acquiring on the cytometer (BD LSRFortessa™) using the BD FACSDiva software (v8.0.1). Data was analyzed using the FlowJo software (v10.10).

MitoTracker, ApoTracker and CFSE labeling

MitoTracker: On day 3 post-seeding, HT-Biowires were first digested (as detailed in ‘Biowire digestion’ section), then the cell pellet was stained in 200nM of MitoTracker Green (Invitrogen Catalog # M7514) for 30 minutes at 37°C. Cells were washed in 1mL of DMEM and pelleted (300g for 5 minutes at 4°C) prior to cell surface staining.

ApoTracker: On day 3 post-seeding, HT-Biowires were first digested (as detailed in ‘Biowire digestion’ section), then the cell pellet was stained in 100μL of 500nM of ApoTracker Green (BioLegend Cat# 427402) with 1:100 of anti-human CD14 (clone M5E2; BioLegend Cat# 301814) for 30 minutes at 4°C. Cells were washed twice in FACS buffer (2% heat-inactivated bovine serum in PBS containing 1mM EDTA) and pelleted (300g for 5 minutes at 4°C). Cells were resuspended in FACS buffer with 1:100 DAPI, filtered through a 40μm filter and acquired on the cytometer (BD LSRFortessa™). Data was analyzed using the FlowJo software.

CFSE: hESC-cardiomyocytes or fibroblasts were pre-labeled with CFSE (BioLegend Catalog # 423801) prior to seeding HT-Biowires. The stock was reconstituted to 5mM in DMSO. A 5uM working solution was made in PBS. Cells were stained in 200μL of the 5μM working solution for 30 minutes at 37°C. After 30 mins, the staining was quenched using 1mL of complete DMEM (containing 10% FBS). Cells were pelleted (300g for 5

minutes at 4°C), and re-suspended in warm complete DMEM for 10 minutes. Cells were then ready to be combined into appropriate groups in hydrogel suspension and to be seeded into HT-Biowires.

Biowire digestion and cell surface staining

HT-Biowires were digested in collagenase type I (1370U/mL; Sigma D4513), hyaluronidase (122U/mL; Sigma H3506), DNase I (146U/mL; Sigma D4513), Dispase (1U/mL) and ROCK inhibitor (1μM) for 40 minutes at 37°C with gentle shaking. For bulk RNA sequencing experiments, the transcription inhibitor Flavopiridol was included during digestion (10μM). After 40 minutes, the digestion mix was pipetted 10 times to physically dissociate cells and was washed in 1mL media. Cells were pelleted (300g for 5 minutes at 4°C) and stained with cell surface antibodies, depending on the experiment.

MitoTracker, ApoTracker and CFSE experiments: Cells were stained in FACS buffer with mouse anti-human CD14 (clone M5E2; BioLegend Cat# 301814; 1:100) for 20 minutes at 4°C.

hESC-macrophage sort for bulk RNA sequencing: In this experiment, Biowires were digested in groups of 5 and then subsequently pooled into 15 microtissues per replicate. Cells were stained in FACS buffer with mouse anti-human CD14 (clone M5E2; BioLegend Cat# 301814; 1:100) and mouse anti-human CD45 (clone 2D1; BioLegend Cat# 368503; 1:100) for 20 minutes at 4°C.

hESC-cardiomyocyte sort for bulk RNA sequencing: In this experiment, two Biowires were pooled for each replicate prior to digestion. Cells were stained in FACS buffer with mouse anti-human CD14 (clone M5E2; BioLegend Cat# 301814; 1:100), mouse anti-human CD90 (clone 5E10; BioLegend Cat#328120; 1:100) and mouse anti-human CD45 (clone 2D1; BioLegend Cat# 368503; 1:100) for 20 minutes at 4°C.

Cells were washed once in FACS buffer (2% heat-inactivated bovine serum in PBS containing 1mM EDTA) and spun down 300xg for 5 minutes at 4°C. Finally, cells were resuspended FACS buffer with 1:100 DAPI, filtered through a 40um filter and acquired on the cytometer (BD LSRFortessa™). For bulk RNA sequencing experiments, samples were resuspended in BD FACS™ Pre-Sort Buffer with 1:100 DAPI and sorted on the Aria Fusion (BD Biosciences) under low pressure (100μm nozzle) directly into 350μL of RLT lysis buffer in DNA lobind tubes.

Gating strategy for bulk RNA sequencing sort experiments: hESC-macrophage sort: DAPI-CD45+CD14+RFP+ live single cells were sorted

hESC-cardiomyocyte sort: DAPI-CD45-CD14-RFP-CD90- live single cells were sorted

LPS stimulation and transcription inhibitor

We aimed to validate the efficacy of the transcription inhibitor Flavopiridol. hESC-macrophages were stimulated with 100ng/mL of LPS for 3 hours at 37°C, with or without 10uM of Flavopiridol. After 3 hours, cells were pelleted (300xg for 5 minutes at 4°C)

and digested with or without Flavopiridol, as described in the 'Biowire digestion' section. Finally, RNA was isolated for qPCR of IL6 and TNF.

Contamination controls for hESC-macrophage bulk RNA sequencing

Three groups were used (1) hESC-macrophages alone, (2) fibroblasts and hESC-macrophages fibroblasts, (3) hESC-cardiomyocytes, fibroblasts and hESC-cardiomyocytes. Cells from each group were digested in collagenase type I (1370U/mL; Sigma D4513), hyaluronidase (122U/mL; Sigma H3506), DNase I (146U/mL; Sigma D4513), Dispase (1U/mL), ROCK inhibitor (1uM) and 10um Flavopiridol for 40 minutes at 37°C with gentle shaking. Cells were pelleted (300g for 5 minutes at 4°C) and stained with with mouse anti-human CD14 (M5E2; BioLegend Cat# 301814; 1:100) and mouse anti-human CD45 (2D1; BioLegend Cat# 368503; 1:100) in FACS buffer for 20 minutes at 4°C. Cells were washed once in FACS buffer (2% heat-inactivated bovine serum in PBS containing 1mM EDTA) and spun down 300xg for 5 minutes at 4°C. Finally, cells were resuspended BD FACS™ Pre-Sort Buffer with 1:100 DAPI, filtered through a 40μm filter and sorted on Aria Fusion (BD Biosciences) under low pressure (100um nozzle) directly into 350μL of RLT lysis buffer in DNA lobind tubes.

RNA isolation and RT-qPCR

Total RNA from hESC-macrophages, hESC-cardiomyocytes, human primary cardiac and dermal fibroblasts (for RT-qPCR) was prepared using the Qiagen RNeasy Micro kit with on-column treatment with RNAase-free DNAase. Reverse transcription to synthesize cDNA was performed using the iScript Reverse Transcription Supermix (Bio-Rad Laboratories). RT-qPCR was performed with 5ng (for fibroblast data in Extended Data Fig. 1) or 20ng (for hESC-macrophage data in Extended Data Fig. 2) of input cDNA using the LightCycler 480 SYBR Green I Master kit, on a Bio-Rad CFX384 Touch Real-Time PCR Detection System. Gene expression in each sample was reported relative (ΔCt) to the housekeeping gene *TBP* (for fibroblast data in Extended Data Fig. 1) or B*2M* (for hESC-macrophage data in Extended Data Fig. 2).

Primer sequences:

Human *TBP*: Forward: TGAGTTGCTCATACCGTGCTGCTA

Reverse: CCCTCAAACCAACTTGTCAACAGC

Human *GATA4*: Forward: CGAATGACGGCATCTGTTTGCCAT

Reverse: ATTTGGTATTAGGGATGCAGGGCG

Human *WT1*: Forward: ATAGGCCAGGGCATGTGTATGTGT

Reverse: AGTTGCCTGGCAGAACTACATCCT

Human *TCF21*: Forward: AGGCAGATCCTGGCTAACGACAAA

Reverse: TCCAGGTACCAAACTCCAAGG TCA

Human β2M: Forward TGCTGTCTCCATGTTTGATGTATCT

Reverse TCTCTGCTCCCCACCTCTAAG

Human TNF: forward ACTTTGGAGTGATCGGCC

reverse GCTTGAGGGTTTGCTACAAC

Human *IL-6*: Forward AGACAGCCACTCACCTCTTCAG

Reverse TTCTGCCAGTGCCTCTTTGCTG

Bulk RNA sequencing and analysis

RNA was isolated as in the 'RNA isolation' section. Library preparation and RNA sequencing was performed at the Princess Margaret Genomic Centre at the University Health Network (Toronto, ON, Canada). Library preparation was performed using Takara SMARTer Stranded Total RNA-seq Kit v3. RNA sequencing was executed on a NovaSeq 6000 (Illumina) using a paired-end 2×100bp protocol and multiplexing to obtain a sequencing depth of 30–35 million paired-end reads per sample. Reads were filtered for quality control and mapped to the human genome (hg19) using STAR aligner (v2.7.9a). Count files containing uniquely mapped reads were generated using htseq-count (v0.11.0), retaining protein-coding genes with non-zero counts. Data were pre-filtered to include only genes expressed by at least one sample. The DESeq2[95] package (v1.42) was used in R Studio (R v4.3.2) to normalize counts and compute differentially expressed genes (DEGs; $\log_2$FoldChange >0.3 and adjusted P value <0.05). Pathway enrichment analysis was performed using gProfiler (GO Biological Processes, GO Cell Component, GO Molecular Processes, KEGG, and Reactome databases) on the set of upregulated or downregulated genes in each comparison. For RNA-seq analyses in Fig. 1 and Extended Data Fig. 2, upregulated DEGs in each comparison noted were first found in contamination controls (Extended Data Fig. 2), and these genes were subsequently removed from comparisons in Biowire groups (Fig. 1). This condensed list of DEGs was then filtered to remove genes with a basemean < 100 to exclude low expressors. This list was used for pathway enrichment analyses.

Single-cell RNA sequencing analysis

We downloaded publicly available single-cell RNA sequencing data of human fetal cardiac tissue[41,48], and human yolk sac data[9]. The Seurat package (v5.0.1)[96–98] was used for all analyses using R 4.3.2, as we have previously done[1,2]. Genes that were not detected in at least three cells, or cells that expressed fewer than 200 genes (low-quality cells) or a high number of genes (putative doublets/multiplets) were removed. Stressed or dying cells with greater than 10 percent (yolk sac and fetal heart in Fig. 4) or 25 percent (fetal heart in Fig. 1) of genes mapping to mitochondrial transcripts were removed. Precise cutoffs were determined for each dataset separately based on the dataset distribution and the presence of outlier cells. In each dataset, different donors were pooled for subsequent combined analysis. Next, we implemented SCTransform to remove technical variation while preserving biological variation. SCTransform normalizes data (negative binomial

regression), finds variable features (variance-stabilizing transformation; top 3000), and scales the data. The number of counts (nCount_RNA) and percentage mitochondrial genes were regressed. Linear dimensionality reduction was performed using principal component analysis. To remove batch effects present across different donors (Fig. 1; Suryawanshi *et al.*), we implemented Harmony (v1.2)[99]. All downstream analyses were performed using Seurat-based clustering ('FindNeighbors' and 'FindClusters' functions). Non-linear dimensionality reduction and visualization was implemented using Uniform Manifold Approximation and Projection (UMAP). Clusters were annotated according to canonical cell type specific genes and based on differentially expressed genes (FindAllMarkers or FindMarkers function; min.pct = 0.25; avg_log_2FC = 0.25, adjusted P value < 0.05).

In vivo gene signature scoring

Human yolk sac signature (Fig. 1): The human yolk sac scRNA-seq dataset was used to generate a gene set signature for human yolk sac macrophages (Popescu *et al.*)[9]. Differentially expressed genes were computed in macrophages relative to the monocyte-macrophage group (min.pct = 0.25; avg_log_2FC = 0.25, adjusted p-value < 0.05). The top 100 genes were used as the yolk sac macrophage signature (ordered by avg_log_2FC).

Human fetal cardiac macrophage signature (Fig. 1): scRNA-seq of human fetal heart was used to generate a gene set signature was generated for human fetal cardiac macrophages (Suryawanshi *et al.*)[48]. Differentially expressed genes were computed in macrophages relative to monocytes (min.pct = 0.25; avg_log_2FC = 0.25, adjusted p-value < 0.05). The top 150 genes were used as the human fetal cardiac macrophage signature (ordered by avg_log_2FC).

Human fetal cardiomyocyte signature (Fig. 5): scRNA-seq of human fetal heart was used to generate a gene set signature for human fetal cardiomyocytes across development (Cui *et al.*)[48]. Differentially expressed genes were computed in ventricular cardiomyocytes relative to immune cells (min.pct = 0.3; avg_log_2FC = 0.3, adjusted p-value < 0.01). For early versus late signatures, comparisons were restricted to 5–9 PCW or 17–24 PCW.

Scoring: Gene set scoring in bulk RNA-seq datasets was performed using the R-based package singscore (v1.22.0)[100]. singscore utilizes rank-based statistics to score gene expression profiles in individual samples based on a provided signature.

Mass spectrometry

Tissue processing—Individual Biowires were washed thoroughly with PBS and frozen at −80°C. Biowires were suspended in 50μL of 8M urea and were homogenized with 10 freeze-thaw cycles in an ethanol / dry ice bath. Samples were reduced with DTT (final concentration 2.5mM in 50mM ammonium bicarbonate) for 1 hour at 37°C. Alkylation was performed with iodoacetamide (final concentration of 5mM in 50mM ammonium bicarbonate) for 30 minutes in the dark at room temperature. Samples were diluted 8-fold using 50mM ammonium bicarbonate. Trypsin/Lys-C mix (mass spectrometry grade; Promega) was added (0.5ug) and incubated overnight at 37°C. The following day, samples were acidified by addition of formic acid to 1% of total volume.

Chromatography and DIA Mass Spectrometry—We analyzed Biowire tryptic peptides by loading 20% of total protein extracted onto C18 tips (Evosep, EV-2001; according to manufacturer's protocols), which was subjected to in-line chromatography using the Evosep One (EV-1000) instrument 15SPD LC protocol. An 88-minute gradient via the Endurance 15cm analytical column (EV-1106) was used, including a stainless-steel emitter (EV-1086) and a spray voltage of 1.9kV. The Q exactive Plus instrument was used for DIA MS data acquisition. Each cycle comprised of one full MS scan (70,000 resolution) with a 30 MS/MS scan windows (17,500 resolution) covering a mass range of 400–951 m/z. We used an AGC target of 3e6 for full MS scans and 5e5 for MS/MS scans. The maximum injection time was set to 200ms for full MS scans, with a normalized collision energy set to 27 for MS/MS scans. Finally, isolation windows were 20 m/z including 1 m/z overlap between scan windows.

Search Parameters—We used the DIA-NN 1.81 software to search RAW files, specifically using an in silico spectral library with canonical and isoform protein sequence FASTA files from UNIPROT (UP000005640_9606, February 2021 release), permitting a maximum of one missed cleavage and one variable modification (methionine oxidation), where carbamidomethylation of cysteines was set as a fixed modification. Next, filtering was performed with a precursor FDR of 0.01, including the features 'match between runs (MBR)', 'unrelated runs' and 'use isotopologues'. 'Robust LC (high precision)' was set for quantification and 'RT & signal-dep' was set for cross-run normalization. Finally, mass accuracy and scan window were determined through built-in features in DIA-NN.

Data analysis—The Perseus software (v2.0.11)[101] was used for data exploration and principal component analysis. The pheatmap R package (v1.0.12) was used to generate heatmaps presented in figures. Differentially expressed proteins were computed by directly comparing groups of interest using an unpaired two-tailed Student's t-test, with P values adjusted for multiple comparisons using Bonferonni correction. Proteins with adjusted P values <0.05 were used for downstream pathway analyses (gProfiler). For the assessment of targeted pathways in Fig. 3, multiple unpaired t-tests was conducted with P values adjusted for multiple comparisons using the Holm-Šídák method. In proteomics analyses for annexin experiments (Fig. 6–7), HT-Biowires with or without hESC-macrophages were first compared directly using multiple unpaired t-tests with P values adjusted for multiple comparisons using the Holm-Šídák method. Then, we performed exploratory analyses to directly compare PBS versus annexin-treated groups in HT-Biowires with hESC-macrophages using multiple unpaired t-tests with P values adjusted for multiple comparisons the false discovery rate (FDR) approach (two-stage step-up, Benjamini, Krieger, and Yekutieli).

Calcium imaging and analysis

Biowires were loaded with 500μL of Fluo-4 NW calcium indicator (Invitrogen, 1X concentration per manufacturer's protocol) and incubated for 45 minutes at 37°C. The dye was removed and replaced with 300μL of Biowire culture media for mapping at 37°C. A complementary metal oxide semiconductor (CMOS) camera system (SciMedia, Ultima-L) was used to acquire data using the Brain Vision software (SciMedia). The camera was

installed on an Olympus MVX10 Microscope. The sensor size of the camera was 1cm and the resolution was 100×100 pixels with a frame rate of 500 images/s and an optical zoom set at 4X, resulting in a field of view of 2.5×2.5mm (25um resolution). The fluorescence was excited using a mercury arc source (X-Cite Exacte). Point stimulation was performed with a twisted pair of AWG#30 silver wires mounted on a micromanipulator and the source was a S88X Square Pulse Stimulator (Grass Technology) with an output of 3V and biphasic pulse width of 8ms. The wires were positioned at one end of the Biowire, allowing for a linear wave propagating towards the other end. The 24-well plate containing the Biowire was placed on a heated plate (MATS-U55S, Olympus) and temperature was regulated at 37°C. Calcium cycling parameters were measured from tissues paced from 2–5Hz. From an area on the optical mapping representing the Biowire, a site was selected for feature analysis (transient duration) of calcium signals using a custom-made MATLAB code. For calcium transient duration analysis, 0 to 50% of repolarization (CaTD50) and 0 to 80% of repolarization (CaTD80) were analyzed, as described previously[102,103].

Current measurements using whole-cell patch-clamp recordings of single cardiomyocytes

Coating, dissociation and plating: Cover slips were coated with 5% Matrigel in DMEM 5 minutes prior to starting tissue dissociation. HT-Biowires were gently dissociated on day 14 post-seeding using collagenase type I (1370U/mL; Sigma D4513), hyaluronidase (122U/mL; Sigma H3506), DNase I (146U/mL; Sigma D4513), Dispase (1U/mL) and ROCK inhibitor (1uM) for 20 minutes in a 37°C water bath. Three HT-Biwoires were pooled for each replicate. After 20 minutes, cells were pipetted 5 times. Cells were pelleted (300xg for 5 minutes at 4°C), resuspended in DMEM containing 10% FBS, and plated on cover slips in 35mm petri dishes. Cells were incubated at 37°C and topped up with Biowire culture media 6 hours later.

Patch-clamp recordings: Isolated hESC-cardiomyocytes were super-fused continuously in a perfusion chamber (placed on the Olympus IX51 microscope stage) with a Tyrode's solution (mM) containing: 140 NaCl, 4 KCl, 1 $MgCl_2$, 1.2 $CaCl_2$, 10 HEPES, 5 D-glucose, 10 $NaHCO_3$, pH = 7.35 adjusted by NaOH. Cardiomyocytes were visualized using a 40X UPlanApo objective (Olympus, Tokyo, Japan) thereby allowing giga seals to be formed between cell membranes and filamented borosilicate glass pipettes (1.5 mm OD, 1.12 mm ID, World Precision Instruments, FL, USA) of 3–6 MΩ resistance that were created with a pipette puller (p-97, Sutter Instrument Company) and polished (Micro Forge MF-90, Narishige Group, Japan). Following giga seal formation, cell membranes were ruptured to gain whole-cell access, and membrane currents were measured and recorded in either the voltage-clamp or current-clamp configurations (Axopatch 200B, Digidata 1440A and pClamp 10.7 Molecular Devices, CA., USA). The recordings were analyzed offline using Clampfit 11.2 (Molecular Devices, CA., USA). All measurements were performed at room temperature.

For voltage-gated Na^+ currents (I_{Na}), the pipette solution contained (mM): 125 K-aspartate, 10 Taurine, 5 NaCl, 20 KCl, 1 $MgCl_2$, 5 MgATP, 10 HEPES, 0.5 EGTA, pH=7.2 adjusted by KOH. The bath solution for local perfusion consisted of (mM): 140 N-methy-D-glucamine, 5 NaCl, 4 KCl, 1 $MgCl_2$, 5 $CaCl_2$, 10 HEPES, 10 D-glucose, 4 4-aminopyridine,

pH=7.35 adjusted by HCl. Before making voltage-clamp recordings, series resistance was compensated by 70–80%. I_{Na} was evoked by applying voltage steps (500 ms) between −70 mV and +50 mV in 5 mV increments from a holding voltage of −100 mV with 5 seconds between steps. Current-clamp measurements were acquired using identical solutions. Action potentials (APs) were recorded immediately following termination (i.e. with anode breaks) of hyperpolarizing current injection, which was used to ensure that resting membrane potentials were ~−85mV thereby ensuring Na^+ channels availability. Recordings were filtered at 2 kHz and sampled at 50 kHz.

For voltage-gated Ca^{2+} currents (I_{Ca}), the pipette solution contained (mM): 135 CsCl, 10 Taurine, 1 $MgCl_2$, 5 MgATP, 10 HEPES, 0.5 EGTA, pH=7.2 adjusted by CsOH. The corresponding bath solution for local perfusion consisted of (mM): 140 N-methy-D-glucamine, 1 $MgCl_2$, 5 $CaCl_2$, 10 HEPES, 10 D-glucose, 4 4-aminopyridine, pH=7.35 adjusted by HCl. Similar to I_{Na}, series resistance was compensated by 70–80%, and current recordings were filtered at 2 kHz while sampled at 50 kHz. The protocol for quantifying I_{Ca} consisted of 1 s voltage steps between −100 mV and +50 mV in 10 mV increments from a holding voltage of −100 mV with 5 seconds between steps.

Peak Na^+ and Ca^{2+} currents (I_{Na}^{peak} and I_{Ca}^{peak}) were estimated for each voltage-step and plotted against the step voltage. Na^+ currents typically peaked around −20 mV and Ca^{2+} currents at 0 mV. The conductance (G_X) was determined using the formula: $G_X = (I_X^{peak}/(V_m - E_{rev}))/G_{max}$, where "X" represents either Na^+ or Ca^{2+}, E_{rev} is the measured reversal potential for Na^+ or Ca^{2+} current and G_{max} is the maximum conductance measured. G_X was fit to the Boltzmann function (GraphPad Prism software, V8.4.3) to estimate $V_{1/2}$ (the voltage for 50% activation) and slope factor (i.e., an estimate of the gating charge).

Cytotoxicity assays

Biowires were seeded with and without hESC-macrophages and culture supernatants were collected on days 3 and 7.

dsDNA: PicoGreen—As a measure of dsDNA released into culture supernatants (day 7 post-seeding) during apoptosis, we used the Quant-iT PicoGreen™ dsDNA Reagent and Kit (Invitrogen). Samples were 5-fold diluted to a final volume of 100μL in TE buffer and mixed with 100μL of the working solution of Quant-iT PicoGreen™ dsDNA Reagent. A standard curve was generated using bacteriophage lambda DNA. Samples were incubated for 5 minutes at room temperature protected from light. Fluorescence of samples read on a PerkinElmer microplate reader using fluorescein wavelengths (excitation 480nm, emission 520nm). dsDNA concentration in each sample was calculated using the standard curve.

Lactate dehydrogenase (LDH)—LDH released from cells is an indicator of cellular toxicity and damage to the plasma membrane. LDH was measured on day 3 post-seeding using the CyQUANT™ LDH Cytotoxicity Assay Kit (Invitrogen). LDH catalyzes lactate to pyruvate conversion through NAD^+ to NADH reduction. Diaphorase then oxidizes NADH while concomitantly results in the reduction of tetrazolium salt to red formazan that is measured at 490nm. Here, samples were 1:2 diluted by mixing 50μL culture supernatant with 50μL substrate mixture and incubated for 30 minutes at room temperature protected

from light. The reaction was stopped using 50μL of stop solution and absorbance was measured at 490nm and 680nm (background signal) using a PerkinElmer microplate reader.

Glucose-6-phosphate dehydrogenase (G6PD) release assay—The CyQUANT™ Cytotoxicity Assay Kit (G6PD Release Assay; Invitrogen) was used to measure G6PD released from damaged or dying cells into culture supernatants day 3 post-seeding. G6PD is a cytosolic enzyme that can be quantified through a reaction that leads to the reduction of resazurin into red-fluorescent resorufin. Briefly, 50μL of culture supernatants was mixed with 50μL of Resazurin/Reaction mixture and incubated for 30 minutes at 37°C. Fluorescence was measured using a PerkinElmer microplate reader (excitation 530–560nm, emission 580–600nm).

Adenylate kinase—The ToxiLight™ bioassay kit (Lonza) was used to measure levels of adenylate kinase, an enzyme present in all cells that is released upon damage to the plasma membrane, indicating cytotoxicity or cytolysis. Here, adenylate kinase is measured via a bioluminescence reaction. First, a substrate of adenylate kinase, ADP, is added and converted to ATP. Second, the enzyme luciferase catalyzes the reaction wherein ATP and luciferin result in the formation of light, which can be measured using a luminometer and is related to the concentration of adenylate kinase present in the sample in a linear relationship. 50μL of culture supernatants from each sample were incubated with 100μL of adenylate kinase detection reagent for 5 minutes. Luminescence was read using a luminometer.

Cell-free mitochondrial DNA assay

Using 100μL of cell supernatant, mitochondrial DNA extraction was performed using QiaAMP DNA mini kit (Cat# 51304, Qiagen) following manufacturer's protocol. DNA was eluted with 50μL Ultra-Pure distilled water free from DNAse and RNAse (Cat# 10977015, Invitrogen). The absolute concentration (copies/μL) of circulating cell free mitochondrial DNA (ccf-mtDNA) was quantified using a commercially synthesized oligonucleotide of the PCR product (Integrated DNA Technologies), of known concentration, serially diluted to concentrations ranging from 10^8 copies/μL to 10^2 copies/μL. Mitochondrially encoded genes ND4 and ND1 were used to represent the major and minor arc, respectively, of the mitochondrial genome. qPCR was run as a duplex reaction using a 20μL TaqMan™ qPCR mixture which contains 10μL of TaqMan™ Fast Advanced Master Mix (Cat# 4444556, ThermoFisher), 4μL DNA, 1μL each of Forward and Reverse primers, and 1μL TaqMan™ probe (IDT Technologies) for each gene. Using BioRad's C1000 Thermal cycle CFX96 Real Time System, qPCR cycling conditions, described by TaqMan™ manufacturer, were as follows: 50°C for 2 minutes, 95°C for 20s, 40 cycles of 95°C for 3 seconds, and 60°C for 30 seconds, followed by a fluorescent read per cycle. The absolute concentration is estimated against the standard curve using a linear equation.

Primers and probes:

ND4: Forward: 5'-CCATTCTCCTCCTATCCCTCAAC-3'

Reverse: 5'-ACAATCTGATGTTTTGGTTAAACTATATTT-3'

Probe: 5′-FAM/CCGACATCA/ZEN/TTACCGGGTTTTCCTCTTG/3IABkFQ/−3′

ND1: Forward: 5’-CCCTAAAACCCGCCACATCT-3’

Reverse: 5’-GAGCGATGGTGAGAGCTAAGGT-3’

Probe: 5′-HEX/CCATCACCC/ZEN/TCTACATCACCGCCC/3IABkFQ/−3′

Cellular reactive oxygen species (ROS)

To assess for cellular oxidative stress, live Biowires (day 7 post-seeding) were incubated with 10uM CellROX Green Reagent (Invitrogen) for 30 minutes at 37°C. Tissues were washed twice with PBS then counterstained with Hoechst 33342 (1:1000 in PBS; NucBlue; Invitrogen) for 10 minutes at room temperature. Images were acquired using the Nikon A1R confocal microscope with resonant scanner.

CKMB ELISA

To quantify the concentration of CKMB in culture supernatants, ELISA was performed according to manufacturer’s instructions (Invitrogen Catalog # EHCKMB) using 100μL of input volume from HT-Biowires with or without hESC-macrophages on day 3 post-seeding.

Multiplex analysis of cytokines using a human cytokine array

The concentration of cytokines in culture supernatants on days 1, 3 and 7 post-seeding in HT-Biowires with or without hESC-macrophages was performed using a Human Cytokine 96-Plex Discovery Assay. Samples were diluted 1.5-fold in culture media. This study used Luminex xMAP technology for multiplexed quantification of 96 Human cytokines, chemokines, and growth factors. The multiplexing analysis was performed using the Luminex™ 200 system (Luminex, Austin, TX, USA) by Eve Technologies Corp. (Calgary, Alberta). Ninety-six markers were simultaneously measured in the samples using Eve Technologies’ Human Cytokine 96-Plex Discovery Assay® which consists of two separate kits; the Panel A 48-plex and the Panel B 48-plex (MilliporeSigma, Burlington, Massachusetts, USA). The assay was ran according to the manufacturer’s protocol. The Panel A 48-plex consisted of sCD40L, EGF, Eotaxin, FGF-2, FLT-3 Ligand, Fractalkine, G-CSF, GM-CSF, GROα, IFN-α2, IFN-γ, IL-1α, IL-1β, IL-1RA, IL-2, IL-3, IL-4, IL-5, IL-6, IL-7, IL-8, IL-9, IL-10, IL-12(p40), IL-12(p70), IL-13, IL-15, IL-17A, IL-17E/IL-25, IL-17F, IL-18, IL-22, IL-27, IP-10, MCP-1, MCP-3, M-CSF, MDC, MIG/CXCL9, MIP-1α, MIP-1β, PDGF-AA, PDGF-AB/BB, RANTES, TGFα, TNF-α, TNF-β, and VEGF-A. The Panel B 48-plex consisted of 6CKine, APRIL, BAFF, BCA-1, CCL28, CTACK, CXCL16, ENA-78, Eotaxin-2, Eotaxin-3, GCP-2, Granzyme A, Granzyme B, HMGB1, I-309, I-TAC, IFNβ, IFNω, IL-11, IL-16, IL-20, IL-21, IL-23, IL-24, IL-28A, IL-29, IL-31, IL-33, IL-34, IL-35, LIF, Lymphotactin, MCP-2, MCP-4, MIP-1δ, MIP-3α, MIP-3β, MPIF-1, Perforin, sCD137, SCF, SDF-1, sFAS, sFASL, TARC, TPO, TRAIL, and TSLP. Assay sensitivities of these markers range from 0.05 – 100 pg/mL for the 96-plex.

ATP assay

We quantified the levels of ATP in tissue lysates using the ATP Colorimetric/Fluorometric Assay Kit according to the manufacturer's instructions (Sigma Catalog #: MAK190). Three microtissues were pooled for each replicate, and homogenized in 200μL of ATP assay buffer, followed by deproteinization using a 10kDa MWCO spin filter. 50μL volume was used for each sample. For each sample, we corrected for background caused by glycerol phosphate by including 'sample blank' that did not include the ATP Converter. Samples were incubated in the colorimetric reaction mix for 30 minutes at room temperature, and absorbance was measured at 570nm.

Transwell co-cultures

Transwell assays were performed using the HTS Transwell®−96 Permeable Support with 0.4 μm Pore Polycarbonate Membrane (Corning 3381). hESC-cardiomyocytes and fibroblasts with or without hESC-macrophages were suspended in a hydrogel matrix and seeded within wells in the bottom chamber. The wells in the top chamber were seeded with either hESC-macrophages as a monolayer (same ratio as HT-Biowires), hESC-macrophages within hydrogel (same ratio as HT-Biowires), or empty, as indicated in Fig. 6A. Culture supernatants were collected on day 3 post-seeding to measure LDH.

Annexin V treatment and assays: hESC-cardiomyocytes were pre-incubated with 40ug per million cells of Purified Annexin V (BioLegend Catalog # 640902) for one hour at 37°C. After 1 hour, cells were washed with 1mL of DMEM and then combined with fibroblasts with or without hESC-macrophages to seed HT-Biowires. On days 3 and 14 post-seeding, culture supernatants were collected for to measure LDH. On day 14 post-seeding, HT-Biowires were imaged for functional assessment. For flow cytometry experiments, hESC-cardiomyocytes were first labeled with 200μL CFSE (5μM in PBS) for 30 minutes at 37°C. Cells were washed in 1mL of complete DMEM (containing 10% FBS) and pelleted (300g for 5 minutes at 4°C). Cells were re-suspended in warm complete DMEM for 10 minutes prior to spinning down (300g at 4°C for 5 mins). Cells were then labeled with Annexin V for 1 hour as above. Cell staining and flow cytometry was performed as detailed above.

Mass cytometry staining and acquisition (CyTOF)

Sample processing—Biowires were digested on day 3 post-seeding as described in the 'Biowire digestion' section, for 40 minutes at 37°C. 8 microtissues were pooled for each replicate, with 6 replicates per group. Cells were resuspended in Fc blocking reagent for 10 min at room temperature, followed immediately by incubation with a cocktail of surface antibodies prepared in cell staining media (CSM; PBS + 2% FBS) for 30 min at 4°C. Cells were then washed and incubated for 30 min at 4°C with anti-APC-162Dy diluted in CSM, to detect APC-conjugated anti-PDGFRβ. Cells were washed with PBS, and dead cell labelling was performed for 15 min at 37°C, using 1uM Cell-ID Intercalator 103Rh (Standard BioTools) prepared in HBSS. Cells were washed and fixed with eBioscience Foxp3 Fixation/Permeabilization (ThermoFisher) buffer for 30 min at 4°C. Cells were then washed with 1X permeabilization wash buffer (ThermoFisher) and stained intracellularly

with anti-cTnT-PE antibody for 1 hour at room temperature. Following this, cells were washed again and resuspended in a cocktail of intracellular metal-tagged antibodies, prepared in 1X permeabilization wash buffer. After incubation for 30 min at 4°C, cells were washed, and then resuspended in 125 uM of Cell-ID Intercalator Ir (Standard BioTools) to stain DNA and detect intact cells. Cells were labelled for 1h at 4°C, and then stored in 1.6% paraformaldehyde (in PBS) until the day of acquisition. On the day of acquisition, cells were washed, filtered, and counted prior to acquiring on a Helios instrument according to standard protocols.

Analysis

First, beads, doublets and ion cloud fusions were excluded using a sequential gating strategy starting with beads, followed by the Gaussian discrimination parameters (Residual, Offset, Center, Width) and finally Event Length. Debris was excluded by gating on the events with the highest DNA staining in both 191Ir and 193Ir channels. Single cell marker intensities from the remaining live and dead cells/events were exported for downstream analysis in R. Data from .fcs files was imported into R using the FlowCore package (read.flowset function; v2.14.2). Data were normalized using Arhsinh transformation and analyzed using the Seurat package. All samples were merged into a single dataset and variable features for clustering included every marker except for Ki67 due to technical limitations. Dimensionality reduction was performed using PCA and clustering was performed using the FindNeighbors and FindClusters functions. Non-linear dimensionality reduction was performed using UMAP and clusters were annotated based on lineage markers present in the panel. To compare sub-clusters across HT-Biowires with or without hESC-macrophages, we performed pseudo-bulk analyses on the average expression of each marker in each replicate. For each sub-cluster of cardiomyocytes or fibroblasts, multiple unpaired t-tests were conducted with P values adjusted for multiple comparisons using the Bonferroni-Dunn method.

Statistics & Reproducibility: Statistical analyses were performed using GraphPad Prism version 10. All data are represented as mean ± standard error of the mean (SEM). Details on statistical tests used are outlined in the figure legends. For proteomics (LC-MS) analyses, we used multiple unpaired (two-tailed) t-tests with correction for multiple comparisons using the Holm-Šídák method. In exploratory analyses of PBS versus annexin-treated microtissues with hESC-macrophages (Fig. 7), we performed multiple unpaired (two-tailed) t-tests were conducted with P values adjusted for multiple comparisons using the false discovery rate (FDR) approach (two-stage step-up, Benjamini, Krieger, and Yekutieli method). For CyTOF analyses (Fig. 4), we used multiple unpaired (two-tailed) t-tests with correction for multiple comparisons using the Bonferroni-Dunn method. For bulk RNA-seq analyses of gene panels (Fig. 1 & Fig. 6), two-way ANOVA was performed and P values were adjusted for multiple comparisons using the Tukey-Kramer test. In all other data, we used an unpaired two-tailed Student’s t-test pairwise comparisons of two groups, or one-way or two-way ANOVA for comparisons of more than two groups. Post hoc multiple comparison tests to determine adjusted P values are specified in figure legends where appropriate. Statistical significance was defined as $P<0.05$. Sample sizes were chosen based on extensive experience with bioengineered cardiac microtissues to account for biological variation in

microtissue generation and function[46], and no statistical method was used to predetermine sample size. No data points were excluded from analyses. All experiments (aside from high throughput sequencing or proteomics) were repeated at least two times using independent differentiations of hESC-macrophages or hESC-cardiomyocytes, and specifics for each experiment are indicated in figure legends. Microtissues were randomized into experimental groups in each experiment, and data was analyzed in a blinded fashion where applicable and unblinded after analyses were complete.

Extended Data

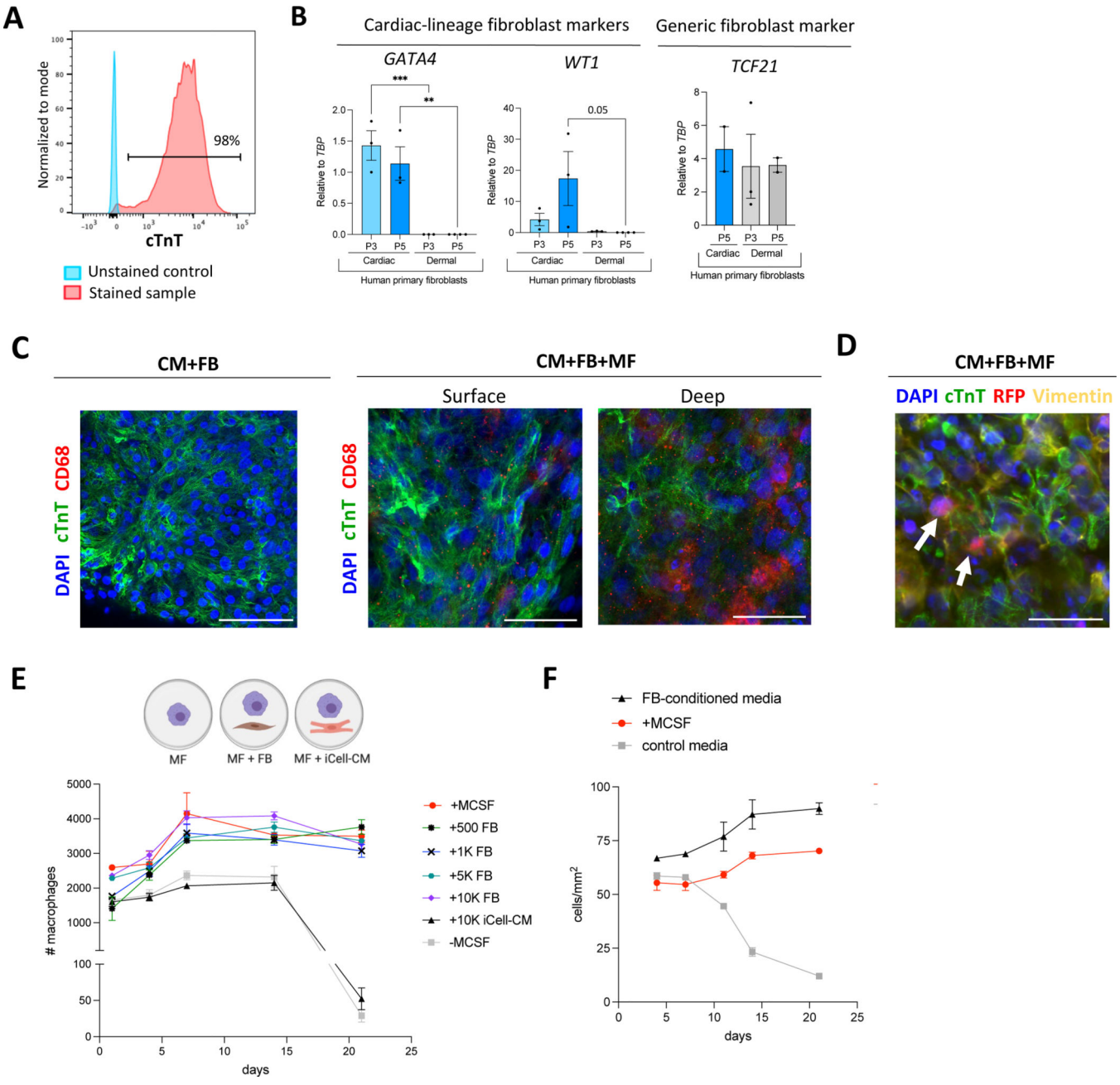

Extended Data Fig. 1: Integration of hESC-macrophages into bioengineered human cardiac microtissues.

(A) Flow cytometry of hESC-cardiomyocytes on day 16 post-differentiation. **(B)** qPCR of generic or cardiac lineage-specific genes in human primary cardiac fibroblasts compared to human primary dermal fibroblasts at passages 3 or 5. n=3 replicates per group from one experiment. (**C-D**) Immunofluorescence confocal imaging of microtissues 14 days post-seeding with or without hESC-macrophages. Images were acquired at the surface or deep within the tissue. Scale bar: 100mm (C, left), 50mm (C, right), 100mm (D). **(E)** hESC-macrophages were seeded either alone or with a range of abundances of human primary cardiac fibroblasts. The number of hESC-macrophages were counted over three weeks. n=3 per group, representative experiment shown, repeated two times. Diagram made with BioRender.com. **(F)** hESC-macrophages were incubated with control or conditioned media from human primary cardiac fibroblasts. The number of hESC-macrophages were counted over three weeks. n=3 per group, representative experiment shown, repeated two times. cTnT: cardiac troponin T; CM: cardiomyocyte; FB: fibroblast; MF: macrophage. One-way ANOVA with P values adjusted for multiple comparisons using the Tukey-Kramer test: $*P<0.05$, $**P<0.01$, $***P<0.001$. Error bars represent mean ± SEM.

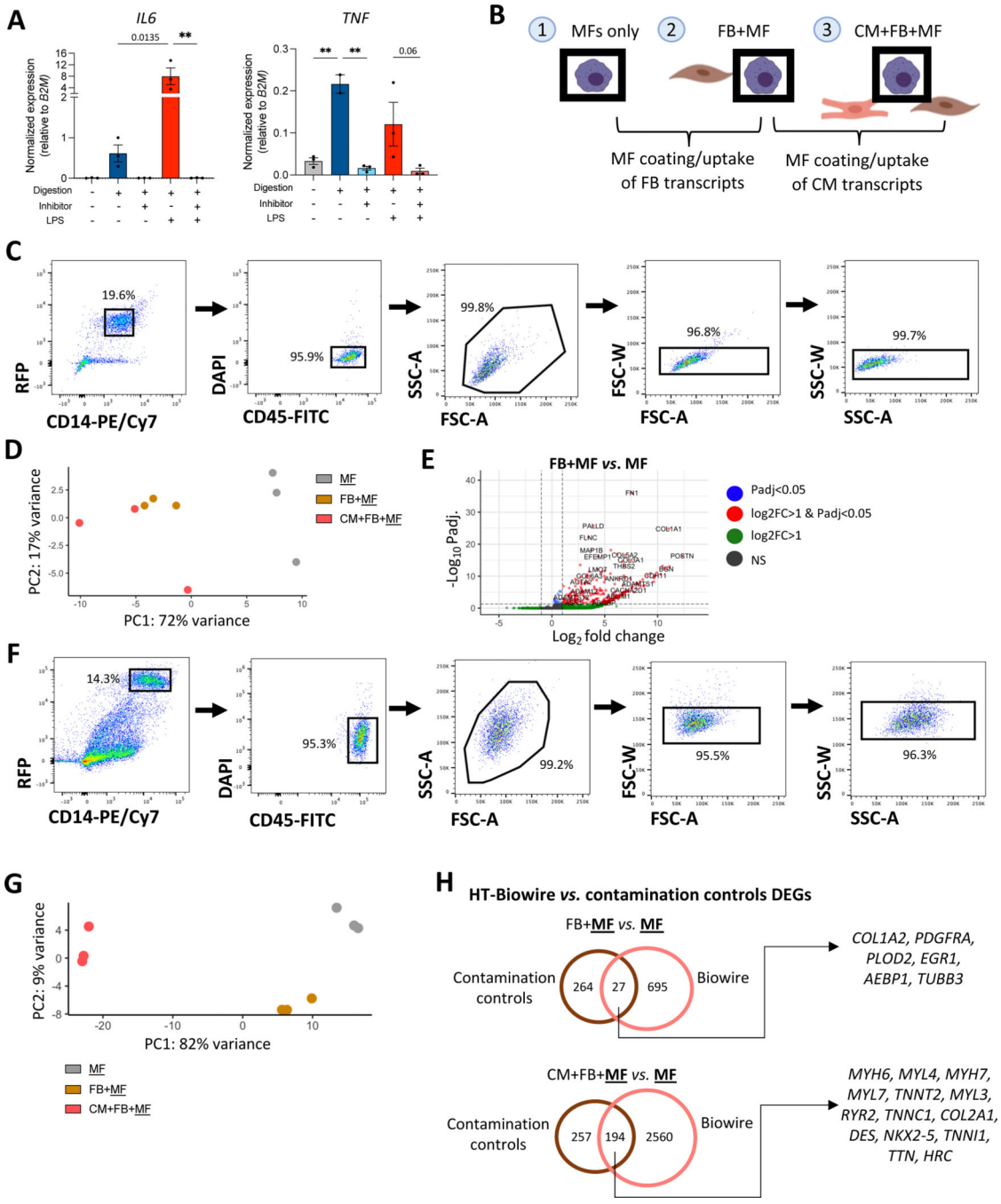

Extended Data Fig. 2: Defining contamination and dissociation-induced gene expression in hESC-macrophages.

(A) hESC-macrophages were stimulated with LPS in the presence or absence of the transcription inhibitor Flavopiridol. qPCR was performed on *IL6* and *TNF* with expression normalized to the housekeeping gene b2M. n=3 replicates per group from one experiment. **(B)** In control experiments, hESC-macrophages were incubated either (1) alone, (2) with fibroblasts or (3) with fibroblasts and hESC-cardiomyocytes during a 40-minute digestion period at 37 degrees Celsius. hESC-macrophages were sorted for bulk RNA

sequencing (n=3 replicates per group from one experiment). **(C)** Representative gating strategy for fluorescence activated cell sorting (FACS) isolation of hESC-macrophages from each digestion control group in (B). CD14+RFP+CD45+DAPI- live single cells were sorted for bulk RNA sequencing. **(D)** Principal component analysis. **(E)** Volcano plots showing differentially expressed genes between CM+FB+MF *vs.* MF and FB+MF *vs.* MF. **(F-G)** Microtissues (HT-Biowires) were seeded in combinations of hESC-cardiomyocytes, human primary cardiac fibroblasts and/or hESC-macrophages. On day 14, hESC-macrophages were sorted for bulk RNA sequencing. **(F)** Representative gating strategy for fluorescence activated cell sorting (FACS) isolation of hESC-macrophages from microtissues. CD14+RFP+CD45+DAPI- live single cells were sorted for bulk RNA sequencing (n=3 microtissues per group from one experiment). **(G)** Principal component analysis of hESC-macrophages sorted from each group in microtissues in (F). **(H)** CM+FB+MF *vs.* FB+MF DEGs compared in Biowire *vs.* digestion controls, or FB+MF *vs.* MF DEGs compared in Biowires *vs.* in digestion controls. CM: cardiomyocyte; FB: fibroblast; MF: macrophage. One-way ANOVA with P values adjusted for multiple comparisons using the Šídák test: *P<0.05, **P<0.01, ***P<0.001. Error bars represent mean ± SEM.

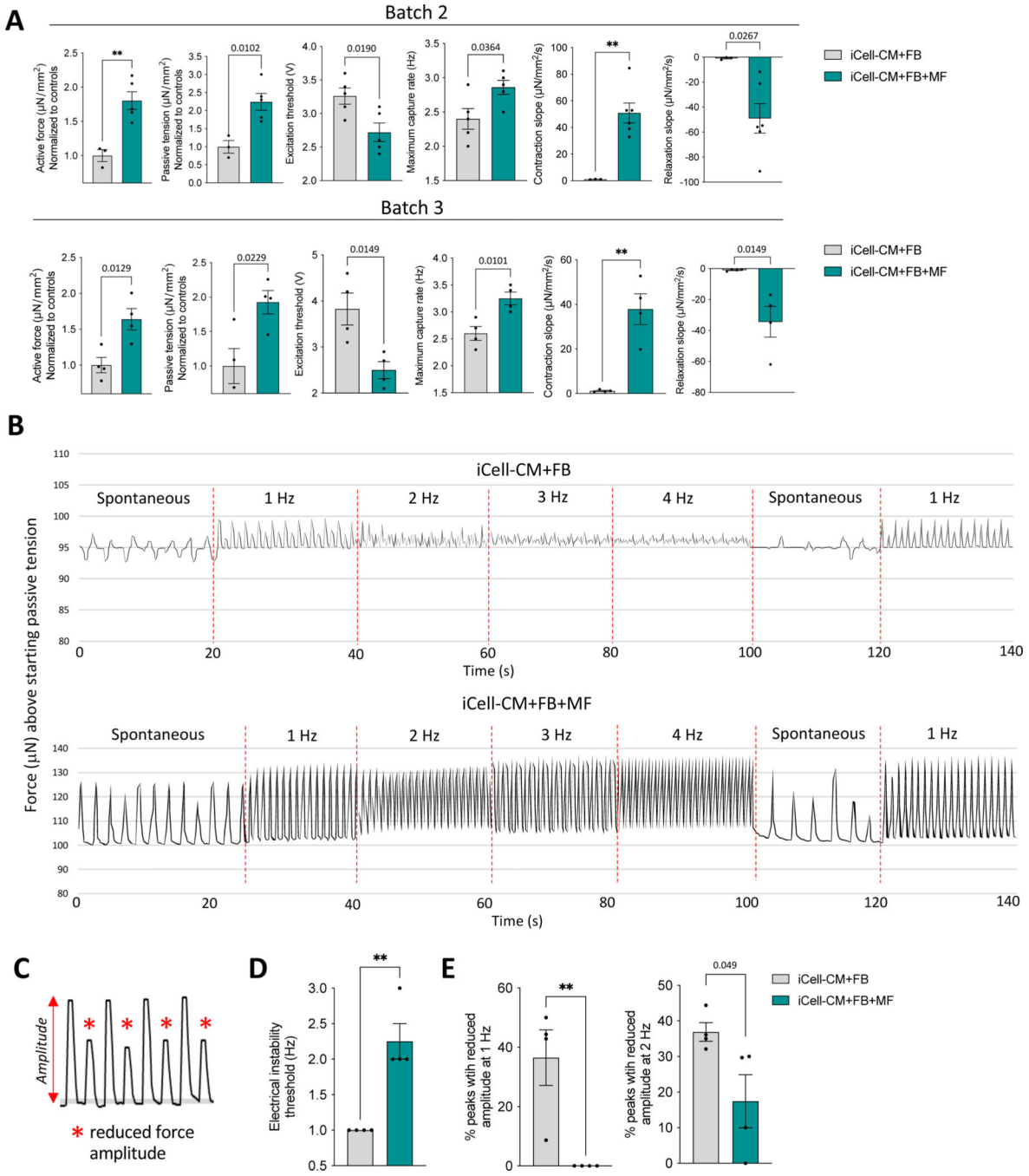

Extended Data Fig. 3: hESC-macrophages improve electromechanical function and reduce electrical instability in iCell-cardiomyocyte containing Biowires.

Microtissues were seeded with iPSC-cardiomyocytes (iCells) and primary human cardiac fibroblasts with or without hESC-macrophages in the Biowire II platform. **(A)** Independent experiments of distinct iPSC-cardiomyocyte and hESC-macrophage batches. Biowires were seeded with or without hESC-macrophages. Force and electrical properties were measured day 11 post-seeding. Batch 2: n=3 (control) or n=5 (hESC-macrophage) microtissues per group from one experiment, except for excitation threshold and maximum capture rate

where n=5 control microtissues. Batch 3: n=4 microtissues per group from one experiment. **(B)** Microtissues were stimulated at increasing frequencies from 1 Hz to 4 Hz. Graph shows the tracking of pixel movement during contraction and relaxation. n=4 per group. **(C)** Schematic depicting the categorization of weak amplitude beats during mechanical alternans. **(D)** Electrical instability threshold representing the minimum frequency at which an alternating reduced force amplitude pattern was observed. n=4 microtissues per group from one experiment. We defined a reduced force amplitude based on whether the amplitude was at least 15% less than the prior measured amplitude. **(E)** Percentage of peaks at 1 Hz or 2 Hz that contain alternating amplitudes were quantified. n=4 microtissues per group, one experiment. CM: cardiomyocyte; FB: fibroblast; MF: macrophage. Unpaired two-tailed t-test (A, D-E): *P<0.05, **P<0.01, ***P<0.001. Error bars represent mean ± SEM.

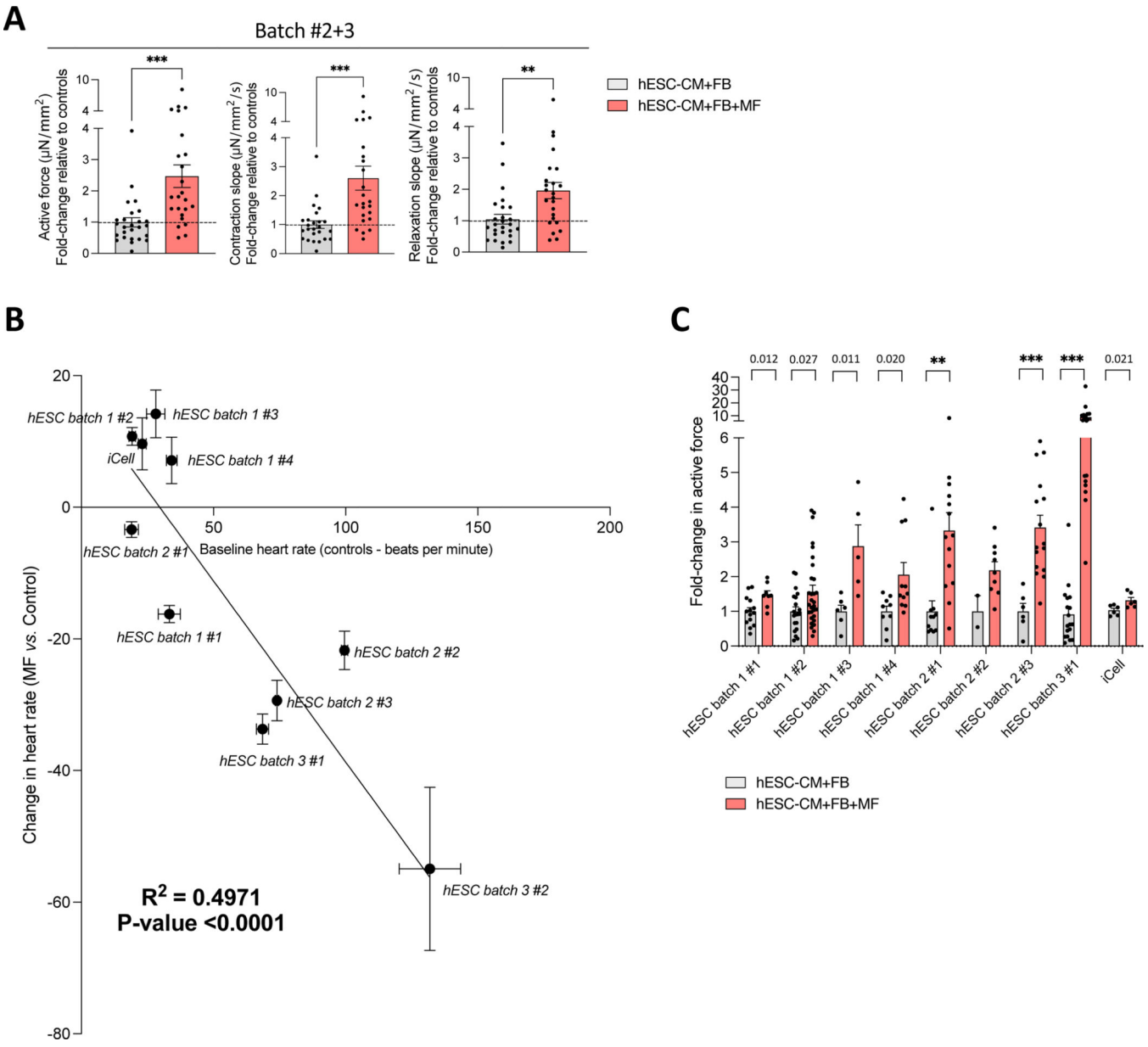

Extended Data Fig. 4: Baseline heart rate correlates with the effect of hESC-macrophages on the heart rate of cardiac microtissues.

(A) Microtissues (HT-Biowires) were seeded with hESC-cardiomyocytes and fibroblasts with or without hESC-macrophages. Active force was measured on day 14 post-seeding. n=26 (control) or n=24 (hESC-macrophage) microtissues per group pooled from two independent experiments. Unpaired t-test was performed. **(B)** Relationship between the baseline heart rate of microtissues (HT-Biowires, except for iCell data point from Biowire II platform) without hESC-macrophages to the change in heart rate upon addition of hESC-macrophages. Each data point represents the average of a distinct experiment, with the batch of cardiomyocytes used indicated. Simple linear regression was performed, reporting R-squared and P value indicating whether the slope is significantly non-zero. **(C)** Fold-change in active force in microtissues (HT-Biowires, except for iCell data from Biowire

II platform) with hESC-macrophages relative to controls in each experiment performed. n=14, 20, 6, 9, 11, 2, 6, 18, 6 control microtissues (left to right) or n= 8, 30, 5, 11, 14, 9, 16, 18, 6 microtissues with hESC-macrophages (left to right). Each group represents an independent experiment. CM: cardiomyocyte; FB: fibroblast; MF: macrophage. Unpaired two-tailed t-test (A, C): **P*<0.05, ***P*<0.01, ****P*<0.001. Error bars represent mean ± SEM.

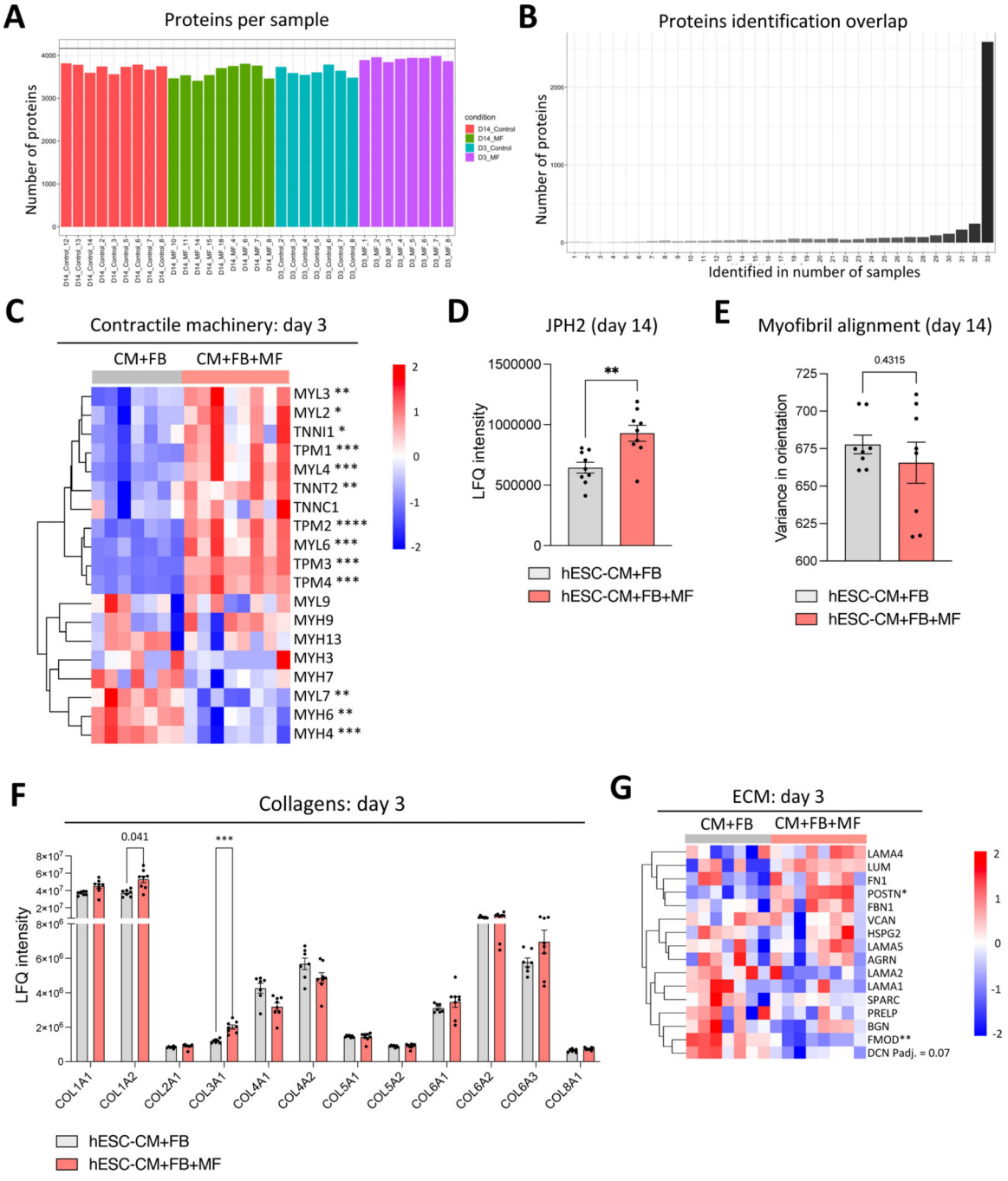

Extended Data Fig. 5: Expression of proteins in mass spectrometry-based proteomics of cardiac microtissues.

Liquid chromatography mass spectrometry was performed on total protein isolated from individual microtissues (HT-Biowires) on day 3 and day 14. **(A)** The number of proteins detected in each sample. **(B)** Histogram showing the number of proteins that are shared across multiple samples as indicated on the x-axis. **(C)** LFQ intensity of contractile machinery proteins in microtissues with or without hESC-macrophages on day 3. **(D)** LFQ intensity of JHP2 in microtissues with or without hESC-macrophages on day 14. n=9 microtissues per group from one experiment. **(E)** Immunofluorescence and confocal microscopy was performed on microtissues with or without hESC-macrophages stained with a-actinin and MLC2v (as in Figure 3G). Myofibril alignment was quantified. n=8 microtissues per group from one experiment. **(F)** LFQ intensity of collagen proteins in microtissues with or without hESC-macrophages on day 3. n=7 (control) or n=8 (hESC-macrophage) microtissues per group from one experiment. **(G)** LFQ intensity of extracellular matrix proteins in microtissues with or without hESC-macrophages on day 3. n=7 (control) or n=8 (hESC-macrophage) microtissues per group from one experiment. CM: cardiomyocyte; FB: fibroblast; MF: macrophage. Multiple unpaired (two-tailed) t-tests were conducted with P values adjusted for multiple comparisons using the Holm-Šídák method (C, F-G). Unpaired two-tailed t-test was performed for pairwise comparisons of two groups (D-E). $*P<0.05$, $**P<0.01$, $***P<0.001$. Error bars represent mean ± SEM.

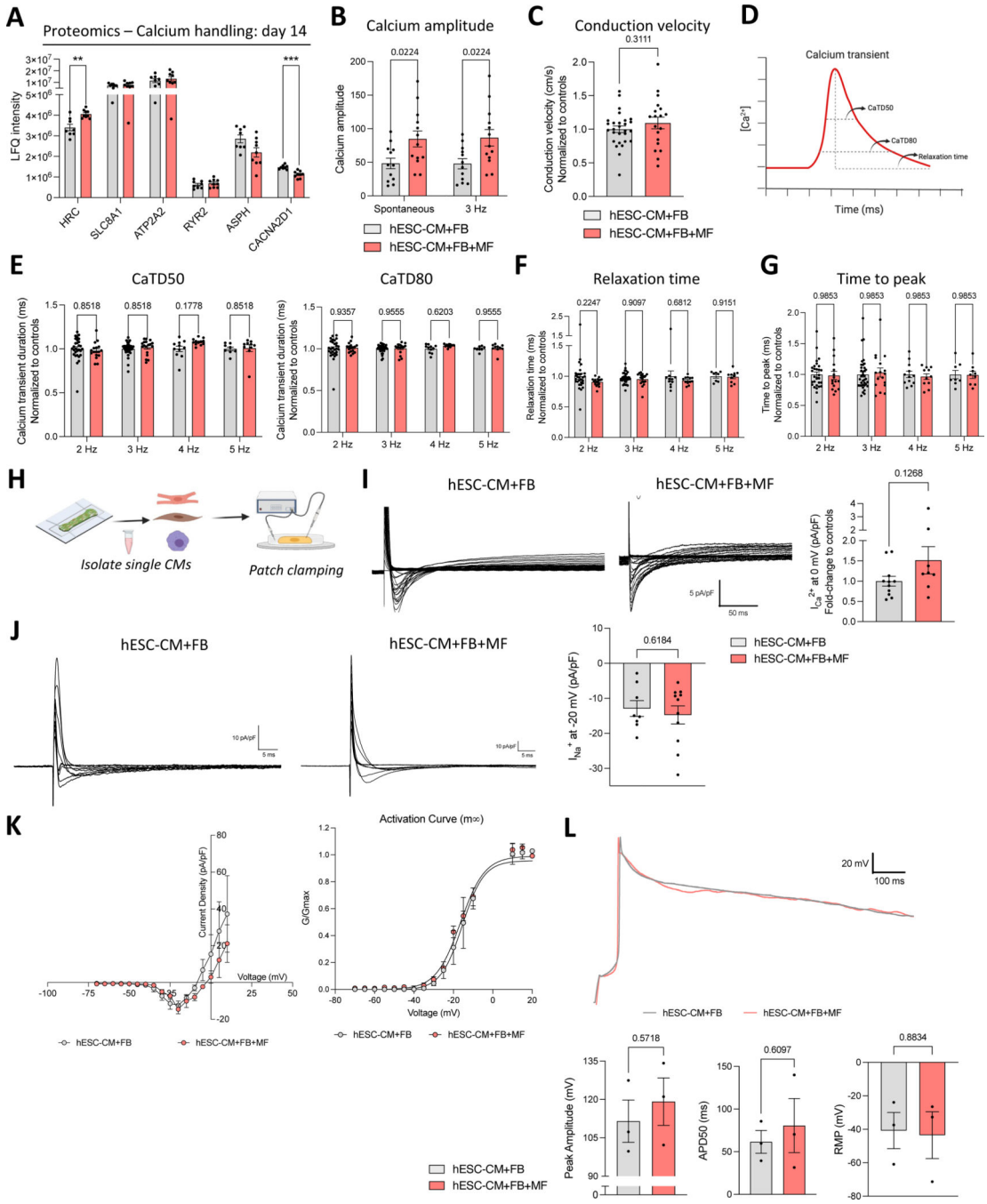

Extended Data Fig. 6: hESC-macrophages increase calcium amplitude in human cardiac microtissues without changes in calcium transients or in single hESC-cardiomyocyte ion channel function.

(A) Liquid chromatography mass spectrometry was performed on total protein isolated from individual microtissues (HT-Biowires). LFQ intensity of calcium handling proteins in microtissues with or without hESC-macrophages on day 14. n=8 (control) n=9 (hESC-macrophage) microtissues per group from one experiment. Multiple unpaired (two-tailed) t-tests were conducted with P values adjusted for multiple comparisons using the Holm-Šídák method. **(B-G)** Microtissues were seeded with hESC-cardiomyocytes and human primary

cardiac fibroblasts with or without hESC-macrophages in a 24-well based HT-Biowire platform. **(B)** Microtissues were incubated with a calcium indicator dye (Fluo-4). Calcium amplitude relative to baseline intensity was measured 14 days post-seeding either during spontaneous beating or while pacing at 3 Hz. n=12, 13, 12 13 microtissues per group (left to right) from one experiment. **(C)** Conduction velocity in microtissues with or without hESC-macrophages paced at 3 Hz. n=28 (control) or n=19 (hESC-macrophage) microtissues per group pooled from two independent experiments. Unpaired two-tailed t-test was performed. **(D-E)** Microtissues were stimulated at increasing frequencies. Calcium transient duration from depolarization to either 50% (CaTD50) or 80% (CaTD80) decay in microtissues with or without hESC-macrophages paced at 2–5 Hz 14 days post-seeding. n=29, 17, 34, 18, 11, 12, 8, 10 microtissues per group (left to right) pooled from two independent. **(F)** Relaxation time (peak to baseline) in microtissues with or without hESC-macrophages paced at 2–5 Hz 14 days post-seeding. n=29, 17, 34, 19, 11, 12, 8, 10 microtissues per group (left to right) pooled from two independent experiments. **(G)** Time to peak from 90% depolarization to 10% repolarization in microtissues with or without hESC-macrophages paced at 2–5 Hz 14 days post-seeding. n=29, 16, 36, 17, 12, 11, 8, 9 microtissues per group (left to right) pooled from two independent experiments. **(H)** Schematic of experimental design made with BioRender.com. Microtissues were seeded with hESC-cardiomyocytes and fibroblasts with or without hESC-macrophages. On day 14, microtissues were dissociated and cells were plated for single cardiomyocyte patch clamp recordings. **(I)** Representative ICa tracings (left). Peak ICa amplitude at 0 mV (right). n=11 (control) or n=8 (hESC-macrophage) cardiomyocytes per group pooled from two independent experiments. **(J)** Representative I_{Na} tracings (left). Peak I_{Na} amplitude at −20mV (right). n=8 (control) or n=11 (hESC-macrophage) cardiomyocytes per group from one experiment. **(K)** $I_{Na}{}^{+}$ Current density-voltage (*I-V*) plot and activation curve with the least-square fits to Boltzmann function. n=8–11 per group, one experiment. **(L)** Representative action potential (AP) tracings along with peak AP amplitude, AP duration at 50% repolarization (APD50) and resting membrane potential (RMP) (left to right). n=3 cardiomyocytes per group from one experiment. CM: cardiomyocyte; FB: fibroblast; MF: macrophage. Two-way ANOVA with P values adjusted for multiple comparisons using the Holm-Šídák method (B, D-G). Unpaired two-tailed t-test (C, I, J, L). *P<0.05, **P<0.01, ***P<0.001. Error bars represent mean ± SEM.

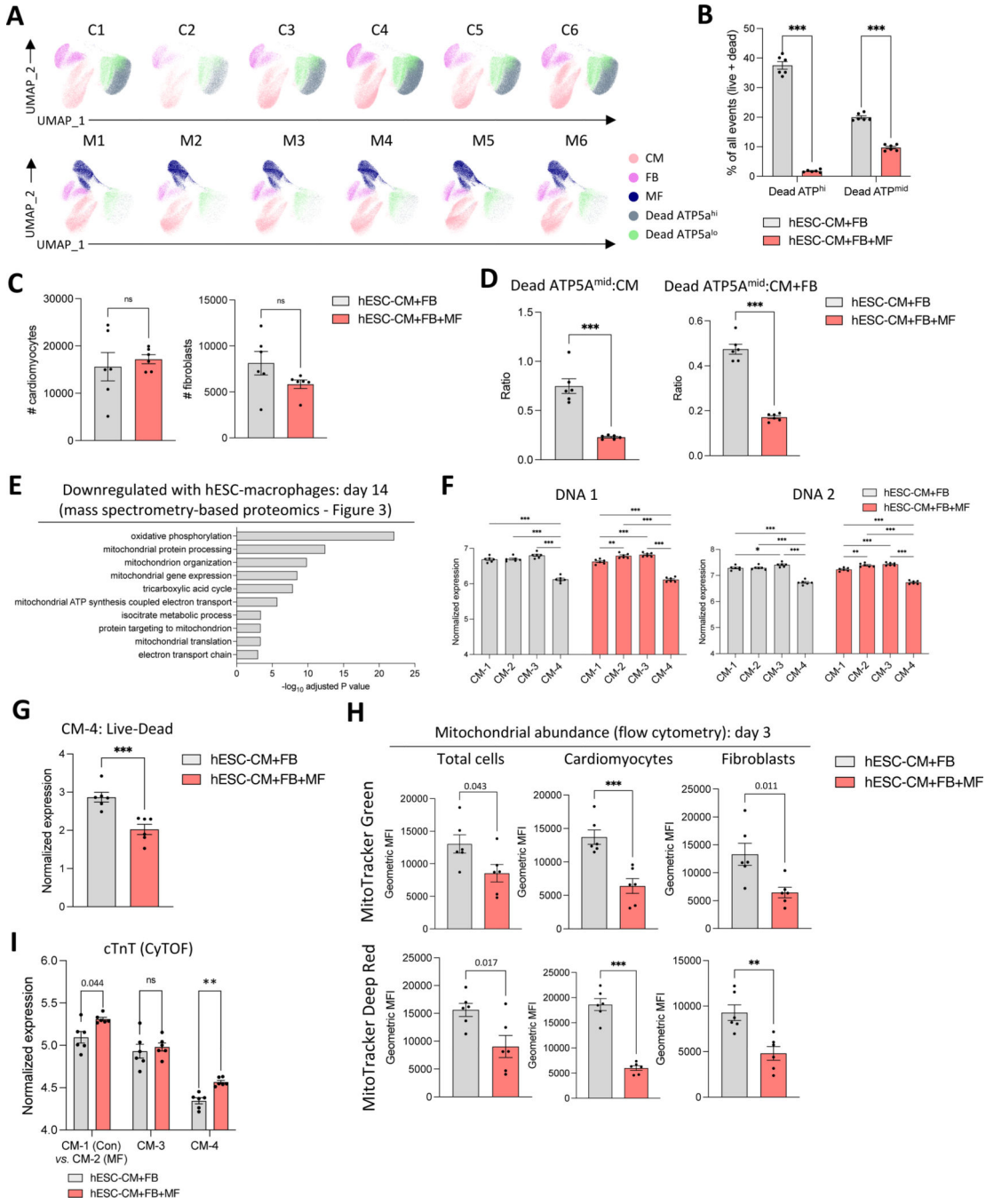

Extended Data Fig. 7: hESC-macrophages reduce accumulation of mitochondrial proteins in cardiac microtissues.

Cytometry by time-of-flight (CyTOF) was performed on microtissues (HT-Biowires) with or without hESC-macrophages on day 3 post-seeding. n=6 replicates per group, each replicate represented 8 pooled microtissues, experiment performed once. **(A)** UMAP visualization of 580,776 live and dead cells following standard quality control filtering, split by replicate in each group. **(B)** Percentage of Dead ATP5^{hi} group relative to all events in each replicate. **(C)** Number of cardiomyocytes or fibroblasts acquired in each

replicate in microtissues with or without hESC-macrophages. **(D)** Percentage of ATP5A^{mid} cells relative to the number of cardiomyocytes (left) or the number of cardiomyocytes and fibroblasts (right) in microtissues with or without hESC-macrophages. **(E)** Pathways downregulated in microtissues with hESC-macrophages on day 14 from mass spectrometry-based proteomics data (as in Figure 3). **(F)** Normalized expression of DNA 1 or DNA 2 in each cardiomyocyte subcluster (averaged in each replicate) in microtissues with or without hESC-macrophages. **(G)** Normalized expression live-dead label in each replicate (averaged) in CM-4 from microtissues with or without hESC-macrophages. **(H)** Microtissues were seeded with hESC-cardiomyocytes and fibroblasts with or without hESC-macrophages. On day 3 post-seeding, microtissues were labelled with the MitoTracker dye and flow cytometry was performed. Geometric mean fluorescence intensity (MFI) of MitoTracker in total cells, cardiomyocytes (CD45^{-}CD14^{-}), or fibroblasts (CD45^{dim}CD14^{dim}) is shown. n=6 microtissues per group, two experiments shown (MitoTracker Green and MitoTracker Deep Red). **(I)** Normalized expression of cardiac troponin T (cTnT) in each replicate (averaged) for all cardiomyocyte subclusters (CyTOF data) in microtissues with or without hESC-macrophages. CM: cardiomyocyte; FB: fibroblast; MF: macrophage. Two-way ANOVA with P values adjusted for multiple comparisons using the Šídák method (B, F, I), or unpaired two-tailed t-test (C, D, E, G, H). *P<0.05, **P<0.01, ***P<0.001. Error bars represent mean ± SEM.

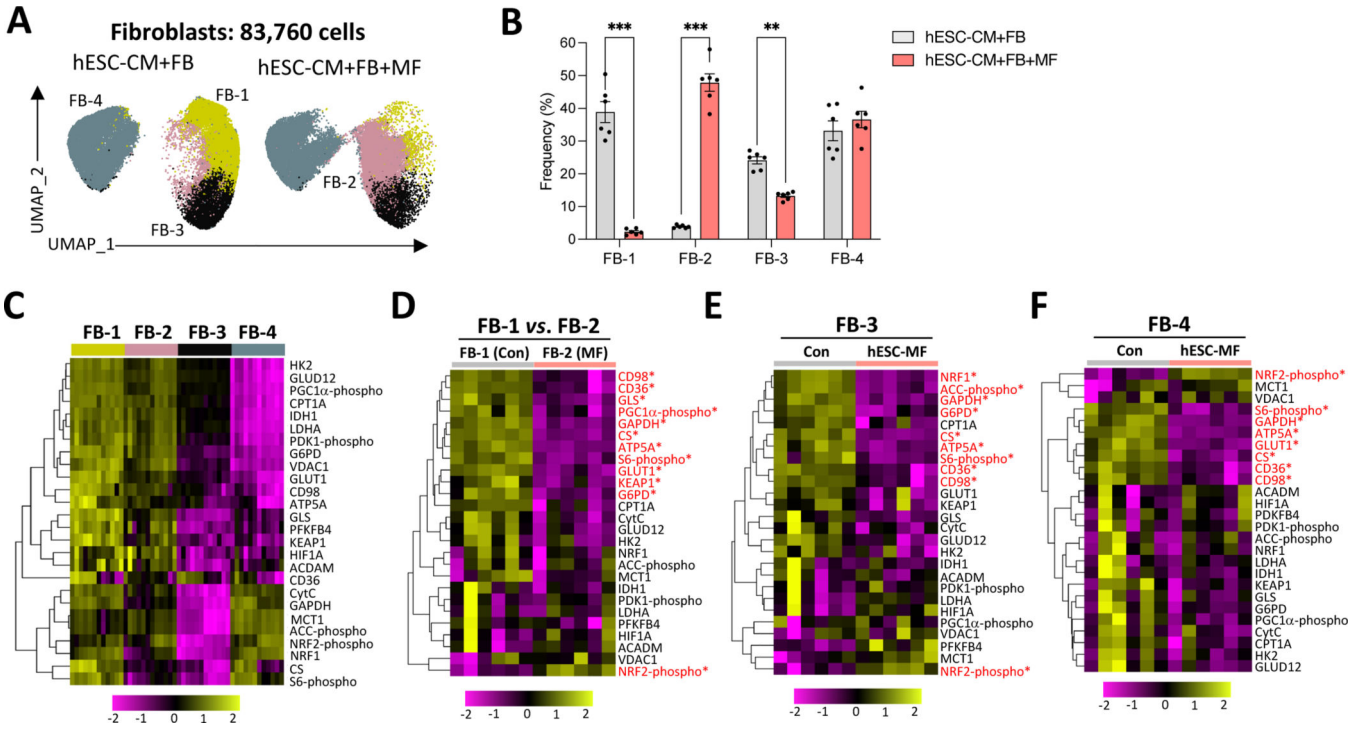

Extended Data Fig. 8: Global downregulation of metabolic proteins in fibroblasts in cardiac microtissues with hESC-macrophages.

(A) CyTOF data of fibroblasts re-clustered showing 5 subclusters. n=6 replicates per group, each replicate represented 8 pooled microtissues, experiment performed once. (A-F). **(B)** Frequency of each subcluster of fibroblasts in microtissues with or without

hESC-macrophages. **(C)** Expression of each marker in each subcluster of fibroblasts. **(D-F)** Expression of each marker in microtissues with or without hESC-macrophages for FB-1 versus FB-2 **(D)**, FB-3 **(E)** or FB-4 **(F)**. CM: cardiomyocyte; FB: fibroblast; MF: macrophage. Multiple unpaired two-tailed t-tests were conducted with P values adjusted for multiple comparisons using the Bonferroni-Dunn method (D-F), or two-way ANOVA was performed with P values adjusted with Šídák method (B). **P*<0.05, ***P*<0.01, ****P*<0.001. Error bars represent mean ± SEM.

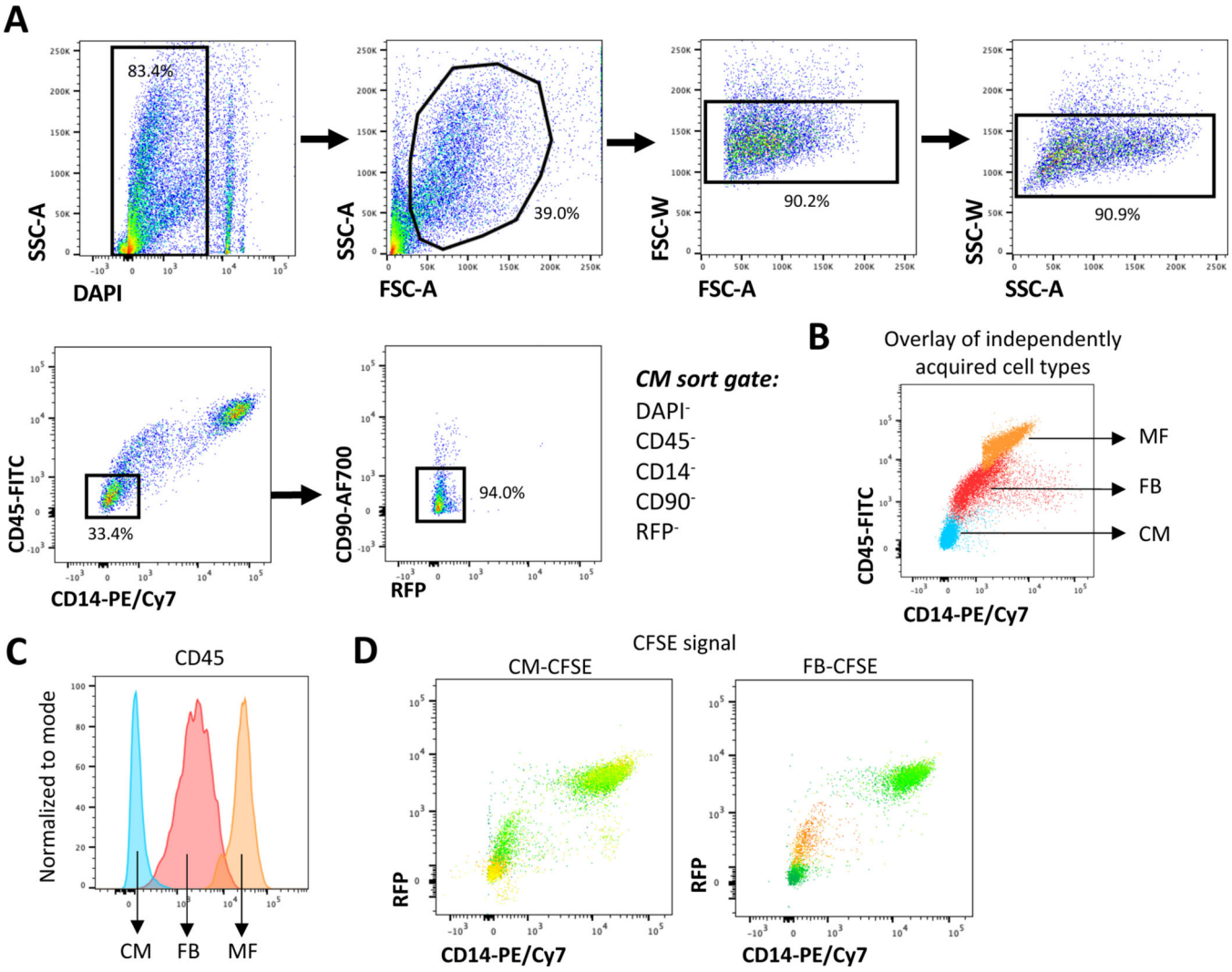

Extended Data Fig. 9: Gating strategy for sorting hESC-cardiomyocytes from microtissues for bulk RNA sequencing.

(A) Microtissues (HT-Biowires) were seeded with hESC-cardiomyocytes and fibroblasts with or without hESC-macrophages for bulk RNA sequencing of hESC-cardiomyocytes on day 3 post-seeding. Representative gating strategy shown. $DAPI^-$ live single cells were first gated, followed by $CD45^-CD14^-CD90^-RFP^-$ cells. **(B)** hESC-cardiomyocytes, fibroblasts and hESC-macrophages were independently stained and acquired for flow cytometry. Data was overlaid into a single plot. $CD45^-CD14^-$ cells were hESC-cardiomyocytes,

$CD45^{dim}CD14^{dim}$ cells were fibroblasts, and $CD45^{+}CD14^{+}$ cells were hESC-macrophages, confirming the gating strategy utilized in (A). **(C)** CD45 expression of populations shown in (B), showing that hESC-cardiomyocytes are $CD45^{-}$, fibroblasts are $CD45^{dim}$ and hESC-macrophages are $CD45^{+}$. **(D)** hESC-cardiomyocytes or fibroblasts were pre-labeled with CFSE prior to seeding microtissues. On day 3, flow cytometry was performed showing that the $CFSE^{+}$ hESC-cardiomyocytes were $CD14^{-}RFP^{-}$, whereas $CFSE^{+}$ fibroblasts were $CD14^{dim}RFP^{dim}$, confirming the gating strategy utilized in (A). CM: cardiomyocyte; FB: fibroblast; MF: macrophage.

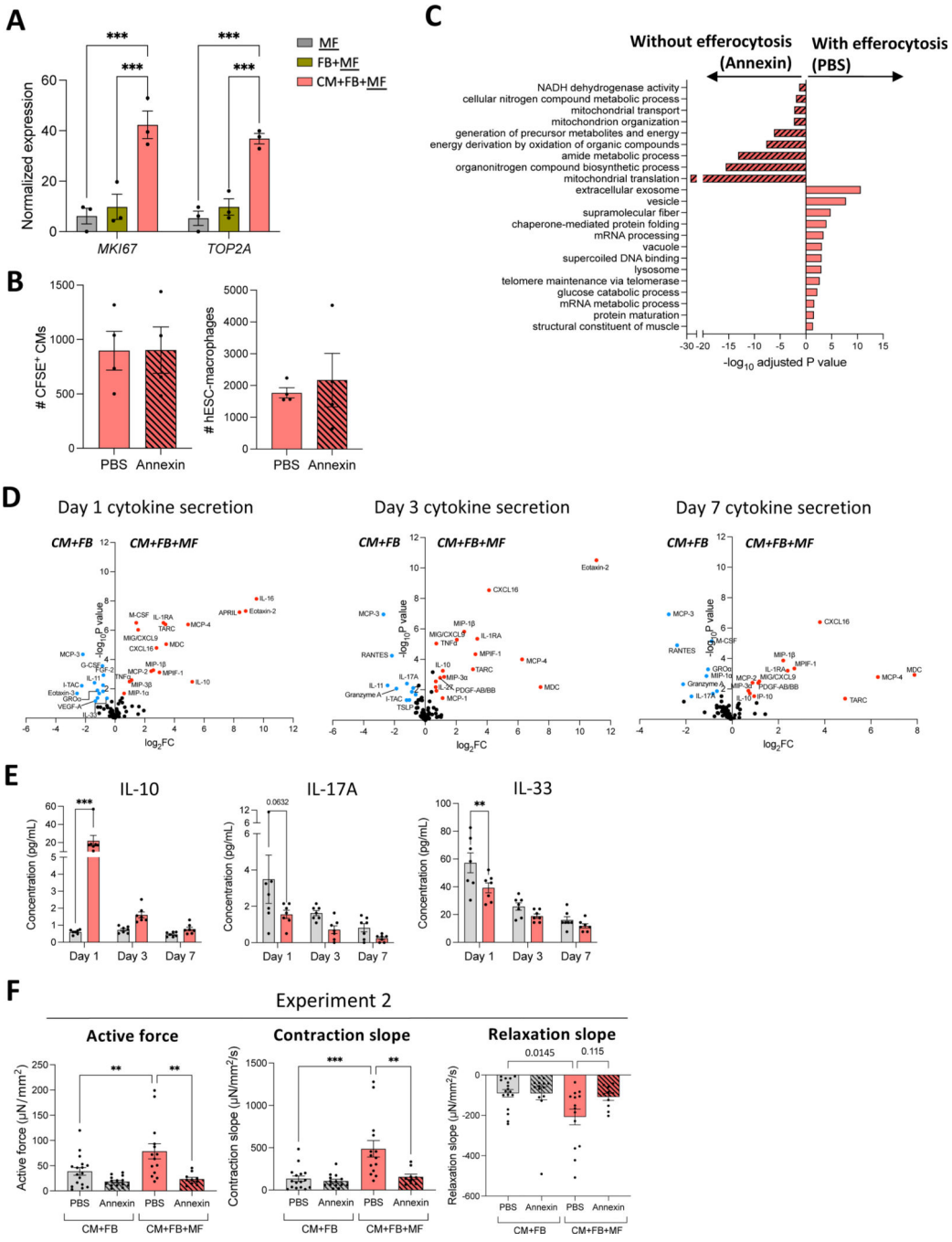

Extended Data Fig. 10: hESC-macrophage efferocytosis alters the total proteome in cardiac microtissues.

(A) Expression of proliferation genes in bulk RNA sequencing data of hESC-macrophages as in Figure 1. n=3 replicates per group from one experiment. **(B)** Number of hESC-cardiomyocytes or hESC-macrophages in microtissues with hESC-macrophages in PBS-treated versus Annexin-treated microtissues assessed using flow cytometry. n=4 microtissues per group from one experiment. **(C)** Pathways enriched in microtissues with hESC-macrophages in PBS treated (with efferocytosis) versus Annexin treated (without

efferocytosis) in liquid chromatography mass spectrometry-based proteomics data. Fisher's one-tailed test was performed with correction for multiple comparisons using the g:SCS method as implemented in gProfiler. **(D)** Human cytokine array (96-plex Discovery Assay) was performed on culture supernatants from microtissues with or without hESC-macrophages on days 1, 3 and 7. Volcano plots show upregulated versus downregulated cytokines at each timepoint. n=7 replicates (collected from n=7 microtissues) per group at each timepoint from one experiment. **(E)** Concentration of key cytokines in culture supernatants at each timepoint in microtissues with or without hESC-macrophages. n=7 replicates (collected from n=7 microtissues) per group at each timepoint from one experiment. **(F)** Microtissues were seeded with or without hESC-macrophages, containing PBS pre-treated versus Annexin pre-treated hESC-cardiomyocytes. On day 14 post-seeding, active force, contraction slope and relaxation slope were measured. n=17, 14, 14, 10 microtissues per group (left to right) from one experiment, first experiment shown in Figure 7. CM: cardiomyocyte; FB: fibroblast; MF: macrophage. One-way ANOVA (F) or two-way ANVOA (A, E) with P values adjusted for multiple comparisons using the Šídák method. Unpaired two-tailed t-test (B, D). $*P<0.05$, $**P<0.01$, $***P<0.001$. Error bars represent mean ± SEM.

Supplementary Material

Refer to Web version on PubMed Central for supplementary material.

Acknowledgments

We would like to thank the Immune Profiling Team at the Tumor Immunotherapy Program (Princess Margaret Cancer Centre, Toronto, Canada) for processing of mass cytometry samples and guidance on experimental design and analysis (Dr. Giselle Boukhaled, Dr. Ben Wang, and Dr. David Brooks). We would also like to thank the Princess Margaret Genomics Centre (Toronto, Canada) for processing of RNA sequencing samples, and the SickKids-UHN Flow Cytometry Facility (Toronto, Canada) for sample sorting. This work was supported by the Canadian Institutes of Health Research (S.E., H.H., M.R.), the Ted Rogers Centre for Heart Research (S.E., H.H.), the Peter Munk Cardiac Centre (S.E.), Ted Roger Centre for Heart Research (S.E.), Medicine by Design (S.E., G.K., M.A.L.), the Stem Cell Network (M.R. [MP-C4R1-3], S.E., H.H.) and National Institutes of Health (M.R. [2R01 HL076485]). The funders had no role in study design, data collection and analysis, decision to publish or preparation of the manuscript.

Data availability

RNA sequencing data generated in this study were deposited to the Gene Expression Omnibus under the accession number GEO: GSE261628. Proteomics data generated in this study were deposited to ProteomeXchange with the identifiers PXD050990 (control vs. macrophage dataset) and PXD050996 (efferocytosis inhibition with annexin dataset). Transcriptomics and proteomics data are available to explore through an interactive web browser (Shiny app) at https://www.epelmanlab.com/resources. Accession codes and sample information for publicly available single-cell RNA sequencing data analyzed in this study are summarized in Supplementary Table 9. All data generated in this study are included in the main article and associated source files.

References

1. Dick SA et al. Self-renewing resident cardiac macrophages limit adverse remodeling following myocardial infarction. Nature Immunology 20, 29–39, doi:10.1038/s41590-018-0272-2 (2019). [PubMed: 30538339]
2. Dick SA et al. Three tissue resident macrophage subsets coexist across organs with conserved origins and life cycles. Sci Immunol 7, eabf7777, doi:10.1126/sciimmunol.abf7777 (2022).
3. Epelman S. et al. Embryonic and adult-derived resident cardiac macrophages are maintained through distinct mechanisms at steady state and during inflammation. Immunity 40, 91–104, doi:10.1016/j.immuni.2013.11.019 (2014). [PubMed: 24439267]
4. Epelman S, Lavine KJ & Randolph GJ Origin and functions of tissue macrophages. Immunity 41, 21–35, doi:10.1016/j.immuni.2014.06.013 (2014). [PubMed: 25035951]
5. Bajpai G. et al. The human heart contains distinct macrophage subsets with divergent origins and functions. Nature Medicine 24, 1234–1245, doi:10.1038/s41591-018-0059-x (2018).
6. Yona S. et al. Fate mapping reveals origins and dynamics of monocytes and tissue macrophages under homeostasis. Immunity 38, 79–91, doi:10.1016/j.immuni.2012.12.001 (2013). [PubMed: 23273845]
7. Ginhoux F. & Guilliams M. Tissue-Resident Macrophage Ontogeny and Homeostasis. Immunity 44, 439–449, doi:10.1016/j.immuni.2016.02.024 (2016). [PubMed: 26982352]
8. Bian Z. et al. Deciphering human macrophage development at single-cell resolution. Nature 582, 571–576, doi:10.1038/s41586-020-2316-7 (2020). [PubMed: 32499656]
9. Popescu D-M et al. Decoding human fetal liver haematopoiesis. Nature 574, 365–371, doi:10.1038/s41586-019-1652-y (2019). [PubMed: 31597962]
10. Hulsmans M. et al. Macrophages Facilitate Electrical Conduction in the Heart. Cell 169, 510–522 e520, doi:10.1016/j.cell.2017.03.050 (2017). [PubMed: 28431249]
11. Lavine K. et al. Distinct Macrophage Lineages Contribute to Disparate Patterns of Cardiac Recovery and Remodeling in the Neonatal and Adult Heart. Proc. Natl. Acad. Sci 111, 16029–16034 (2014). [PubMed: 25349429]
12. Aurora AB et al. Macrophages are required for neonatal heart regeneration. J. Clin. Invest 124, 1382–1392, doi:72181 [pii];10.1172/JCI72181 [doi] (2014). [PubMed: 24569380]
13. Bajpai G. et al. Tissue Resident CCR2- and CCR2+ Cardiac Macrophages Differentially Orchestrate Monocyte Recruitment and Fate Specification Following Myocardial Injury. Circ Res 124, 263–278, doi:10.1161/circresaha.118.314028 (2019). [PubMed: 30582448]
14. Epelman S, Liu PP & Mann DL Role of innate and adaptive immune mechanisms in cardiac injury and repair. Nature Reviews Immunology 15, 117–129, doi:10.1038/nri3800 (2015).
15. Epelman S. & Mann DL Communication in the heart: the role of the innate immune system in coordinating cellular responses to ischemic injury. J. Cardiovasc. Transl. Res 5, 827–836, doi:10.1007/s12265-012-9410-7 [doi] (2012). [PubMed: 23054658]
16. Wong A, Hamidzada H. & Epelman S. A cardioimmunologist's toolkit: genetic tools to dissect immune cells in cardiac disease. Nat Rev Cardiol 19, 395–413, doi:10.1038/s41569-022-00701-0 (2022). [PubMed: 35523863]
17. Wong NR et al. Resident Cardiac Macrophages Mediate Adaptive Myocardial Remodeling. bioRxiv, 2021.2001.2028.428724, doi:10.1101/2021.01.28.428724 (2021).
18. Zaman R, Hamidzada H. & Epelman S. Exploring cardiac macrophage heterogeneity in the healthy and diseased myocardium. Curr Opin Immunol 68, 54–63, doi:10.1016/j.coi.2020.09.005 (2020). [PubMed: 33128959]
19. Zaman R. et al. Selective loss of resident macrophage-derived insulin-like growth factor-1 abolishes adaptive cardiac growth to stress. Immunity, doi:10.1016/j.immuni.2021.07.006 (2021).
20. Wan E. et al. Enhanced Efferocytosis of Apoptotic Cardiomyocytes Through Myeloid-Epithelial-Reproductive Tyrosine Kinase Links Acute Inflammation Resolution to Cardiac Repair After Infarction. Circulation Research 113, 1004–1012, doi:doi:10.1161/CIRCRESAHA.113.301198 (2013). [PubMed: 23836795]

21. Glinton KE et al. Macrophage-produced VEGFC is induced by efferocytosis to ameliorate cardiac injury and inflammation. The Journal of Clinical Investigation 132, doi:10.1172/JCI140685 (2022).
22. Morioka S, Maueröder C. & Ravichandran KS Living on the Edge: Efferocytosis at the Interface of Homeostasis and Pathology. Immunity 50, 1149–1162, doi:10.1016/j.immuni.2019.04.018 (2019). [PubMed: 31117011]
23. Valentin JE, Stewart-Akers AM, Gilbert TW & Badylak SF Macrophage participation in the degradation and remodeling of extracellular matrix scaffolds. Tissue Eng Part A 15, 1687–1694, doi:10.1089/ten.tea.2008.0419 (2009). [PubMed: 19125644]
24. Doran AC, Yurdagul A. & Tabas I. Efferocytosis in health and disease. Nature Reviews Immunology 20, 254–267, doi:10.1038/s41577-019-0240-6 (2020).
25. Leid JM et al. Primitive Embryonic Macrophages are Required for Coronary Development and Maturation. Circ. Res, doi:CIRCRESAHA.115.308270 [pii];10.1161/CIRCRESAHA.115.308270 [doi] (2016).
26. Cahill TJ et al. Tissue-resident macrophages regulate lymphatic vessel growth and patterning in the developing heart. Development 148, doi:10.1242/dev.194563 (2021).
27. Lewis-Israeli YR et al. Self-assembling human heart organoids for the modeling of cardiac development and congenital heart disease. Nature Communications 12, 5142, doi:10.1038/s41467-021-25329-5 (2021).
28. Wang EY et al. Biowire Model of Interstitial and Focal Cardiac Fibrosis. ACS Central Science 5, 1146–1158, doi:10.1021/acscentsci.9b00052 (2019). [PubMed: 31403068]
29. Thomas D, Choi S, Alamana C, Parker KK & Wu JC Cellular and Engineered Organoids for Cardiovascular Models. Circulation Research 130, 1780–1802, doi:doi:10.1161/CIRCRESAHA.122.320305 (2022). [PubMed: 35679369]
30. Drakhlis L. et al. Human heart-forming organoids recapitulate early heart and foregut development. Nature Biotechnology 39, 737–746, doi:10.1038/s41587-021-00815-9 (2021).
31. Hofbauer P. et al. Cardioids reveal self-organizing principles of human cardiogenesis. Cell 184, 3299–3317.e3222, doi:10.1016/j.cell.2021.04.034 (2021). [PubMed: 34019794]
32. Filippo Buono M. et al. Human Cardiac Organoids for Modeling Genetic Cardiomyopathy. Cells 9, doi:10.3390/cells9071733 (2020).
33. Marini V. et al. Long-term culture of patient-derived cardiac organoids recapitulated Duchenne muscular dystrophy cardiomyopathy and disease progression. Frontiers in Cell and Developmental Biology 10, doi:10.3389/fcell.2022.878311 (2022).
34. Micheu MM & Rosca AM Patient-specific induced pluripotent stem cells as “disease-in-a-dish” models for inherited cardiomyopathies and channelopathies - 15 years of research. World J Stem Cells 13, 281–303, doi:10.4252/wjsc.v13.i4.281 (2021). [PubMed: 33959219]
35. Silva AC et al. Co-emergence of cardiac and gut tissues promotes cardiomyocyte maturation within human iPSC-derived organoids. Cell Stem Cell 28, 2137–2152.e2136, doi:10.1016/j.stem.2021.11.007 (2021). [PubMed: 34861147]
36. Ergir E. et al. Generation and Maturation of Human iPSC-derived Cardiac Organoids in Long Term Culture. bioRxiv, 2022.2003.2007.483273, doi:10.1101/2022.03.07.483273 (2022).
37. Feric NT & Radisic M. Maturing human pluripotent stem cell-derived cardiomyocytes in human engineered cardiac tissues. Adv Drug Deliv Rev 96, 110–134, doi:10.1016/j.addr.2015.04.019 (2016). [PubMed: 25956564]
38. Liang P-Y, Chang Y, Jin G, Lian X. & Bao X. Wnt signaling directs human pluripotent stem cells into vascularized cardiac organoids with chamber-like structures. Frontiers in Bioengineering and Biotechnology 10, doi:10.3389/fbioe.2022.1059243 (2022).
39. Helms HR, Jarrell DK & Jacot JG Generation of Cardiac Organoids Using Cardiomyocytes, Endothelial Cells, Epicardial Cells, and Cardiac Fibroblasts Derived From Human Induced Pluripotent Stem Cells. The FASEB Journal 33, lb170-lb170, doi:10.1096/fasebj.2019.33.1_supplement.lb170 (2019).
40. Kahn-Krell A. et al. A three-dimensional culture system for generating cardiac spheroids composed of cardiomyocytes, endothelial cells, smooth-muscle cells, and cardiac fibroblasts

derived from human induced-pluripotent stem cells. Frontiers in Bioengineering and Biotechnology 10, doi:10.3389/fbioe.2022.908848 (2022).

41. Cui Y. et al. Single-Cell Transcriptome Analysis Maps the Developmental Track of the Human Heart. Cell Reports 26, 1934–1950.e1935, doi:10.1016/j.celrep.2019.01.079 (2019). [PubMed: 30759401]
42. Nicolás-Ávila JA et al. A Network of Macrophages Supports Mitochondrial Homeostasis in the Heart. Cell 183, 94–109.e123, doi:10.1016/j.cell.2020.08.031 (2020). [PubMed: 32937105]
43. Atkins MH et al. Modeling human yolk sac hematopoiesis with pluripotent stem cells. J Exp Med 219, doi:10.1084/jem.20211924 (2022).
44. Sturgeon CM, Ditadi A, Awong G, Kennedy M. & Keller G. Wnt signaling controls the specification of definitive and primitive hematopoiesis from human pluripotent stem cells. Nat Biotechnol 32, 554–561, doi:10.1038/nbt.2915 (2014). [PubMed: 24837661]
45. Nunes SS et al. Biowire: a platform for maturation of human pluripotent stem cell-derived cardiomyocytes. Nat. Methods 10, 781–787, doi:nmeth.2524 [pii];10.1038/nmeth.2524 [doi] (2013). [PubMed: 23793239]
46. Zhao Y. et al. A Platform for Generation of Chamber-Specific Cardiac Tissues and Disease Modeling. Cell 176, 913–927.e918, doi:10.1016/j.cell.2018.11.042 (2019). [PubMed: 30686581]
47. Wu Q. et al. Automated fabrication of a scalable heart-on-a-chip device by 3D printing of thermoplastic elastomer nanocomposite and hot embossing. Bioactive Materials 33, 46–60, doi:10.1016/j.bioactmat.2023.10.019 (2024). [PubMed: 38024233]
48. Suryawanshi H. et al. Cell atlas of the foetal human heart and implications for autoimmune-mediated congenital heart block. Cardiovasc Res 116, 1446–1457, doi:10.1093/cvr/cvz257 (2020). [PubMed: 31589297]
49. Dhahri W. et al. In Vitro Matured Human Pluripotent Stem Cell-Derived Cardiomyocytes Form Grafts With Enhanced Structure and Function in Injured Hearts. Circulation 145, 1412–1426, doi:10.1161/circulationaha.121.053563 (2022). [PubMed: 35089805]
50. Kattman SJ et al. Stage-specific optimization of activin/nodal and BMP signaling promotes cardiac differentiation of mouse and human pluripotent stem cell lines. Cell Stem Cell 8, 228–240, doi:10.1016/j.stem.2010.12.008 (2011). [PubMed: 21295278]
51. Euler DE Cardiac alternans: mechanisms and pathophysiological significance. Cardiovascular Research 42, 583–590, doi:10.1016/s0008-6363(99)00011-5 (1999). [PubMed: 10533597]
52. Kim R. et al. Mechanical alternans is associated with mortality in acute hospitalized heart failure: prospective mechanical alternans study (MAS). Circ Arrhythm Electrophysiol 7, 259–266, doi:10.1161/circep.113.000958 (2014). [PubMed: 24585716]
53. Chen B. et al. Critical roles of junctophilin-2 in T-tubule and excitation-contraction coupling maturation during postnatal development. Cardiovasc Res 100, 54–62, doi:10.1093/cvr/cvt180 (2013). [PubMed: 23860812]
54. Rienks M, Papageorgiou A-P, Frangogiannis NG & Heymans S. Myocardial Extracellular Matrix. Circulation Research 114, 872–888, doi:doi:10.1161/CIRCRESAHA.114.302533 (2014). [PubMed: 24577967]
55. Singh JP & Young JL The cardiac nanoenvironment: form and function at the nanoscale. Biophysical Reviews 13, 625–636, doi:10.1007/s12551-021-00834-5 (2021). [PubMed: 34765045]
56. Chen QM & Maltagliati AJ Nrf2 at the heart of oxidative stress and cardiac protection. Physiol Genomics 50, 77–97, doi:10.1152/physiolgenomics.00041.2017 (2018). [PubMed: 29187515]
57. Segawa K. & Nagata S. An Apoptotic ‘Eat Me’ Signal: Phosphatidylserine Exposure. Trends Cell Biol 25, 639–650, doi:10.1016/j.tcb.2015.08.003 (2015). [PubMed: 26437594]
58. Naeini MB, Bianconi V, Pirro M. & Sahebkar A. The role of phosphatidylserine recognition receptors in multiple biological functions. Cell Mol Biol Lett 25, 23, doi:10.1186/s11658-020-00214-z (2020). [PubMed: 32226456]
59. Gerlach BD et al. Efferocytosis induces macrophage proliferation to help resolve tissue injury. Cell Metab 33, 2445–2463.e2448, doi:10.1016/j.cmet.2021.10.015 (2021). [PubMed: 34784501]
60. Gomes MT et al. Phosphatidylserine externalization by apoptotic cells is dispensable for specific recognition leading to innate apoptotic immune responses. J Biol Chem 298, 102034, doi:10.1016/j.jbc.2022.102034 (2022). [PubMed: 35588784]

61. Krahling S, Callahan MK, Williamson P. & Schlegel RA Exposure of phosphatidylserine is a general feature in the phagocytosis of apoptotic lymphocytes by macrophages. Cell Death Differ 6, 183–189, doi:10.1038/sj.cdd.4400473 (1999). [PubMed: 10200565]
62. Liao YH et al. Interleukin-17A contributes to myocardial ischemia/reperfusion injury by regulating cardiomyocyte apoptosis and neutrophil infiltration. J Am Coll Cardiol 59, 420–429, doi:10.1016/j.jacc.2011.10.863 (2012). [PubMed: 22261166]
63. Chang S-L et al. Interleukin-17 enhances cardiac ventricular remodeling via activating MAPK pathway in ischemic heart failure. Journal of Molecular and Cellular Cardiology 122, 69–79, doi:10.1016/j.yjmcc.2018.08.005 (2018). [PubMed: 30096409]
64. Baldeviano GC et al. Interleukin-17A Is Dispensable for Myocarditis but Essential for the Progression to Dilated Cardiomyopathy. Circulation Research 106, 1646–1655, doi:doi:10.1161/CIRCRESAHA.109.213157 (2010). [PubMed: 20378858]
65. Gosselin D. et al. Environment drives selection and function of enhancers controlling tissue-specific macrophage identities. Cell 159, 1327–1340, doi:10.1016/j.cell.2014.11.023 (2014). [PubMed: 25480297]
66. Gosselin D. et al. An environment-dependent transcriptional network specifies human microglia identity. Science 356, eaal3222, doi:10.1126/science.aal3222 (2017).
67. Lavin Y. et al. Tissue-Resident Macrophage Enhancer Landscapes Are Shaped by the Local Microenvironment. Cell 159, 1312–1326, doi:10.1016/j.cell.2014.11.018 (2014). [PubMed: 25480296]
68. Zhou X. et al. Circuit Design Features of a Stable Two-Cell System. Cell 172, 744–757.e717, doi:10.1016/j.cell.2018.01.015 (2018). [PubMed: 29398113]
69. Bonnardel J. et al. Stellate Cells, Hepatocytes, and Endothelial Cells Imprint the Kupffer Cell Identity on Monocytes Colonizing the Liver Macrophage Niche. Immunity 51, 638–654.e639, doi:10.1016/j.immuni.2019.08.017 (2019). [PubMed: 31561945]
70. Israeli-Rosenberg S, Manso AM, Okada H. & Ross RS Integrins and integrin-associated proteins in the cardiac myocyte. Circ Res 114, 572–586, doi:10.1161/circresaha.114.301275 (2014). [PubMed: 24481847]
71. Song R. & Zhang L. Cardiac ECM: Its Epigenetic Regulation and Role in Heart Development and Repair. Int J Mol Sci 21, doi:10.3390/ijms21228610 (2020).
72. Scott CL et al. The Transcription Factor ZEB2 Is Required to Maintain the Tissue-Specific Identities of Macrophages. Immunity 49, 312–325.e315, doi:10.1016/j.immuni.2018.07.004 (2018). [PubMed: 30076102]
73. Schulz C. et al. A lineage of myeloid cells independent of Myb and hematopoietic stem cells. Science 336, 86–90 (2012). [PubMed: 22442384]
74. Kelly LM, Englmeier U, Lafon I, Sieweke MH & Graf T. MafB is an inducer of monocytic differentiation. Embo j 19, 1987–1997, doi:10.1093/emboj/19.9.1987 (2000). [PubMed: 10790365]
75. Aziz A, Soucie E, Sarrazin S. & Sieweke MH MafB/c-Maf deficiency enables self-renewal of differentiated functional macrophages. Science 326, 867–871, doi:10.1126/science.1176056 (2009). [PubMed: 19892988]
76. T'Jonck W, Guilliams M. & Bonnardel J. Niche signals and transcription factors involved in tissue-resident macrophage development. Cellular Immunology 330, 43–53, doi:10.1016/j.cellimm.2018.02.005 (2018). [PubMed: 29463401]
77. Ueno M. et al. Layer V cortical neurons require microglial support for survival during postnatal development. Nature Neuroscience 16, 543–551, doi:10.1038/nn.3358 (2013). [PubMed: 23525041]
78. Wakselman S. et al. Developmental neuronal death in hippocampus requires the microglial CD11b integrin and DAP12 immunoreceptor. J Neurosci 28, 8138–8143, doi:10.1523/jneurosci.1006-08.2008 (2008). [PubMed: 18685038]
79. Marín-Teva JL et al. Microglia promote the death of developing Purkinje cells. Neuron 41, 535–547, doi:10.1016/s0896-6273(04)00069-8 (2004). [PubMed: 14980203]
80. Grune J. et al. Neutrophils incite and macrophages avert electrical storm after myocardial infarction. Nature Cardiovascular Research 1, 649–664, doi:10.1038/s44161-022-00094-w (2022).

81. Jia D. et al. Cardiac Resident Macrophage-Derived Legumain Improves Cardiac Repair by Promoting Clearance and Degradation of Apoptotic Cardiomyocytes After Myocardial Infarction. Circulation 145, 1542–1556, doi:doi:10.1161/CIRCULATIONAHA.121.057549 (2022). [PubMed: 35430895]
82. Koivumäki JT et al. Structural Immaturity of Human iPSC-Derived Cardiomyocytes: In Silico Investigation of Effects on Function and Disease Modeling. Front Physiol 9, 80, doi:10.3389/fphys.2018.00080 (2018). [PubMed: 29467678]
83. Karbassi E. et al. Cardiomyocyte maturation: advances in knowledge and implications for regenerative medicine. Nat Rev Cardiol 17, 341–359, doi:10.1038/s41569-019-0331-x (2020). [PubMed: 32015528]
84. Lundy SD, Zhu WZ, Regnier M. & Laflamme MA Structural and functional maturation of cardiomyocytes derived from human pluripotent stem cells. Stem Cells Dev 22, 1991–2002, doi:10.1089/scd.2012.0490 (2013). [PubMed: 23461462]
85. Ronaldson-Bouchard K. et al. Advanced maturation of human cardiac tissue grown from pluripotent stem cells. Nature 556, 239–243, doi:10.1038/s41586-018-0016-3 (2018). [PubMed: 29618819]
86. Tiburcy M. et al. Defined Engineered Human Myocardium With Advanced Maturation for Applications in Heart Failure Modeling and Repair. Circulation 135, 1832–1847, doi:10.1161/circulationaha.116.024145 (2017). [PubMed: 28167635]
87. Guo Y. & Pu WT Cardiomyocyte Maturation. Circulation Research 126, 1086–1106, doi:doi:10.1161/CIRCRESAHA.119.315862 (2020). [PubMed: 32271675]
88. Park DS et al. iPS-cell-derived microglia promote brain organoid maturation via cholesterol transfer. Nature 623, 397–405, doi:10.1038/s41586-023-06713-1 (2023). [PubMed: 37914940]
89. Patterson AJ & Zhang L. Hypoxia and fetal heart development. Curr Mol Med 10, 653–666, doi:10.2174/156652410792630643 (2010). [PubMed: 20712587]
90. Irion S. et al. Identification and targeting of the ROSA26 locus in human embryonic stem cells. Nature Biotechnology 25, 1477–1482, doi:10.1038/nbt1362 (2007).
91. Reubinoff BE, Pera MF, Fong CY, Trounson A. & Bongso A. Embryonic stem cell lines from human blastocysts: somatic differentiation in vitro. Nat Biotechnol 18, 399–404, doi:10.1038/74447 (2000). [PubMed: 10748519]
92. Thomson JA et al. Embryonic stem cell lines derived from human blastocysts. Science 282, 1145–1147, doi:10.1126/science.282.5391.1145 (1998). [PubMed: 9804556]
93. Funakoshi S. et al. Generation of mature compact ventricular cardiomyocytes from human pluripotent stem cells. Nature Communications 12, 3155, doi:10.1038/s41467-021-23329-z (2021).
94. Fernandes I, Funakoshi S, Hamidzada H, Epelman S. & Keller G. Modeling cardiac fibroblast heterogeneity from human pluripotent stem cell-derived epicardial cells. Nature Communications 14, 8183, doi:10.1038/s41467-023-43312-0 (2023).
95. Love MI, Huber W. & Anders S. Moderated estimation of fold change and dispersion for RNA-seq data with DESeq2. Genome Biology 15, 550, doi:10.1186/s13059-014-0550-8 (2014). [PubMed: 25516281]
96. Butler A, Hoffman P, Smibert P, Papalexi E. & Satija R. Integrating single-cell transcriptomic data across different conditions, technologies, and species. Nature Biotechnology 36, 411–420, doi:10.1038/nbt.4096 (2018).
97. Stuart T. et al. Comprehensive Integration of Single-Cell Data. Cell 177, 1888–1902.e1821, doi:10.1016/j.cell.2019.05.031 (2019). [PubMed: 31178118]
98. Hao Y. et al. Dictionary learning for integrative, multimodal and scalable single-cell analysis. Nature Biotechnology, doi:10.1038/s41587-023-01767-y (2023).
99. Korsunsky I. et al. Fast, sensitive and accurate integration of single-cell data with Harmony. Nature Methods 16, 1289–1296, doi:10.1038/s41592-019-0619-0 (2019). [PubMed: 31740819]
100. Foroutan M. et al. Single sample scoring of molecular phenotypes. BMC Bioinformatics 19, 404, doi:10.1186/s12859-018-2435-4 (2018). [PubMed: 30400809]
101. Tyanova S. et al. The Perseus computational platform for comprehensive analysis of (prote)omics data. Nature Methods 13, 731–740, doi:10.1038/nmeth.3901 (2016). [PubMed: 27348712]

102. Azam MA et al. Effects of Late Sodium Current Blockade on Ventricular Refibrillation in a Rabbit Model. Circ Arrhythm Electrophysiol 10, doi:10.1161/circep.116.004331 (2017).

103. Si D. et al. Essential role of ryanodine receptor 2 phosphorylation in the effect of azumolene on ventricular arrhythmia vulnerability in a rabbit heart model. J Cardiovasc Electrophysiol 29, 1707–1715, doi:10.1111/jce.13737 (2018). [PubMed: 30203424]

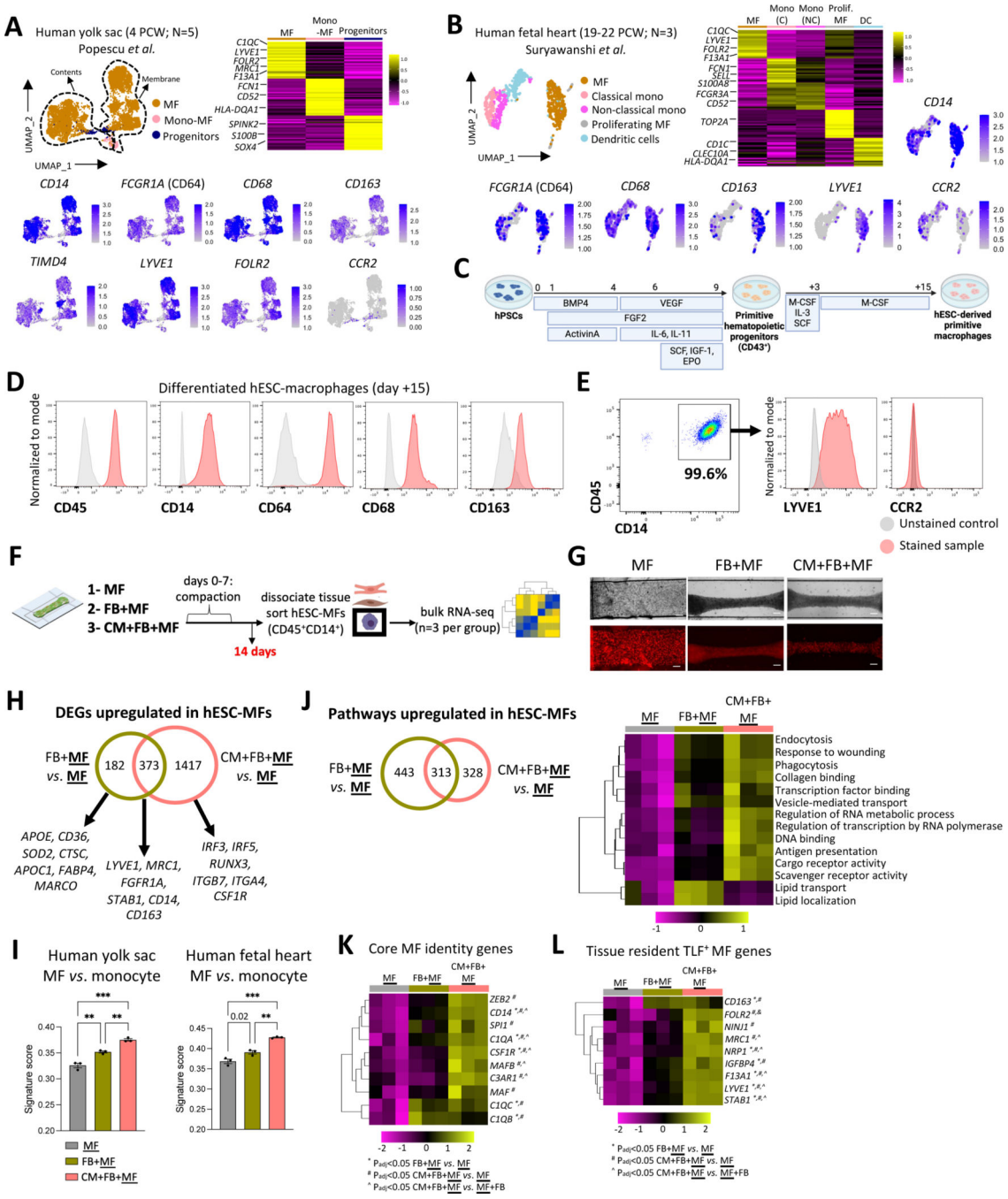

Figure 1: hESC-macrophages undergo stepwise *in vivo* yolk sac tissue macrophage programming in bioengineered human cardiac microtissues.

(A) Single-cell RNA sequencing analysis of publicly available data (Popescu *et al.*) of human yolk sac macrophages [4 post-conception weeks (PCW)], transitioning monocytes to macrophages (Mono-MF) and progenitors from the contents or membrane of the yolk sac. Uniform manifold approximation and projection (UMAP) dimensionality reduction and Seurat-based clustering was performed. Heatmap shows the average expression of the top 30 differentially expressed genes (DEGs) in each group. Feature plots depict single

cell gene expression. **(B)** Single-cell RNA sequencing analysis of publicly available data (Suryawanshi *et al.*) of human fetal cardiac myeloid cells (1001 cells) at 19–22 PCWs (N=3 pooled patients). UMAP dimensionality reduction and Seurat-based clustering identified a population of macrophages, monocytes and dendritic cells. Feature plots depict single cell gene expression of macrophage (*C1QC, LYVE1, CD163*), monocyte (*FCN1, CCR2*) and dendritic cell (*CD1C*) markers. **(C)** Timeline of the differentiation of human embryonic stem cells to hematopoietic progenitors and hESC-macrophages. **(D-E)** Flow cytometric analysis of immune and macrophage markers **(D)** and macrophage lineage-specific markers **(E)** on day 15 of the differentiation of hematopoietic progenitors. **(F)** Schematic of bulk RNA sequencing experiment (created with BioRender.com). Cells were seeded in 3 groups within a hydrogel (Matrigel + collagen): (1) hESC-macrophages alone, (2) hESC-macrophages and fibroblasts, (3) hESC-macrophages, fibroblasts and hESC-cardiomyocytes. hESC-macrophages were sorted from each group on day 14 (n=3 replicates per group from one experiment; each replicate represents 15 pooled microtissues) and bulk RNA sequencing was performed. **(G)** Images of microtissues from each group on day 14. hESC-macrophages are RFP-expressing and shown with red fluorescence signal. Representative images shown, experiment repeated 5 times. Scale bar: 200mm. **(H)** DEGs were computed in FB+MF *vs.* MF (effect of fibroblasts) and CM+FB+MF *vs.* MF (combined effect of fibroblasts and cardiomyocytes). Venn diagram shows the number of genes that were unique to each comparison or shared across comparisons. **(I)** A human yolk sac macrophage signature was generated by computing the top 100 DEGs (ordered by avg_log_2FC) in total yolk sac macrophages relative to the monocyte-macrophage population in the Popsecu *et al.* data in (A). A signature for human fetal cardiac macrophages was generated by computing the top 150 DEGs (ordered by avg_log_2FC) in TLF^+ macrophages relative to monocytes in the Suryawanshi *et al.* in (B). Bulk RNA sequencing data from sorted hESC-macrophages from each group were scored for both the yolk sac macrophage and human fetal cardiac macrophage signature. n=3 replicates per group from one experiment. One-way ANOVA was performed with P values adjusted for multiple comparisons using the Tukey-Kramer test. **(J)** Pathway enrichment analysis was performed in hESC-macrophages from FB+MF *vs.* MF and in CM+FB+MF *vs.* MF. Venn diagram shows the number of unique or shared pathways that were significant based on the - log_{10} of adjusted P value. Heatmap shows the average expression of gene sets from each GO term, including pathways that were induced by fibroblasts or by the combination of fibroblasts and cardiomyocytes. **(K-L)** Log_{10} transformed expression of core macrophage survival or identity genes **(K)** or tissue resident macrophage genes, defined as the TLF^+ macrophage signature in Dick *et al.* 2022 **(L)**. n=3 replicates per group from one experiment. In K-L, two-way ANOVA was performed and P values were adjusted for multiple comparisons using the Tukey-Kramer test. CM: cardiomyocyte; FB: fibroblast; MF: macrophage. *P<0.05, **P<0.01, ***P<0.001. Error bars represent mean ± SEM.

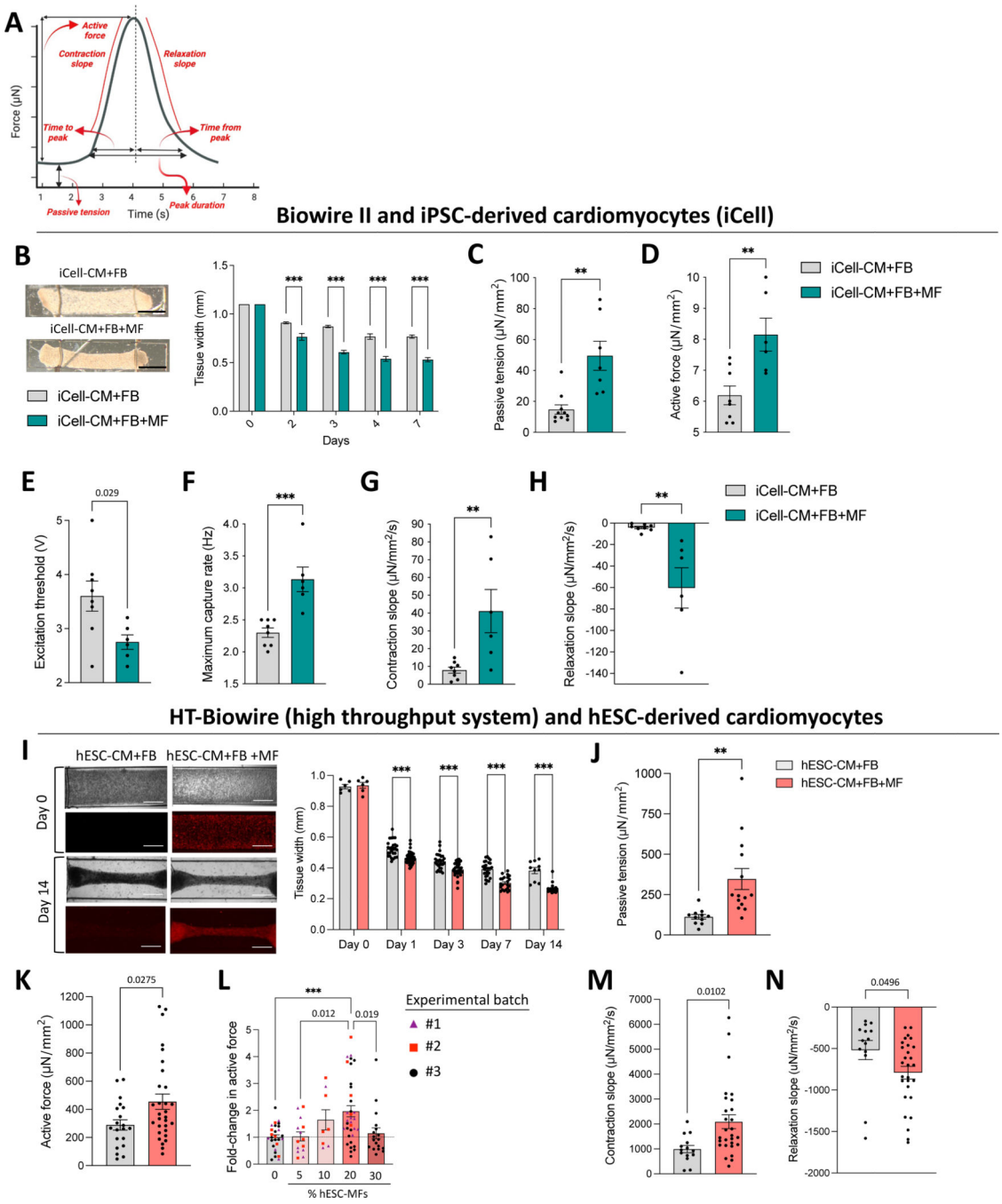

Figure 2: hESC-macrophages enhance mechanical and electrical properties of human cardiac microtissues across cell source and platforms.

(A) Diagram of the parameters that were tracked to assess contraction and relaxation properties in each cardiac cycle. **(B-H)** The Biowire II platform was seeded with human iPSC-cardiomyocytes (iCells) and primary human cardiac fibroblasts with or without hESC-macrophages in a collagen-Matrigel hydrogel, paced at 1 Hz and measurements were performed on day 11 post-seeding. **(B)** Tissue width on days 0, 2, 3, 4 and 7 post-seeding in Biowires with or without hESC-macrophages. n=10 (control) or n=8

(hESC-macrophages) microtissues per group measured repeatedly across time from 1 representative experiment, repeated 3 times. Scale bar = 1mm. **(C)** Passive tension generated by Biowires with or without hESC-macrophages while at rest (in between contractions). n=10 (control) or n=7 (hESC-macrophages) microtissues per group from 1 representative experiment, repeated 3 times. **(D)** Active force upon tissue contraction in Biowires II with or without hESC-macrophages. n=8 (control) or n=6 (hESC-macrophages) microtissues per group from 1 representative experiment, repeated 3 times. **(E)** The excitation threshold, or voltage required to stimulate synchronized contraction, in Biowires with or without hESC-macrophages. n=8 (control) or n=6 (hESC-macrophage) microtissues per group from 1 representative experiment, repeated 3 times. **(F)** Biowires were stimulated at increasing frequencies and maximum capture rate at which the tissue contracts synchronously was measured. n=8 (control) or n=6 (hESC-macrophages) microtissues per group from 1 representative experiment, repeated 3 times. **(G-H)** Contraction and relaxation slope measured in Biowires with or without hESC-macrophages. n=8 (control) or n=6 (hESC-macrophage) microtissues per group from 1 representative experiment, repeated 3 times. **(I-N)** Microtissues were seeded with hESC-cardiomyocytes and primary human cardiac fibroblasts with or without hESC-macrophages in a high throughput 96-well based Biowire platform (HT-Biowires), and measurements were performed on day 14 post-seeding. **(I)** Tissue width was measured (days 0–14) post-seeding. n=6, 27, 29, 29, 10 (control) or n=6, 35, 33, 22, 24 (hESC-macrophage) microtissues per group, representative experiment shown, repeated 7 times. Scale bar: 0.5mm. **(J)** Passive tension generated in HT-Biowires with or without hESC-macrophages was measured in between contractions (day 14). n=19 (control) or n=21 (hESC-macrophage) microtissues per group, representative experiment shown, repeated 7 times. **(K)** Active force generated during contraction by HT-Biowires. n=20 (control) or n=30 (hESC-macrophage) microtissues per group, representative experiment shown, repeated 7 times. **(L)** Active force of HT-Biowires seeded with a range of hESC-macrophage concentrations. Percentages represent the proportion of macrophages over the base numbers (cardiomyocytes + fibroblasts). n=27, 14, 8, 35, 18 microtissues per group (left to right), pooled from 3 independent experiments. **(M-N)** Contraction and relaxation slope of HT-Biowires with or without hESC-macrophages on day 14 post-seeding. n=14 (control) or n=28 (hESC-macrophage) microtissues per group, representative data shown, repeated 7 times. CM: cardiomyocyte; FB: fibroblast; MF: macrophage. One-way ANOVA (L) or two-way ANOVA (B, I) corrected for multiple comparisons using the Tukey-Kramer test, or unpaired two-tailed t-test (C-H, J, K, M, N): $*P<0.05$, $**P<0.01$, $***P<0.001$. Error bars represent mean ± SEM.

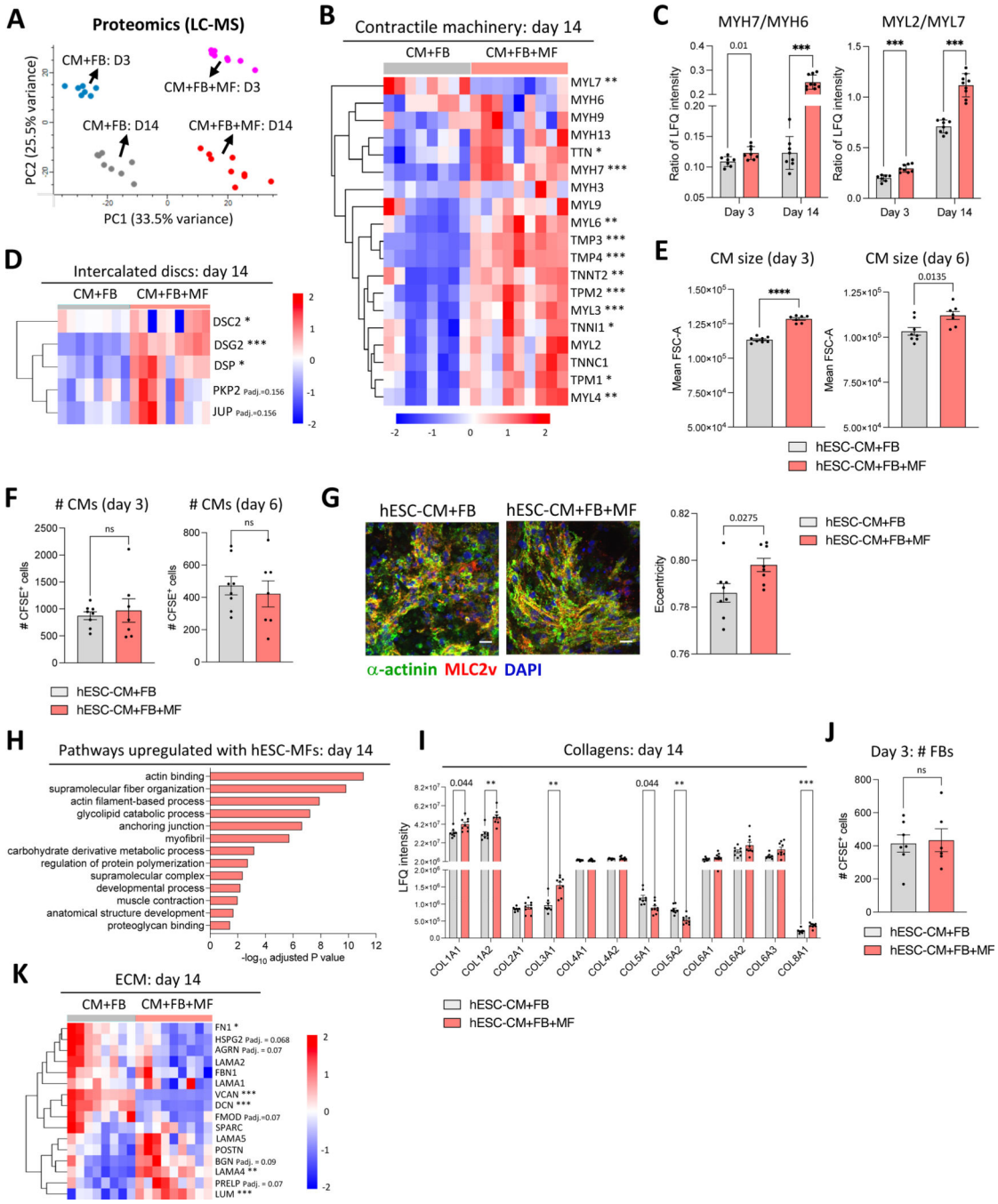

Figure 3: hESC-macrophages induce maturation of cardiomyocyte sarcomeric apparatus and alter extracellular matrix composition in human cardiac microtissues

Liquid chromatography mass spectrometry (LC-MS) was performed on total protein isolated from individual microtissues (HT-Biowires) on day 3 and day 14. **(A)** Principal component analysis of day 3 and day 14 microtissues with or without hESC-macrophages. **(B)** LFQ intensity of contractile machinery proteins in microtissues with or without hESC-macrophages on day 14. n=8 (control) or n=9 (hESC-macrophage) microtissues per group from one experiment. **(C)** Ratio of LFQ intensity of adult to fetal isoforms of contractile

machinery proteins on day 3 and day 14. n=7, 8, 8, 9 (left to right) microtissues per group from 1 experiment. **(D)** LFQ intensity of proteins comprising intercalated discs in microtissues with or without hESC-macrophages on day 14. n=8 (control) or n=9 (hESC-macrophage) microtissues per group from one experiment. **(E)** hESC-cardiomyocytes were pre-labeled with CFSE prior to microtissue seeding. Flow cytometry was performed on day 3 or day 6 and the size of CFSE+ cardiomyocytes was assessed using the forward scatter area (FSC-A) parameter. n=7 (control) or n=8 (hESC-macrophage) microtissues per group from 1 representative experiment performed 3 times. **(F)** hESC-cardiomyocytes were pre-labeled with CFSE prior to microtissue seeding. Flow cytometry was performed on day 3 or day 6 and the number of CFSE+ cardiomyocytes were quantified. n=8, 7, 8, 6 microtissues per group (left to right) from 1 representative experiment performed 3 times. **(G)** Immunofluorescence and confocal microscopy of microtissues with or without hESC-macrophages stained with a-actinin and MLC2v. Sarcomere elongation (eccentricity) was quantified. n=8 microtissues per group, one representative experiment performed 2 times. Scale bar = 20mm. **(H)** Pathway enrichment analysis of proteins significantly upregulated in microtissues with hESC-macrophages (gProfiler). Fisher's one-tailed test was performed with correction for multiple comparisons using the g:SCS method as implemented in gProfiler. **(I)** LFQ intensity of collagen proteins on day 14 in microtissues with or without hESC-macrophages on day 14. n=8 (control) or n=9 (hESC-macrophage) microtissues per group from one experiment. **(J)** Human primary cardiac fibroblasts were pre-labeled with CFSE prior to microtissue seeding. Flow cytometry was performed on day 3 and the number of CFSE+ fibroblasts were quantified. n=7 (control) or n=8 (hESC-macrophage) microtissues per group from one experiment. **(K)** LFQ intensity of extracellular matrix proteins (proteoglycans and glycoproteins) in microtissues with or without hESC-macrophages on day 14. n=8 (control) or n=9 (hESC-macrophage) microtissues per group from one experiment. CM: cardiomyocyte; FB: fibroblast; MF: macrophage. Multiple unpaired t-tests (two-tailed) were conducted with P-values adjusted for multiple comparisons using the Holm-Šídák method (B-D, I, K). Unpaired two-tailed t-test was performed for pairwise comparisons of two groups (E-G, J). $*P<0.05$, $**P<0.01$, $***P<0.001$. Error bars represent mean ± SEM.

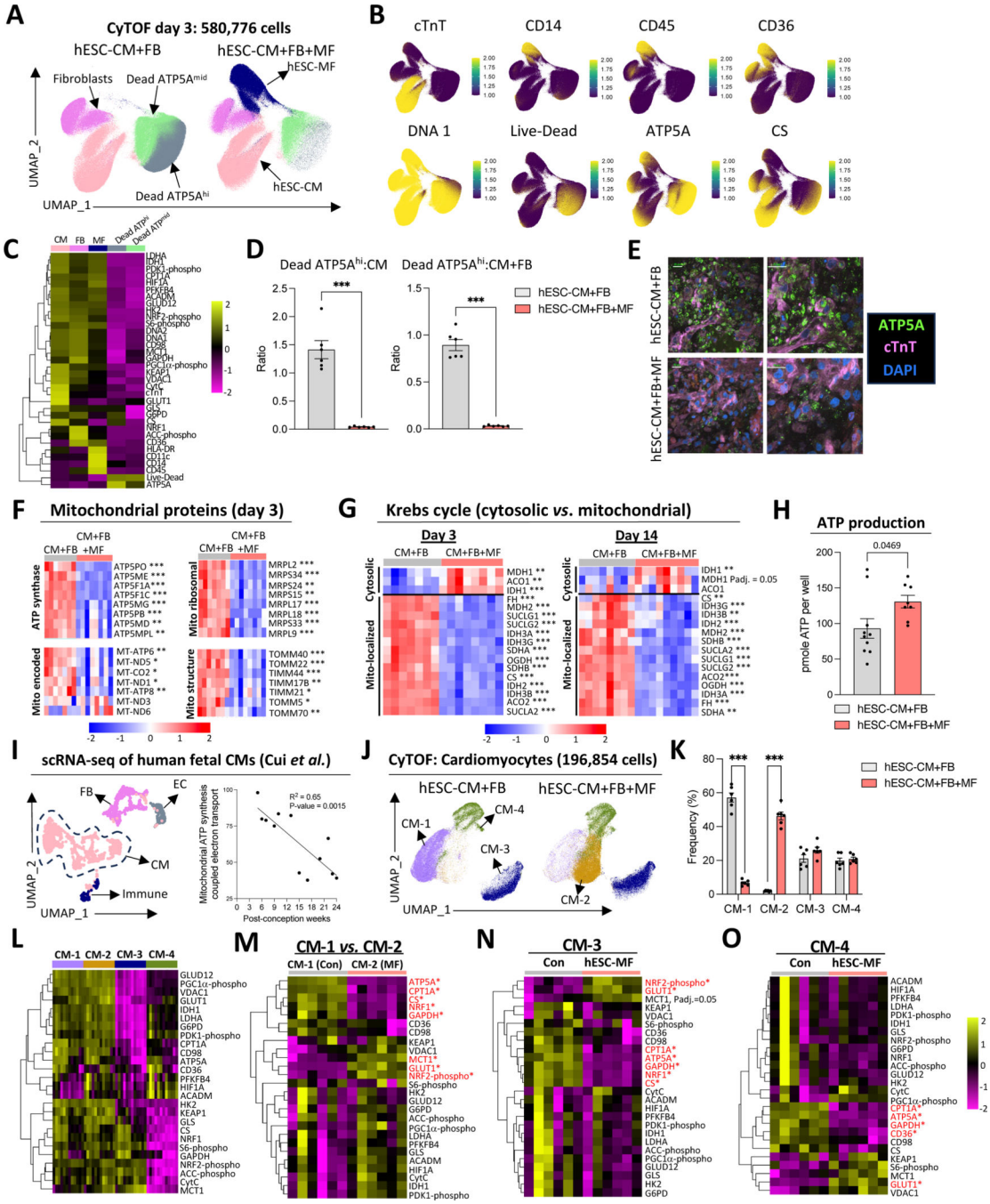

Figure 4: Multi-dimensional CyTOF analyses reveal hESC-macrophages reduce mitochondrial debris, increase ATP production and realign cardiomyocyte metabolism to approximate early fetal ventricular cardiomyocytes.

Cytometry by time-of-flight (CyTOF) was performed on microtissues (HT-Biowires) with or without hESC-macrophages on day 3 post-seeding. n=6 replicates per group; each replicate represents 8 pooled microtissues; experiment performed twice, one representative experiment is shown. **(A)** Uniform manifold approximation and projection (UMAP) visualization of 580,776 live and dead cells following standard quality control filtering. **(B)** Feature plots showing single cell expression of cell type (cTnT, CD45, CD14, CD36)

markers, mitochondrial markers (ATP5A, Citrate synthase ([CS]), DNA and cell death markers. **(C)** Heatmap showing expression of all markers in each major cluster identified in (A). **(D)** Percentage of $ATP5A^{hi}$ cells relative to the number of cardiomyocytes (left) or the number of cardiomyocytes and fibroblasts (right) in microtissues with or without hESC-macrophages. Unpaired two-tailed t-test was performed. **(E)** Immunofluorescence staining and confocal microscopy of ATP5 and cTnT expression in microtissues with or without hESC-macrophages. Scale bar: 20mm. **(F-G)** Mass spectrometry-based proteomics as in Figure 3. LFQ intensity of mitochondrial proteins from a variety of pathways **(F)** or Krebs cycle proteins **(G)** in microtissues with or without hESC-macrophages on day 3 or day 14 post-seeding as indicated. n=7 (control; day 3), n=8 (hESC-macrophage; day 3), n=8 (control; day 14), or n=9 (hESC-macrophage; day 14) microtissues per group from one experiment **(H)** ATP production measured in tissue lysates of total microtissues with or without hESC-macrophages. n=10 (control) or n=8 (hESC-macrophage) replicates per group; each replicate represents 3 pooled microtissues; experiment performed once. Unpaired two-tailed t-test performed. **(I)** Single-cell RNA sequencing analysis of human fetal ventricular cardiomyocytes from Cui *et al*. UMAP showing ventricular cardiomyocyte population (left). Average expression of genes comprising the mitochondrial ATP synthesis electron transport pathway from 5–24 post-conception weeks (right). **(J)** CyTOF data of hESC-cardiomyocytes re-clustered showing 4 subsets. **(K)** Frequency of each hESC-cardiomyocyte subcluster in microtissues with or without hESC-macrophages. Two-way ANOVA was performed with P values adjusted for multiple comparisons using the Šídák method. **(L)** Expression of each marker in each subcluster of hESC-cardiomyocytes. **(M-O)** Expression of each marker in microtissues with or without hESC-macrophages for CM-1 versus CM-2 **(M)**, CM-3 **(N)** or CM-4 **(O)**. CM: cardiomyocyte; FB: fibroblast; MF: macrophage. Multiple unpaired (two-tailed) t-tests were conducted with P values adjusted for multiple comparisons using the Holm-Šídák method (F-G) or Bonferroni-Dunn method (M-O). $*P<0.05$, $**P<0.01$, $***P<0.001$. Error bars represent mean ± SEM.

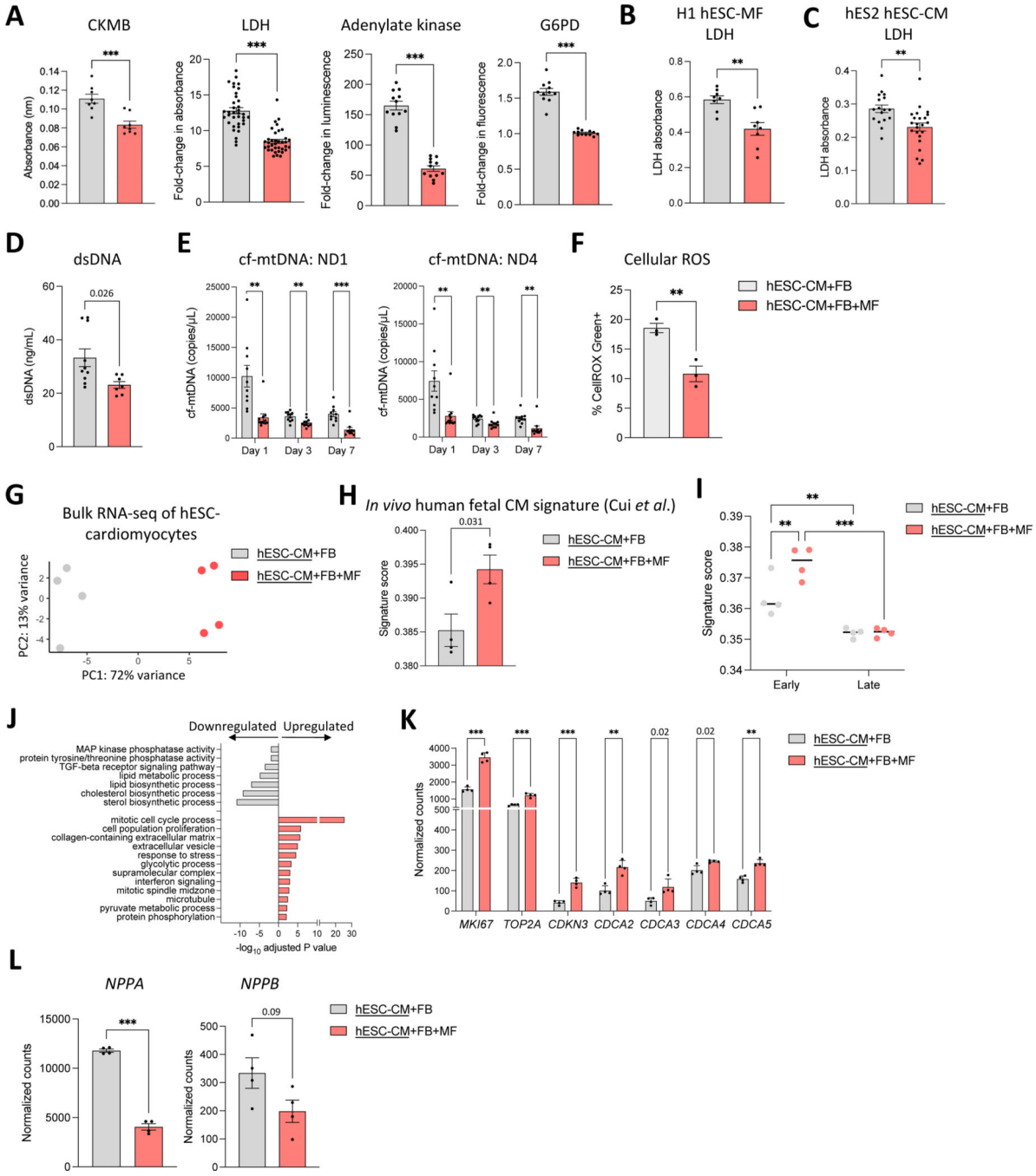

Figure 5: hESC-macrophage incorporation into cardiac microtissues results in reduced cytotoxicity and increased differentiation of cardiomyocytes towards *in vivo* human fetal cardiomyocytes.

(A) Markers of cytotoxicity were measured in culture supernatants from microtissues on day 3 post-seeding, including creatine kinase MB (CKMB; n=8 per group from one experiment), lactate dehydrogenase (LDH; n=36 per group, two pooled experiments shown, 10 experiments performed), adenylate kinase (n=12 per group from one experiment) and glucose-6-phosphate dehydrogenase (G6PD; n=11 per group from one experiment). **(B)** LDH release in supernatants on day 3 post-seeding from microtissues seeded with hESC-

cardiomyocytes and fibroblasts with or without H1 hESC-macrophages. n=8 microtissues per group, two experiments pooled. **(C)** LDH release in supernatants on day 3 post-seeding from microtissues seeded with hES2 GFP^+ hESC-cardiomyocytes and fibroblasts with or without hESC-macrophages. n=8 per group, two experiments pooled. **(D)** The release of double-stranded DNA (dsDNA) in culture supernatants from microtissues on day 3 post-seeding. n=10 (control) or n=7 (hESC-macrophage) microtissues per group from one experiment. **(E)** Cell-free mitochondrial DNA (cf-mtDNA) was measured in culture supernatants on day 1, 3 and 7 post-seeding. Genes in both the minor (ND1) and major (ND4) arc of the mitochondrial genome were assessed. n=10, 11, 11, 11, 10, 10 microtissues per group (left to right) from one experiment. **(F)** Cellular reactive oxygen species were measured in live microtissues on day 7 post-seeding. Percentage of microtissue area positive for CellROX Green. n=3 microtissues per group from one experiment. **(G)** hESC-cardiomyocytes ($DAPI^-CD45^-CD14^-CD90^-RFP^-$ live single cells) were sorted from microtissues with or without hESC-macrophages on day 3 post-seeding for bulk RNA sequencing (n=4 replicates per group; each replicate represents two pooled microtissues; one experiment). Principal component analysis showing that the major driver of variation was the presence or absence of hESC-macrophages. **(H)** A signature for *in vivo* human fetal ventricular cardiomyocytes was generated using the top differentially expressed genes in ventricular cardiomyocytes relative to immune cells in Cui *et al.* dataset. hESC-cardiomyocytes from microtissues with or without hESC-macrophages were scored for this signature. n=4 replicates per group, one experiment. **(I)** Similar to (H), except the signature was generated for early (5–9 post-conception weeks) versus late (17–24 post-conception weeks) separately. n=4 replicates per group, one experiment. Two-way ANOVA was performed. **(J)** Pathways enriched in hESC-cardiomyocytes from microtissues with or without hESC-macrophages (gProfiler). Fisher's one-tailed test was performed with correction for multiple comparisons using the g:SCS method as implemented in gProfiler. **(K)** Expression levels of proliferation genes in in hESC-cardiomyocytes from microtissues with or without hESC-macrophages. n=4 replicates per group, one experiment. **(L)** Expression levels of *NPPA* and *NPPB* in in hESC-cardiomyocytes from microtissues with or without hESC-macrophages. n=4 replicates per group, one experiment. CM: cardiomyocyte; FB: fibroblast; MF: macrophage. Multiple unpaired (two-tailed) t-tests was performed with P values adjusted for multiple comparisons using the Holm-Šídák method (K), or unpaired two-tailed t-test for pairwise comparisons (A-F, H, L). $*P<0.05$, $**P<0.01$, $***P<0.001$. Error bars represent mean ± SEM.

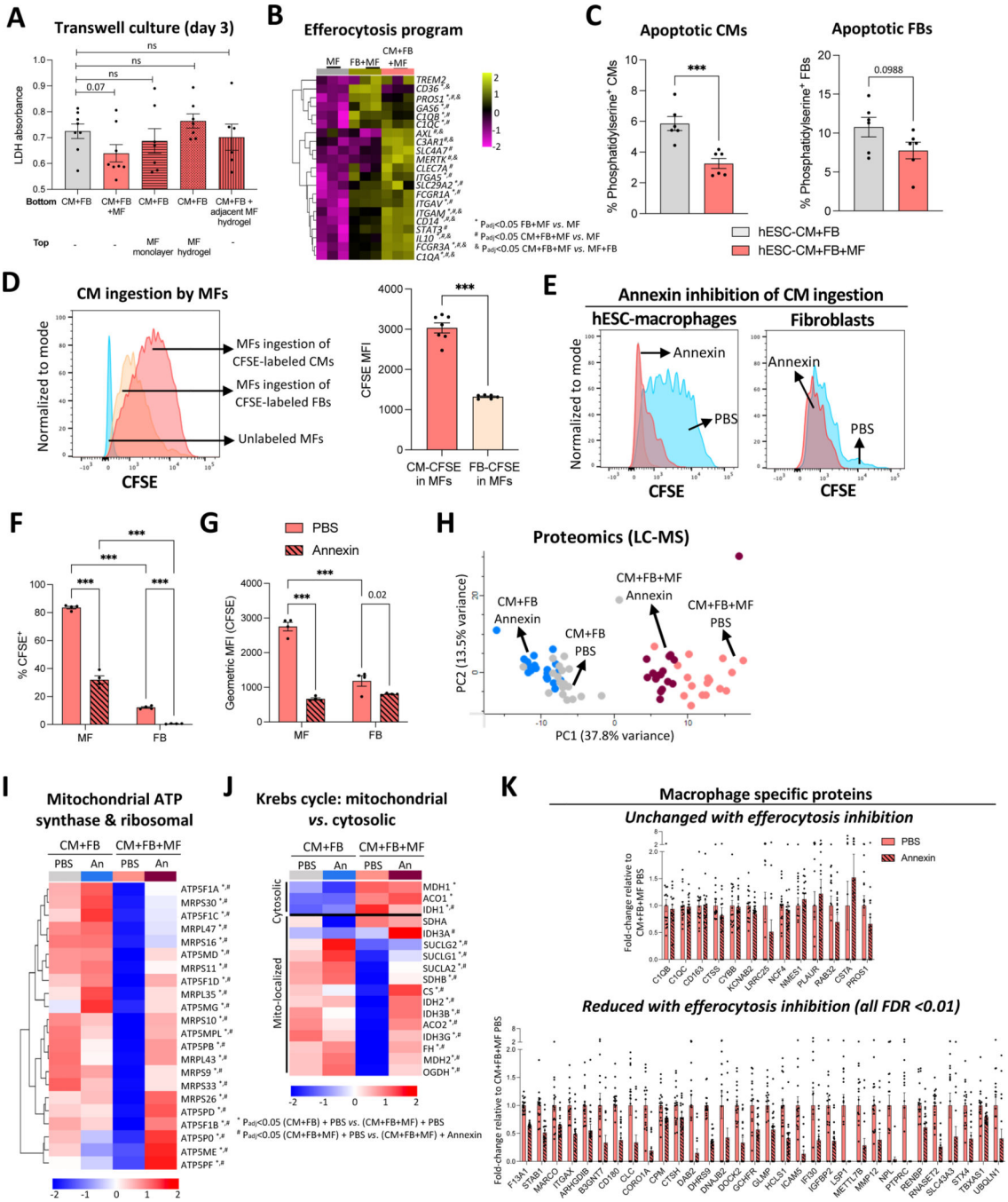

Figure 6: Efferocytic uptake of cardiomyocytes by hESC-macrophages is driven by phosphatidylserine recognition and is required for full macrophage maturation.

(A) Transwell co-cultures were performed with each combination of cells specified. LDH was measured in culture supernatants on day 3. n=7, 7, 5, 5, 5 microtissues per group (left to right) from one experiment. **(B)** Log transformed expression of efferocytosis or phagocytosis related genes from bulk RNA sequencing of hESC-macrophages as in Figure 1. Two-way ANOVA was performed and P values were adjusted for multiple comparisons using the Tukey-Kramer test. **(C)** Microtissues were seeded with or without

hESC-macrophages and flow cytometry was performed on day 1 post-seeding. The percentage of ApoTracker^{+}DAPI^{-} cardiomyocytes (left; CD14^{-}CD45^{-}) or fibroblasts (right; CD45^{dim}CD14^{dim}) is shown. n=6 microtissues per group from one experiment. **(D)** hESC-cardiomyocytes or fibroblasts were pre-labeled with CFSE prior to seeding microtissues. Flow cytometry was performed on day 3 post-seeding, and the intensity of CFSE within hESC-macrophages (CD45^{+}CD14^{+}) cells is shown. n=7 (CM-CFSE) or n=6 (FB-CFSE) microtissues per group; two experiments performed, representative experiment shown. **(E)** hESC-cardiomyocytes were pre-incubated with Annexin V to block exposed phosphatidylserine, then pre-labeled with CFSE prior to seeding microtissues. On day 3, flow cytometry was performed and the intensity of CFSE within hESC-macrophages (CD45^{+}CD14^{+}) or in fibroblasts (CD45^{dim}CD14^{dim}) is shown. **(F)** Percentage of hESC-macrophages or fibroblasts that are CFSE^{+} on day 3 post-seeding in microtissues containing PBS pre-treated versus Annexin pre-treated hESC-cardiomyocytes. n=4 microtissues per group from one experiment. **(G)** Geometric MFI of CFSE within hESC-macrophages or fibroblasts on day 3 post-seeding in microtissues containing PBS pre-treated versus Annexin pre-treated hESC-cardiomyocytes. n=4 microtissues per group from one experiment. **(H)** Liquid chromatography mass spectrometry was performed on individual whole microtissues with or without hESC-macrophages, containing PBS pre-treated versus Annexin pre-treated hESC-cardiomyocytes (4 groups) on day 14. n=19 (control PBS), n=19 (control Annexin), n=17 (hESC-macrophage PBS), or n=16 (hESC-macrophage Annexin) microtissues per group from one experiment (H-K). Principal component analysis is shown. **(I-J)** LFQ intensity of mitochondrial proteins **(I)** or Krebs cycle proteins **(J)** in each group. The top 10 mitochondrial ribosomal proteins are shown (based on fold-change of annexin *vs.* PBS microtissues with hESC-macrophages). **(K)** LFQ intensity of macrophage-specific proteins that were detected only in microtissues with hESC-macrophages in either PBS or Annexin groups (normalized to PBS group). All pairwise comparisons in “reduced” graph were significantly different (FDR<0.01). An: Annexin; CM: cardiomyocyte; FB: fibroblast; MF: macrophage. Multiple unpaired (two-tailed) t-tests were conducted with P values adjusted for multiple comparisons using the false discovery rate (FDR) approach (two-stage step-up, Benjamini, Krieger, and Yekutieli method). I-K: * indicates discoveries below desired FDR of 0.05. Two-way ANVOA for multiple groups (F-G) or unpaired two-tailed t-test for pairwise comparisons (A, C, D) were performed. *P<0.05, **P<0.01, ***P<0.001. Error bars represent mean ± SEM.

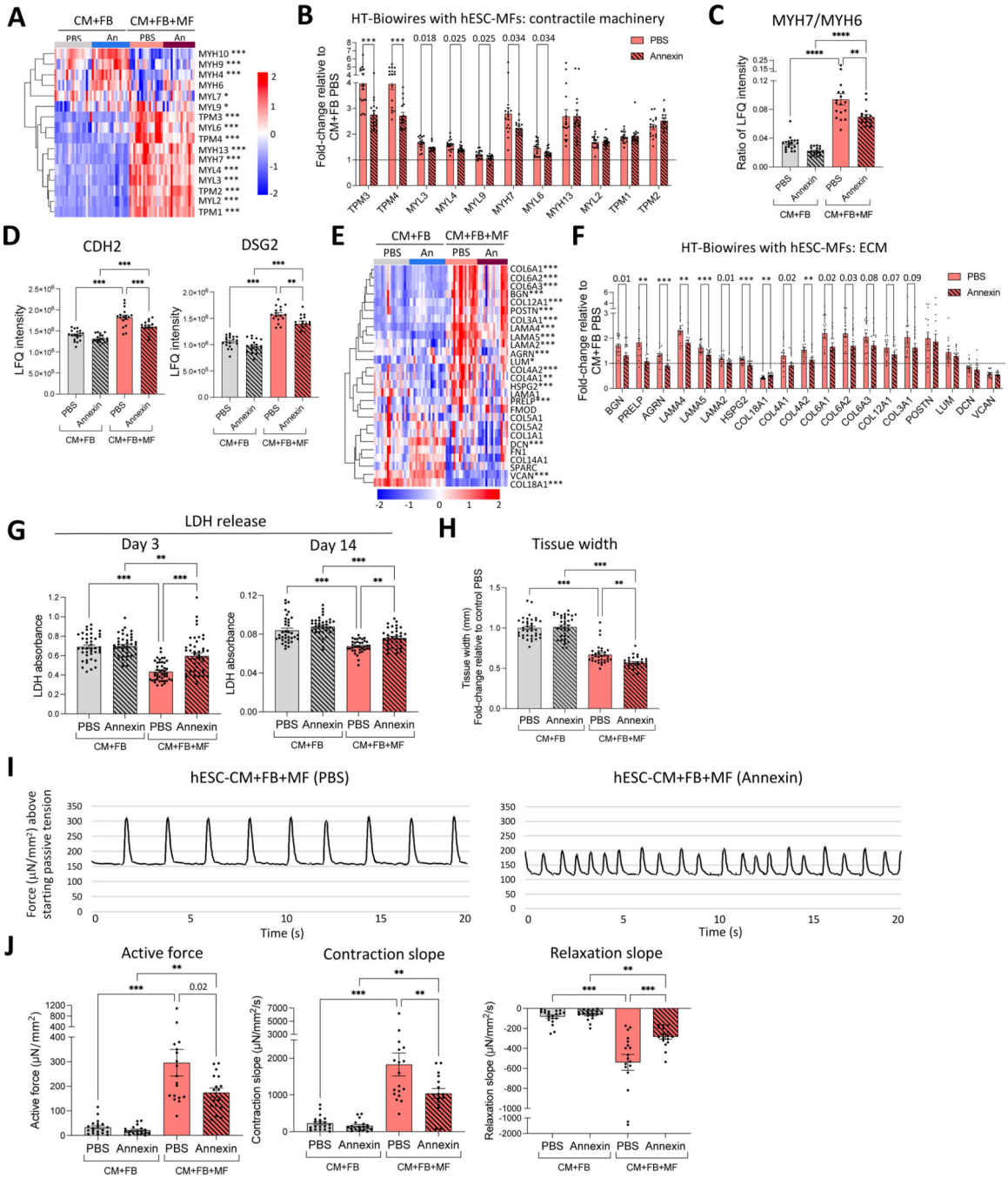

Figure 7: Inhibiting hESC-macrophage efferocytosis of cardiomyocytes leads to blunted cardiomyocyte maturation, increased cytotoxicity and impaired microtissue function.

(A-F) Liquid chromatography mass spectrometry was performed on individual microtissues (HT-Biowires) with or without hESC-macrophages, containing PBS pre-treated versus Annexin pre-treated hESC-cardiomyocytes (4 groups) on day 14 post-seeding. n=19 (control PBS), n=19 (control Annexin), n=17 (hESC-macrophage PBS), or n=16 (hESC-macrophage Annexin) microtissues per group from one experiment. **(A)** LFQ intensity of contractile machinery proteins is shown in microtissues with or without hESC-macrophages. **(B)**

Contractile machinery proteins that were upregulated with hESC-macrophages in (A) are shown as a direct comparison between microtissues with hESC-macrophages in PBS versus Annexin treated groups. Fold change of LFQ intensity relative to control microtissues without hESC-macrophages. **(C)** Ratio of LFQ intensity of MYH7 to MYH6 in each group. **(D)** LFQ intensity of CDH2 and DSG2 in each group. **(E)** LFQ intensity of collagen proteins is shown in microtissues with or without hESC-macrophages. **(F)** Collagen proteins that were significantly upregulated or downregulated with hESC-macrophages in (E) are shown as a direct comparison between microtissues with hESC-macrophages in PBS versus Annexin treated groups. Fold change of LFQ intensity relative to control microtissues without hESC-macrophages. **(G-J)** Microtissues were seeded with or without hESC-macrophages, containing PBS pre-treated versus Annexin pre-treated hESC-cardiomyocytes. **(G)** LDH was measured in culture supernatants on day 3 or day 14 post-seeding. n=41, 41, 45, 45 (day 3, left to right) microtissues per group from three independent experiments pooled or n=37 microtissues per group (day 14) from two independent experiments pooled. **(H)** Tissue width was measured on day 14. n=38, 37, 33, 28 microtissues per group (left to right) from two independent experiments pooled. **(I)** Force traces showing the measured force above passive tension across time in microtissues with hESC-macrophages in PBS versus Annexin treated groups. Representative traces shown. **(J)** On day 14 post-seeding, active force, contraction slope and relaxation slope were measured. n=20, 18, 18, 16 microtissues per group (left to right) from one representative experiment; second experiment shown in Figure S10. An: Annexin; CM: cardiomyocyte; FB: fibroblast; MF: macrophage. One-way ANOVA with P values adjusted for multiple comparisons using the Šídák method (C-D, G-H, J). Multiple unpaired (two-tailed) t-tests with P values adjusted for multiple comparisons using the Holm-Šídák method (A, E) or the false discovery rate approach (two-stage step-up, Benjamini, Krieger, and Yekutieli; [B, F]). *P<0.05, **P<0.01, ***P<0.001. Error bars represent mean ± SEM.

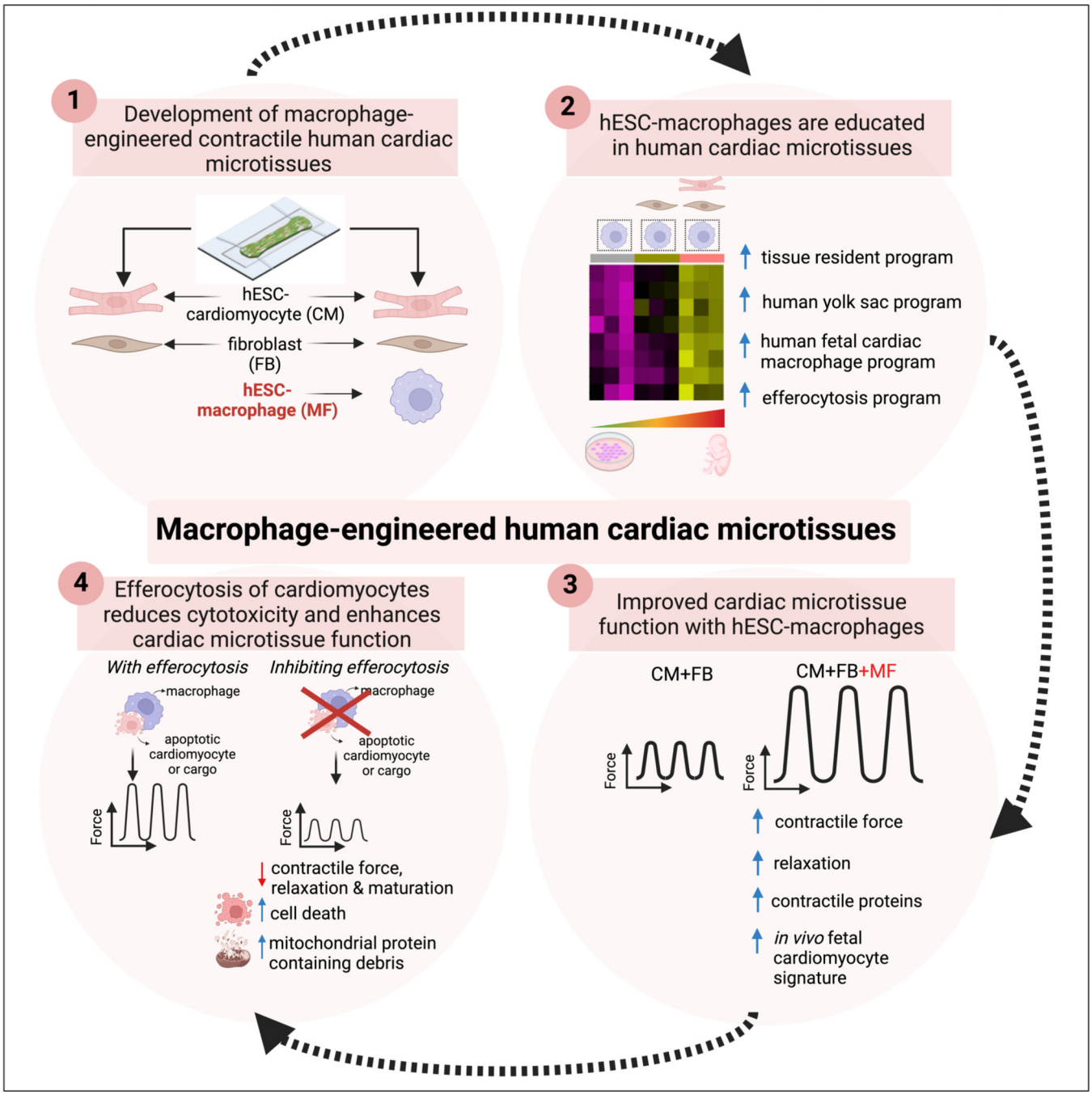

Figure 8: Graphical summary of findings.
Created with BioRender.com.